Order Number 1346741

Characterization and comparison of noise generation for quasi-resonant and pulse-width-modulated converters

Hsiu, Leng-nien, M.S.

The University of Arizona, 1991

U·M·I
300 N. Zeeb Rd.
Ann Arbor, MI 48106

Characterization and Comparison of Noise Generation for Quasi-resonant and Pulse-width-modulated Converters

by
Leng-nien Hsiu

A Thesis Submitted to the Faculty of the
DEPARTMENT OF ELECTRICAL AND COMPUTER ENGINEERING
In Partial Fulfillment of the Requirements
For the Degree of
MASTER OF SCIENCE
WITH A MAJOR IN ELECTRICAL ENGINEERING
In the Graduate College
THE UNIVERSITY OF ARIZONA

1991

STATEMENT BY AUTHOR

This thesis has been submitted in partial fulfillment of requirements for an advanced degree at The University of Arizona and is deposited in the University Library to be made available to borrowers under rules of the library.

Brief quotations from this thesis are allowable without special permission, provided that accurate acknowledgement of source is made. Requests for permission for extended quotation from or reproduction of this manuscript in whole or in part may be granted by the head of the major department or the Dean of the Graduate College when in his or her judgement the proposed use of the material is in the interests of scholarship. In all other instances, however, permission must be obtained from the author.

SIGNED: Longnien Hsiu

APPROVAL BY THESIS DIRECTOR

This thesis has been approved on the date shown below:

Arthur F Witulski — 12/12/91

Arthur F. Witulski — Date

Assistant Professor of
Electrical and Computer Engineering

Acknowledgements

At the moment that the thesis becomes reality, I have to express my sincere thanks to all the people who have helped me. I would like to thank my parents and families first. They always are my firmest support in any situation. I give my special gratitude to Dr. A. F. Witulski who has been patient in guiding me to acomplish this thesis. I also thank Dr. Kerwin and R. Carlsten (IBM, Tucson) for their helpful suggestion about this research. Finally, I would like to acknowledge the IBM Power Electronics Group for their generous support of this research project.

Table of Contents

List of Figures

List of Tables

Abstract

A buck converter with a given output filter is operated with pulse-width modulated and quasi-resonant switching schemes at the same nominal load and switching frequency. Electromagnetic interference generated by the natural switching action of the converter is examined by Fourier spectral analysis. Interference caused by excitation of parasitic elements is examined experimentally. Quasi-resonant converters are found to have a lower switching frequency harmonic bandwidth than the equivalent pulse-width modulated converter. The most significant parasitic responses are the turn-on current and turn-off voltage of the catch diode, and the gate charge current of the MOSFET switch. A significant decrease in radiated and conducted noise is obtained when the gate drive voltage rise and fall times are increased, which is possible without loss of efficiency using quasi-resonant switching.

CHAPTER 1
INTRODUCTION

Electromagnetic interference (EMI) is a critical issue in the design of electronic power processing systems. It is especially important in more demanding applications, such as distributed power systems, in which the converter is mounted directly on the circuit board and is very near the signal processing components. Higher packaging density also increases the importance of EMI considerations because the proximity of power supply and processing circuitry increases the likelihood of undesired interactions. This is especially important in instrumentation electronics with sensitive transducers, where EMI must be severely limited to obtain accurate and reliable measurements.

Electromagnetic interference must be carefully defined. In power converter circuits, noise is translated to be the periodical or random deviations from the ideal converter waveforms. The ideal dc-to-dc converter is a device in which only frequencies that contribute to the actual power transfer (dc in this case) appear at the input or output ports of the converter or are radiated to the surrounding environment (Fig. 1-1(a)). The traditional linear regulator fits this description well. The instantaneous input power $P_i(t)$ is equal to the average input power $\langle P_i(t) \rangle$ because both input voltage and current are dc. The generated fields are also independent of time and hence do not induce voltages or currents in the surrounding components. A switching regulator such as a buck converter (Fig. 1-1(b)), on the other hand, has a square-wave input current containing infinite switching frequency harmonics, of which only the dc component contributes to average power transfer. Hence the instantaneous input power is not equal to the average input power. The switching frequency harmonics can be considered conducted interference. The

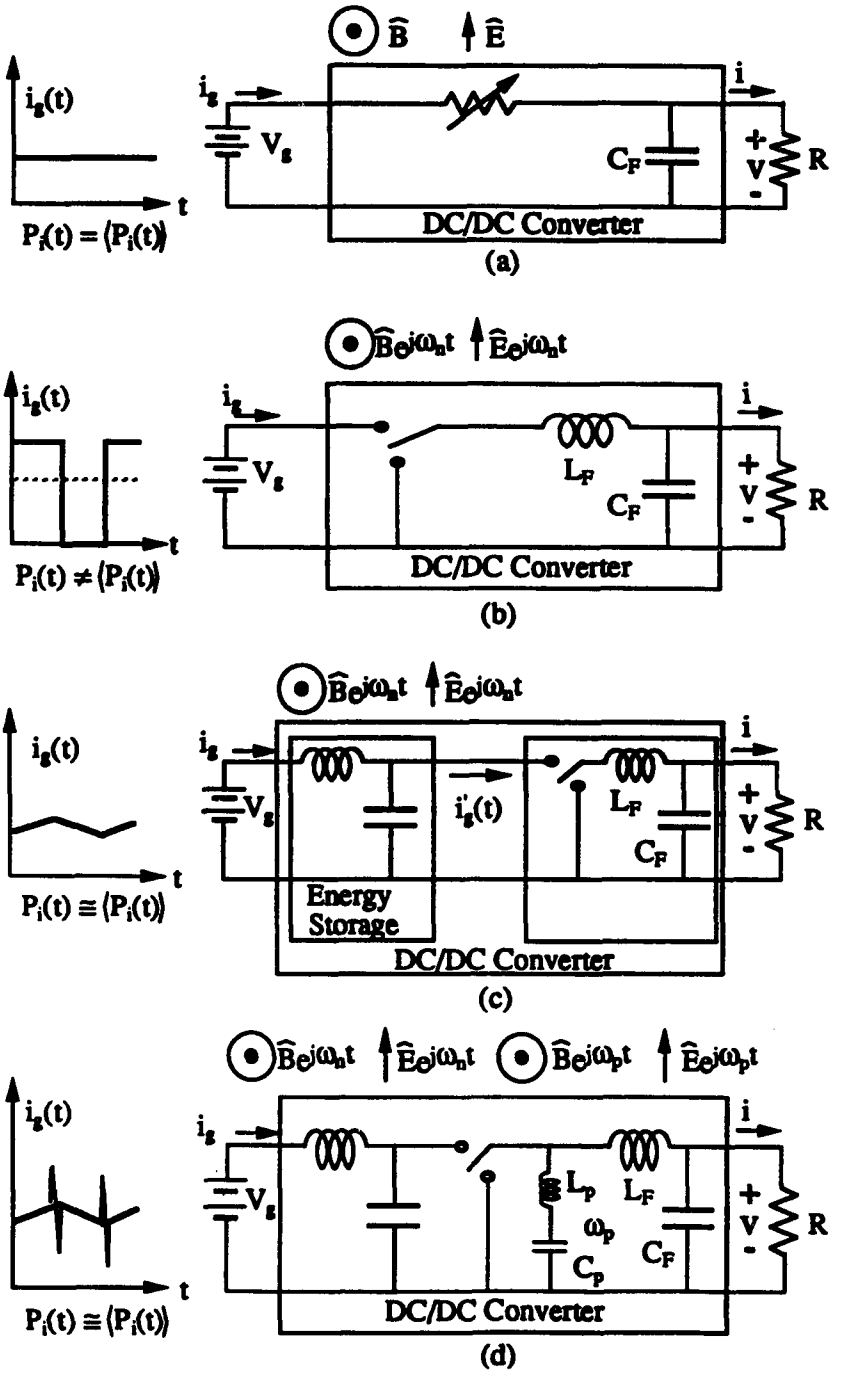

Fig. 1-1 Interference characteristics of: (a) traditional linear regulator, (b) switching regulator, (c) switching regulator with input and output filters, (d) switching regulator with parasitic oscillations.

radiated fields are also time-varying and therefore tend to induce currents and voltages in nearby conductors. In order to prevent the switching frequency harmonics from being conducted to the source, an energy storage element must be provided to absorb the difference between instantaneous and average power (Fig. 1-1(c)). Hence filters must be used if near-ideal dc-to-dc terminal characteristics are to be obtained, although in practice some switching frequency harmonics are still present when finite filter elements are used. Of course, the problem with radiated fields remains unchanged. Obtaining near-ideal performance with switching converters is further complicated by the fact that the switching action excites various parasitic elements in the converter, which results in conducted and radiated energy at unpredictable frequencies (Fig. 1-1(d)). In practice it is these parasitic oscillation frequencies which are most difficult to filter, and which often cause the most interference with signal processing circuitry.

1.1 Background

Before a comparison between quasi-resonant and PWM converters can be performed, the operation of these converters must be discussed to enhance understanding of the following material. Converter operation is reviewed in 1.1.1 and 1.1.2. Some previous work related to this research is mentioned in 1.1.3.

1.1.1 Review of PWM converter

In the traditional linear regulator (Fig. 1(a)), the input current and input voltage both are continuous (the transistor is always on). Moreover, the transistor through which the full regulator output current is flowing has a significant voltage drop (transistor operates in

the active region). Hence, there is large amount of continuous power consumption in the switch of the traditional linear regulators.

The pulse-width modulated (PWM) converter, however, is controlled such that the switch-on time is controlled by the switching duty cycle D (Fig. 1-2). Therefore, the unnecessary power consumption of the switch (conduction loss) can be greatly reduced and the efficiency of the regulator improved over the linear regulator. The average output voltage of the PWM converter is equal to DV_g. By changing the switching duty cycle, the average output voltage can be adjusted to a specific value without changing the switching frequency. Hence, the PWM converter is a constant-frequency-controlled converter. Nevertheless, the switching action of the PWM converters introduces the square switch current and voltage waveforms, as shown in Fig. 1-2, that can cause serious problems with electromagnetic interference (EMI) for the circuit and its environment.

1.1.2 Review of Quasi-resonant Converter

Although PWM converters reduce the switch conduction loss, they introduce switching loss, which is due to non-zero switch current and voltage during turn-on and turn-off. Further attempts to reduce the switching power losses and the EMI generation of the PWM converters at the same time leads to the development of the quasi-resonant converters. There are four basic types of quasi-resonant converters: half wave zero-current switching (ZCS-1/2), full wave zero-current switching (ZCS-1), half wave zero-voltage switching (ZVS-1/2), full wave zero-voltage switching (ZVS-1). Either zero-current switching (switch current is zero at turn-on and turn-off) or zero-voltage switching (switch voltage is zero at turn-on and turn-off) converters have lower switching losses than the PWM converters. Moreover, the quasi-sinusoidal switch current or voltage waveforms of

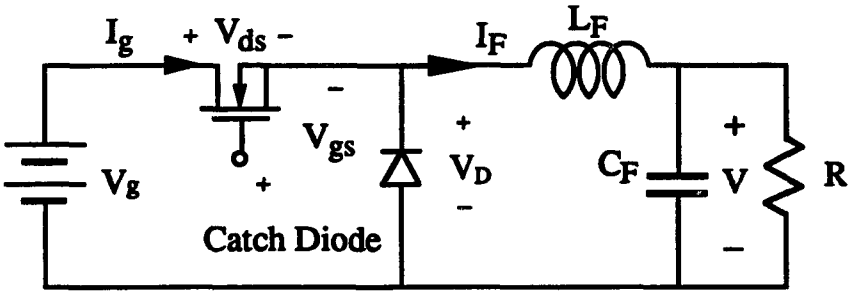

PWM

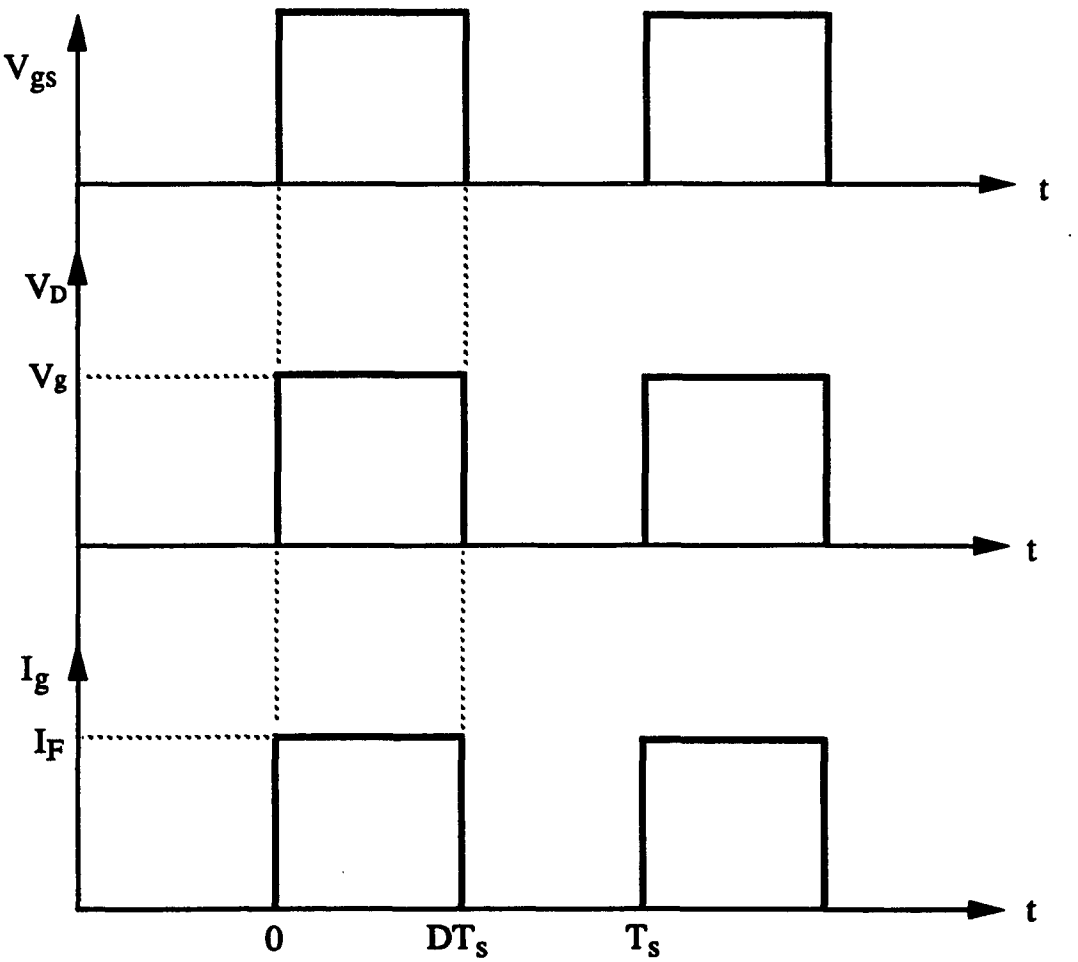

Fig. 1-2 PWM converter circuit and waveforms of V_{gs}, V_D, and I_g.

these converters intuitively seem better than the square waveforms of PWM converters in reducing the generation of EMI.

The operation of these quasi-resonant converters is briefly reviewed here for better understanding of the following work. Detailed explanation of their operation can be found in [1-3]. The circuit and resonant inductor current (switch current) and resonant capacitor voltage waveforms of ZCS-1/2 are shown in Fig. 1-3. In the first interval, when the switch is on, the catch diode (labeled in Fig. 1-3) will still be on until the resonant inductor current ramps up to the filter inductor current. In the second interval, the catch diode is off and the resonant inductor and capacitor begin to resonate. When the resonant inductor current reaches zero, the switch is turned off and the second interval ends. In the third interval, the resonant capacitor voltage discharges to zero through the filter inductor. In the fourth interval, the catch diode turns on again. The operation of ZCS-1, shown in Figure 1-4, is slightly different from ZCS-1/2 in the second interval. For ZCS-1, the resonant inductor current can continue to resonate to negative current because of the anti-parallel mode diode (labeled in Fig. 1-4) across the switch.

The circuit and resonant inductor current and resonant capacitor voltage (switch voltage) waveforms of ZVS-1/2 are shown in Fig. 1-5. In the first interval, when the switch is off, the resonant capacitor voltage ramps up to the input voltage through the filter inductor current. In the second interval, the catch diode (labeled in Fig. 1-5) is on and the resonant capacitor and inductor begin to resonate. When the resonant capacitor voltage reaches zero, the switch turns on and the second interval ends. In the third interval, the resonant inductor current ramps up to the filter inductor current. In the fourth interval, the catch diode is off. The difference between ZVS-1/2 and ZVS-1 arises because the resonant

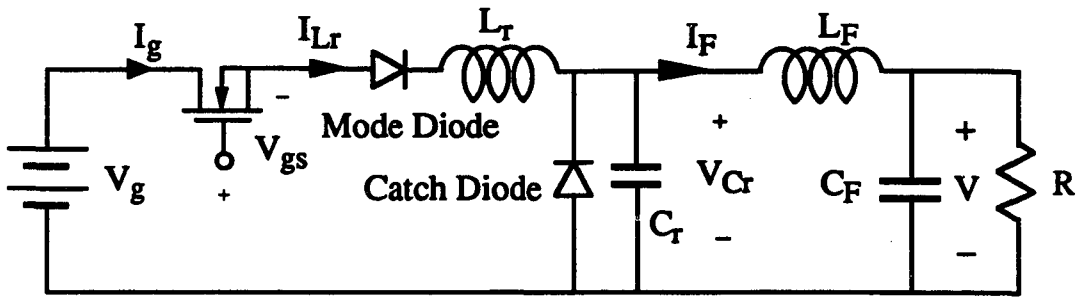

ZCS-1/2

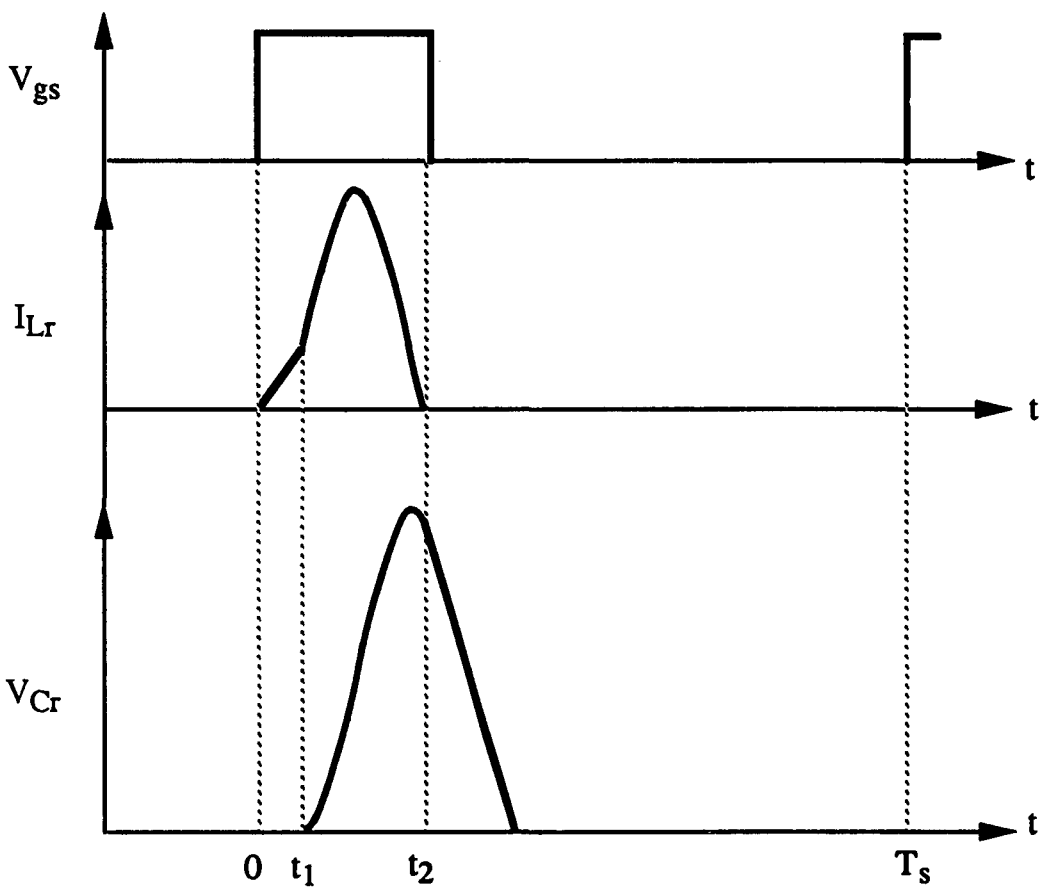

Fig. 1-3 ZCS-1/2 QRC circuit and the waveforms of V_{gs}, I_{Lr}, and V_{Cr}.

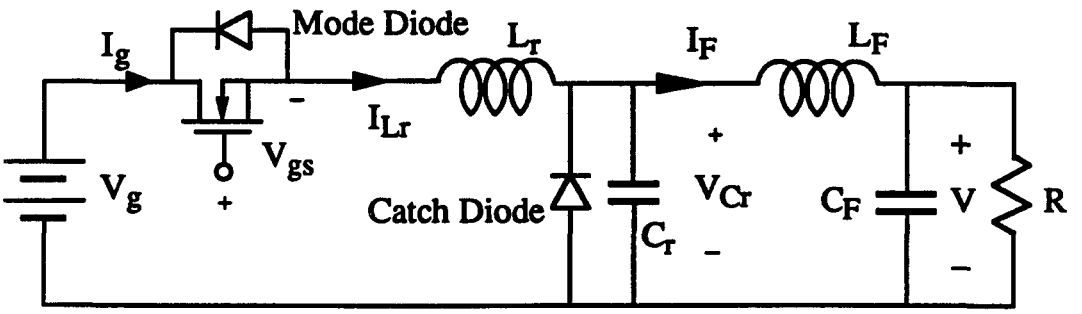

ZCS-1

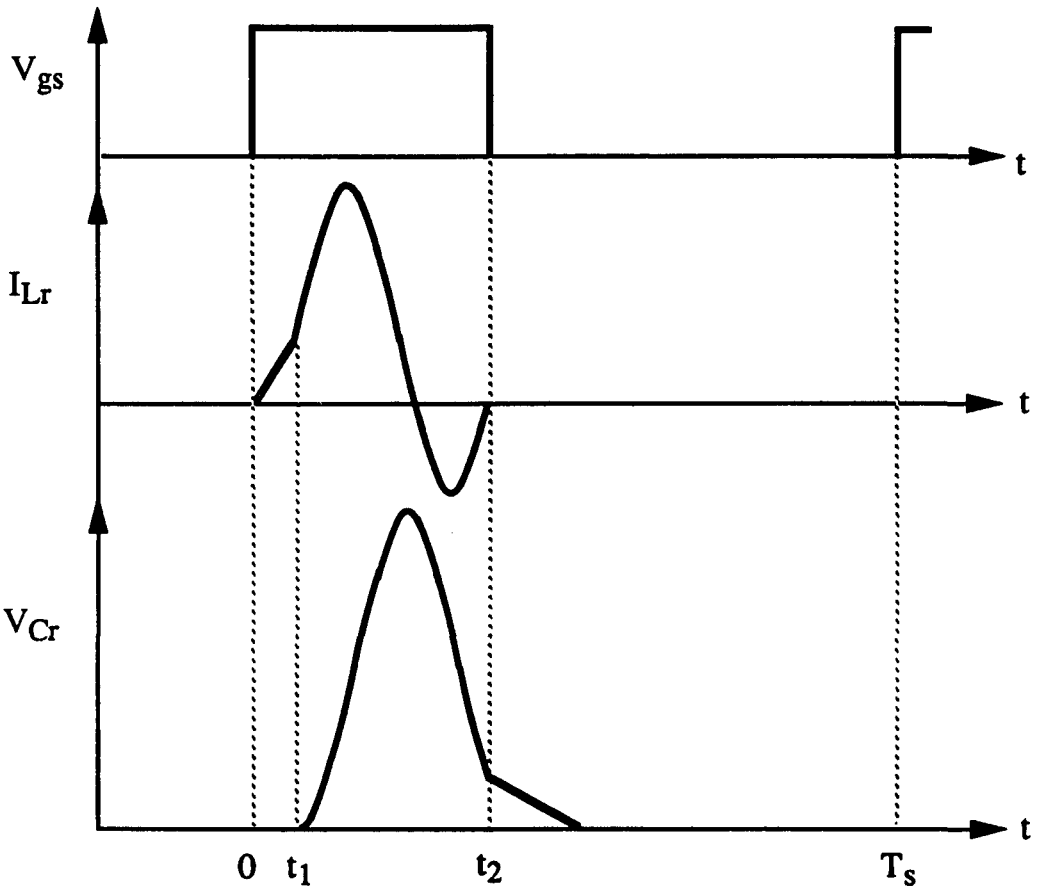

Fig. 1-4 ZCS-1 QRC circuit and waveforms of V_{gs}, I_{Lr}, and V_{Cr}.

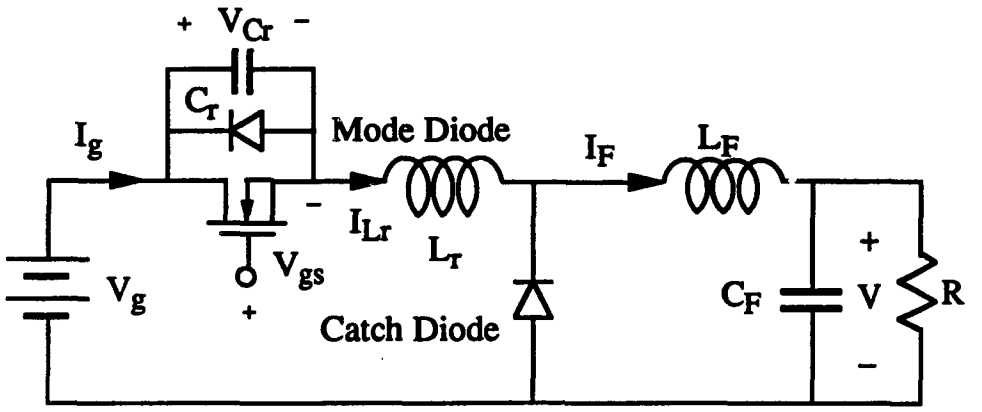

ZVS-1/2

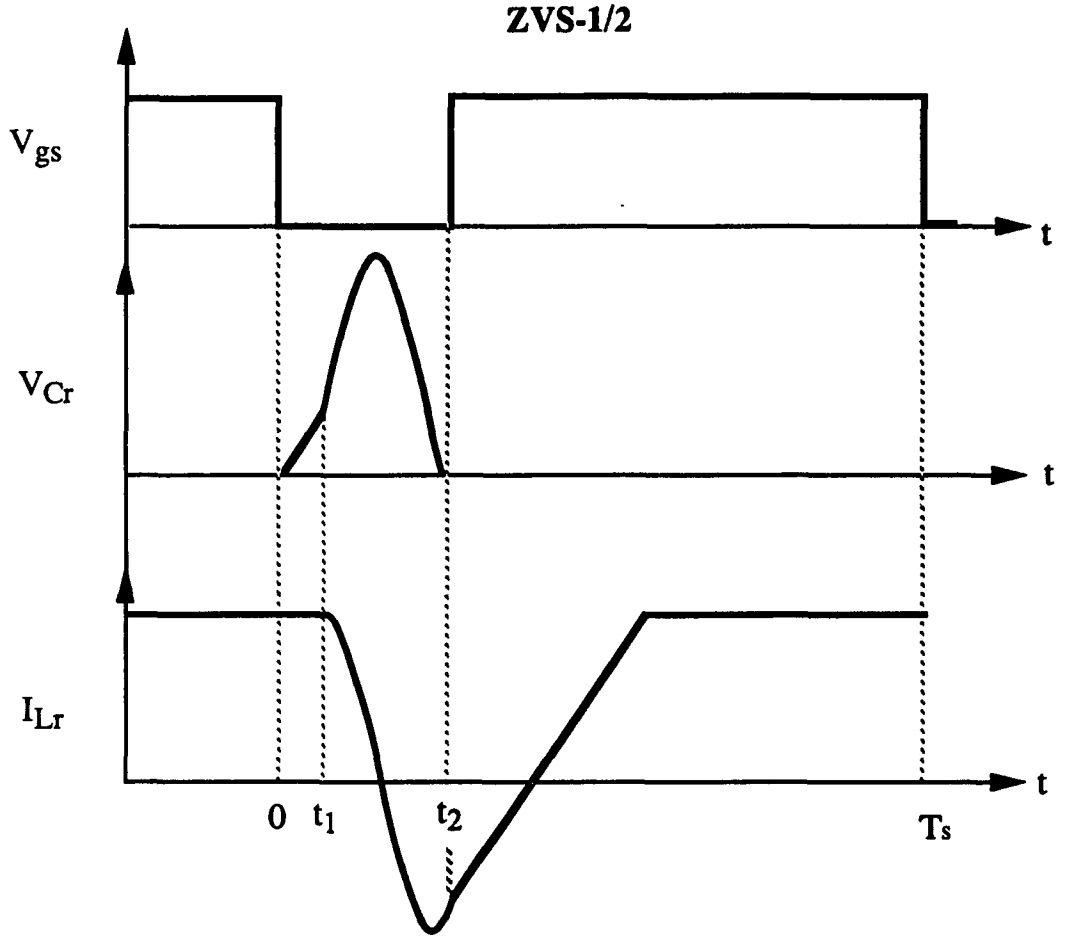

Fig. 1-5 ZVS-1/2 QRC circuit and the waveforms of V_{gs}, V_{Cr}, and I_{Lr}.

capacitor voltage can continue to resonate to negative voltage in the ZVS-1 because of the conduction-blocking mode diode (labeled in Fig. 1-6) in series with the switch. The operation of ZVS-1 is shown in Fig. 1-6.

1.1.3 Previous Work

Earlier study of noise generation in switching converters has found that noise is generated whenever there is a difference between an input or output current waveform and its corresponding voltage waveform [4]. For example, the buck converter has a dc input voltage, but the input current is pulsating. Hence, the obvious difference between the input voltage and current indicates noise generation in the buck converter. These waveform differences usually involve undesired current waveforms having high harmonic contents that are difficult to filter and cause conducted or radiated interference. In [4], two types of switching frequency harmonic noise are defined: pulsating noise and ripple noise. The pulsating component is present if the current has pulsed waveform, i.e. is zero for some portion of the switching cycle. The ripple component consists of a small ac waveform superimposed on a large dc level. It is important to realize that both of them are caused by the switching function and have the switching frequency harmonic interference generation. The methods introduced in [4] to reduce noise are well-known today. The principle is to keep the corresponding input or output current and voltage waveforms as much the same as possible. Hence, the pulsating noise is reduced by putting a shunt capacitor, and the ripple noise is reduced by adding a large enough LC filter.

Besides these switching frequency noise mentioned above, some higher frequency parasitic-induced noise taking place at switching instants has also been found in the

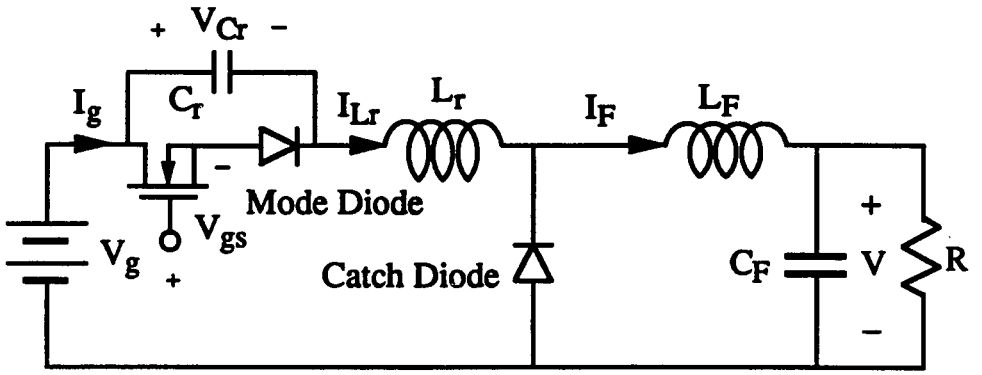

ZVS- 1

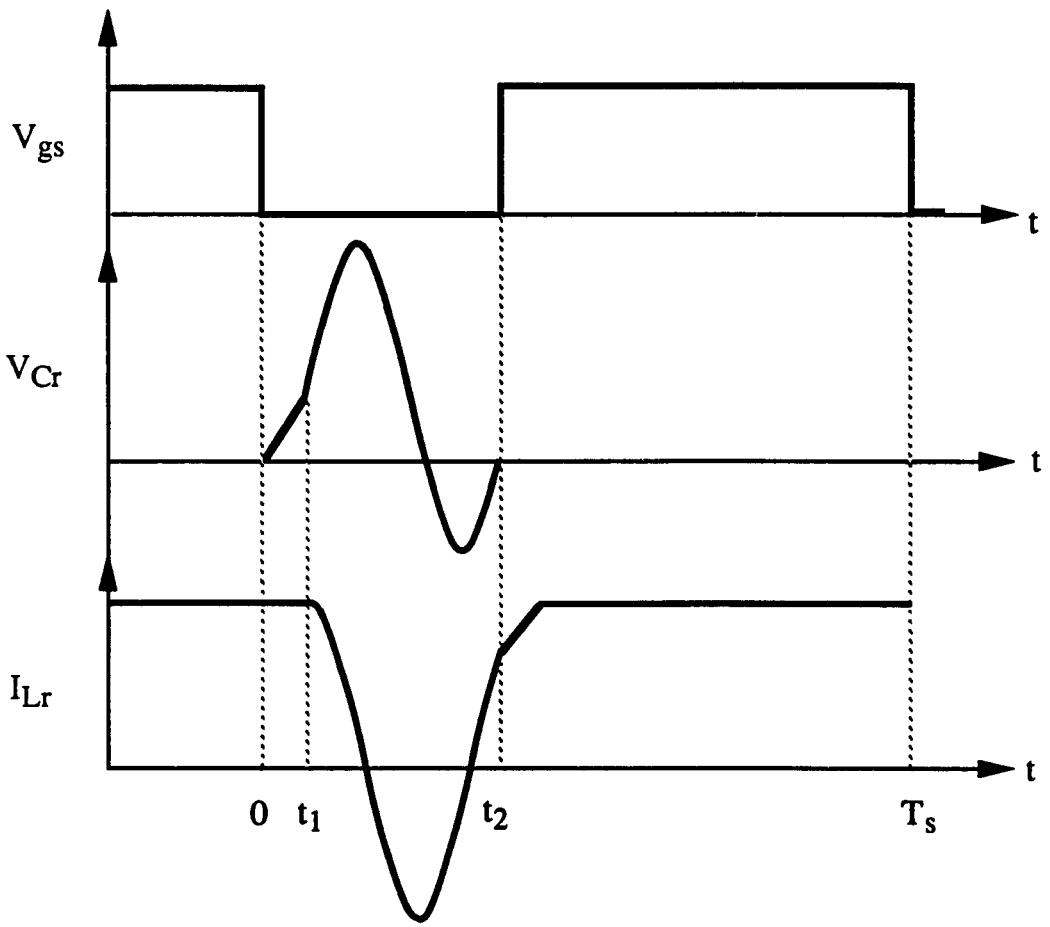

Fig. 1-6 ZVS-1 QRC circuit and the waveforms of V_{gs}, V_{Cr}, and I_{Lr}.

switching converter. Later research on higher frequency parasitic noise generation was done through some analysis of different equivalent high frequency converter circuit models at several turn-on and turn-off switching operation intervals [5-7]. These equivalent high frequency circuits are formed by some high frequency circuit models for the transistor and diodes, and include some parasitic inductance of the wire or the lead and stray capacitances of the transformer windings. The computer-aided numerical circuit analysis and the experimental results of the study show that these higher parasitic frequency noise generation relates to the switching speed (rise time and fall time), the depletion capacitance of the transistor, and the stored charge and depletion capacitance of the catch diode.

Although these studies cover the whole range of the noise generated from switching converters, only the PWM converters were analyzed. Since the quasi-resonant converters can further reduce converter size and weight and increase the operating switching frequency compared to PWM converters, they are preferred in some special applications. Therefore, it becomes necessary to understand their noise generation behavior which is investigated in this study. Moreover, a comparison between the quasi-resonant and PWM converters is performed to quantify the relative merits.

1.2 Statement of Problem

Switching converters are more efficient than the traditional linear converters as explained in section 1.1.1. They also have the advantages of reduced component size and weight. However, the switching converters cause serious electromagnetic interference problems, because of the fast-switching sharp-edged component waveforms from the natural switching action. In addition, these fast-switching waveforms will inevitably excite

some high-frequency parasitic oscillations from parasitic inductive and capacitive elements in the circuits. Both these characteristics could generate conducted and radiated noise that may affect the desired circuit functions and therefore should be eliminated or reduced to an acceptable magnitude.

Among these switching converters, the pulse-width modulated (PWM) switching converters, which have square switch voltage and current waveforms, are the most widely-used power converters. Recently some quasi-resonant converters (QRCs) have attracted a lot of interest among researchers in power electronics. They can further reduce the component size and weight and operate more efficiently in higher switching frequencies than the PWM converter. Moreover, their quasi-sinusoidal waveforms intuitively seem much better than the square waveforms of the PWM converters in producing less interference.

Although the previous work has pointed out the correlation between noise generation and the parasitic elements or the switching speed in the switching converters, the actual mechanisms for the noise generation and the efficient methods to suppress these noise have not been addressed. Furthermore, the relatively quantitative comparison of the noise magnitude and bandwidth at the same output power delivery between several different widely-used switching converters has not been done yet. In this thesis, the noise-generation behavior of the quasi-resonant and PWM converters will be characterized, and efficient methods to eliminate or reduce the noise are demonstrated. On the other hand, the question of whether or not quasi-resonant converters actually generate less interference than PWM converters will be investigated in a quantitative manner.

The approach used to study the interference of the switching converters in this research is depicted in Fig. 1-7. Fourier analysis of switching waveforms is used to study the conducted and radiated behavior of switching frequency harmonics. Experiments are used to study the conducted and radiated behavior of parasitic frequency interference.

In this work, Fourier analysis is first applied to several possibly noise-inducing waveforms (switch current and voltage; catch diode current and voltage) in quasi-resonant and PWM converters to get the Fourier spectral content of these waveforms. The analysis also includes several load variations of the quasi-resonant and the PWM converters. As explained in section 1.1.1, for the PWM converters there is no switching frequency change when the load changes. Hence, the Fourier spectra of the PWM converters will not change significantly when load current is changed. However, this is not the case for the quasi-resonant converters. For quasi-resonant converters, the output voltage is a function of both the load current and the switching frequency. When the output voltage is fixed in quasi-resonant converters, the load current change is obtained by changing the switching frequency. Therefore, the Fourier spectra of the quasi-resonant converter waveforms change since the switching frequencies of the quasi-resonant converters change when the load current changes.

The quantitative comparison of the noise magnitude and bandwidth between these converters with the same output power becomes possible when the relative spectral content magnitudes are known. Two types of noise bandwidth (shown in Fig. 1-8) are useful to compare and judge the relative EMI generated by these converters. The noise total bandwidth (which is the harmonic whose magnitude is one hundredth of the magnitude of the dc component) indicates how high the frequency is for which the filter must remain

Approach	Interference	Conducted	Radiated
Fourier Analysis	Switching Frequency Harmonics	Conducted Harmonics	Radiated Harmonics
Experiments	Parasitic Interference	Conducted Parasitic	Radiated Parasitic

Fig. 1-7 Research approach illustration.

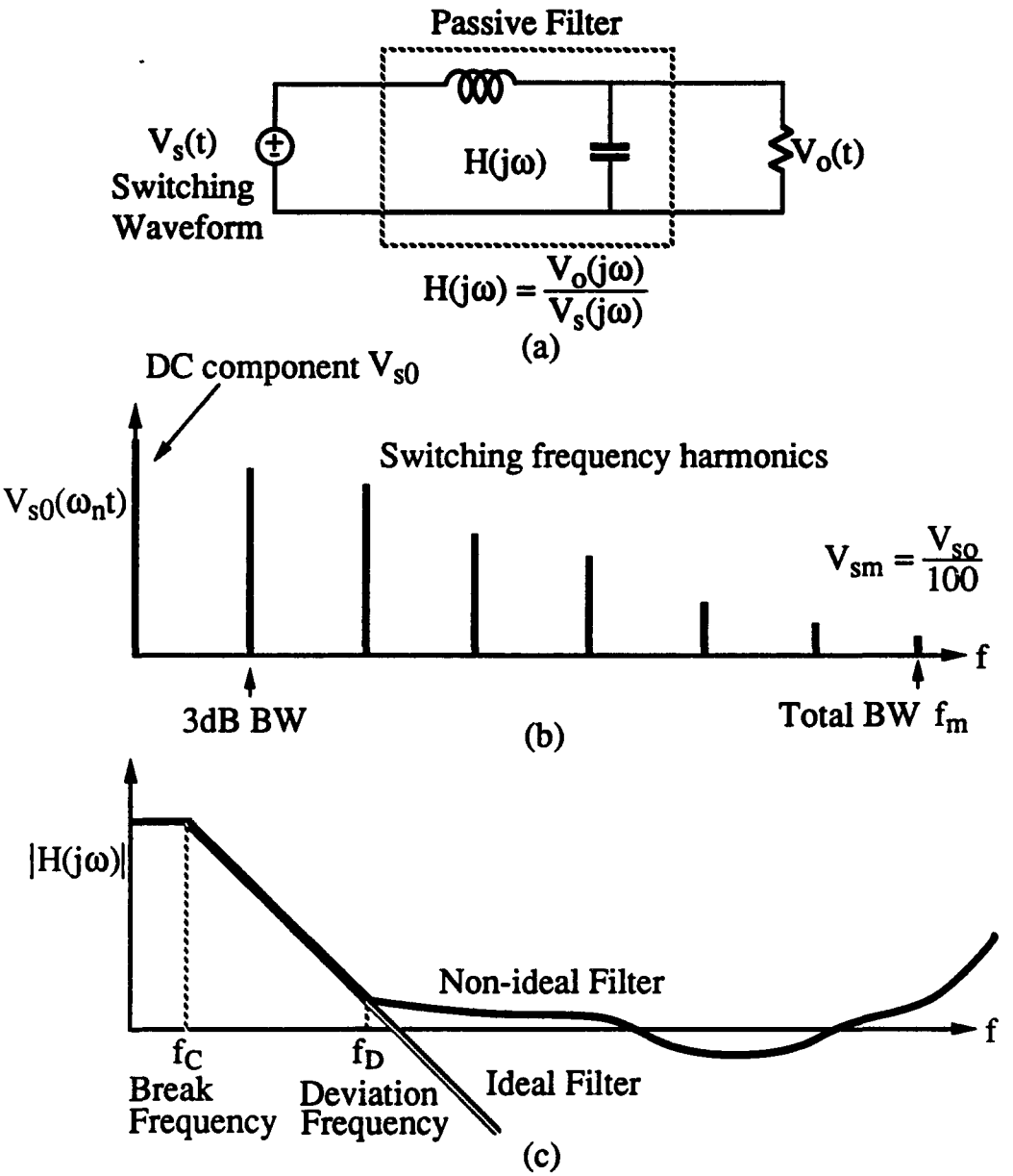

Fig. 1-8 (a) Typical filter model.
(b) Fourier spectrum of switching converter waveform.
(c) Comparison of ideal and non-ideal filter transfer characteristics.

ideal to eliminate the higher switching frequency harmonic interference. Since ideal filter components do not exist, if the filter cannot function ideally up to the total bandwidth, the higher switching frequency harmonics can cause interference problems. The noise 3dB bandwidth (which is the frequency whose magnitude is $1/\sqrt{2}$ times of the magnitude of the dc component) shows how low the cutoff frequency the filter should be to suppress the high power lower switching frequency harmonics to obtain a dc waveform.

On the other hand, an experimental approach is used to identify the parasitic oscillation interference sources of these switching converters and to find successful methods for suppressing these oscillation. First, several noise pick-up traces around the converter prototype are utilized to extract the induced signal, from which the interference sources are identified. The most significant interference source of these switching converters then can be found. The interference effect of parasitic oscillations on the input current and output voltage is explored. The methods to suppress these respective interference sources are then demonstrated.

1.3 Overview of the results

Two different approaches to compare and characterize the noise behavior of the quasi-resonant and the PWM switching converters have been employed, as mentioned in section 1.2. The ideal converter waveforms are analyzed by Fourier analysis. The experimental approach is used to identify the interference sources of these converters, to study the effect induced from these interference on input current and output voltage, and to find efficient methods to suppress these interference sources.

From Fourier analysis of ideal converter waveforms in chapter 2, the input current of quasi-resonant converters is found to have lower total bandwidth than that of the PWM converter, even though there is switching frequency change from the load current change in quasi-resonant converters. Hence low-noise quasi-resonant converters are easier to physically realize the input filter than the PWM converter, because ideal filter function is not required at high frequency in the quasi-resonant converters. However, the 3dB bandwidth of quasi-resonant converters is higher than that of the PWM converter; therefore, quasi-resonant converter will need a lower filter cutoff frequency to achieve the same ripple limitation as PWM converter.

The results from experiments in chapter 4 show that besides the natural switching frequency harmonic interference, two other higher parasitic frequency interference mechanisms are identified from the induced signal by the noise pick-up method. Both the natural switching frequency harmonics and two parasitic frequency interferences affect the output voltage and input current of these switching converters. One of the parasitic interferences from the MOSFET gate charge current spike can be alleviated by the slow switching for the MOSFET in quasi-resonant converters. The other parasitic interference from the catch diode parasitic oscillation can be reduced by adding the ferrite beads on the catch diode leads.

CHAPTER 2
FOURIER ANALYSIS OF IDEAL CONVERTER WAVEFORMS

2.0 Introduction

Fourier analysis of the converter waveforms provides a comparison between quasi-resonant and PWM switching converters operated with the same average power and switching frequency by quantifying the relative spectral content. In the following, a derivation of the spectra of the ideal converter waveforms is shown in 2.1. All the switching converters are specified to operate at the same input voltage, output voltage, and output current I_o so that the comparison is based on all the converters delivering the same output power. The switching frequency of these converters is specified to be as much the same as possible (true for nominal operating point only), such that the comparison is based on the same switching frequency harmonic spectral content. The comparison of several other operating points of each switching scheme with the same output power delivery at each operating point requires the measure definition of total and 3dB bandwidth, because there are different switching frequencies resulting from changing the output load current for the quasi-resonant converters. The result of the comparison on several operating points by this measure is shown in Table I in section 2.2. The discussion of the result from Fourier analysis is presented in 2.3. It is found that the quasi-resonant converters have a lower total bandwidth than the PWM converter of equivalent power even with variable switching frequency control, however, they have a higher 3dB bandwidth than the PWM converters.

2.1 Derivation of Fourier Spectra of Ideal Converter Waveforms

In the derivation of Fourier spectra of ideal converter waveforms, all the converters are specified to operate at the same input voltage V_g (26 V), the same output voltage V_o (13 V), and the same output current I_o such that the comparison is based on the same output power delivery. At the nominal operating point discussed in this particular section with $I_o = 4$ A, the switching frequency is specified to be 100 kHz for both quasi-resonant and PWM converters.

In the following, among all the converter waveforms, the reason for analyzing only the current waveforms is first explained in 2.1.1. A few definitions concerning the normalization are introduced in 2.1.2 to facilitate the Fourier analysis. An example of Fourier analysis procedure on ZCS-1/2 resonant inductor current then is given in 2.1.3.

2.1.1 Rationale for Current Waveform Analysis

Fourier analysis is applied to those converter waveforms that are more likely to cause significant radiated and conducted EMI. These waveforms include the switch current and voltage of the PWM converters, the resonant inductor current and the resonant capacitor voltage of the quasi-resonant converters, and the catch diode current and voltage of quasi-resonant and PWM converters. For the PWM converters, all the converter waveforms are similar square waveforms. Therefore, the analysis result of the switch current can adequately represent all of the PWM converter waveforms. On the other hand, because of the duality relationship between zero-current switching resonant inductor current (resonant capacitor voltage) and zero-voltage switching resonant capacitor voltage (resonant

inductor current), the analysis of the quasi-resonant converter resonant inductor current actually includes the analysis result of the quasi-resonant converter resonant capacitor voltage. Similarly, the duality relationship between ZCS catch diode voltage (catch diode current) and ZVS catch diode current (catch diode voltage) saves half of the analytic work. Therefore, in the following work, Fourier analysis is applied to the quasi-resonant and PWM converter current waveforms only.

2.1.2 Terminology of Normalization

A few definitions about normalization are introduced here for convenience in the Fourier analysis of the converter waveforms. Define the characteristic impedance as

$$R_o = \sqrt{L/C} = \omega_o L = 1 / \omega_o C \qquad (2\text{-}1)$$

where ω_o is the radian resonant frequency

$$\omega_o = 1 / \sqrt{LC} \qquad (2\text{-}2)$$

Second, define the normalized current J as

$$J = I / (V_g / R_o) \qquad (2\text{-}3)$$

where I is the current to be normalized and V_g / R_o is the base current of normalization. Define the normalized voltage m as

$$m = \frac{V}{V_g} \qquad (2\text{-}4)$$

where V is the voltage to be normalized and V_g is the input voltage. Define the normalized frequency γ as

$$\gamma = \pi \frac{f_o}{f_s} \qquad (2\text{-}5)$$

where f_o is the resonant frequency and f_s is the switching frequency.

2.1.3 Fourier Analysis Example of ZCS-1/2 Resonant Inductor Current

In the following example, the quasi-resonant converter waveform is first normalized so that a general result of the Fourier spectral content magnitude is obtained independent of the component values and power levels. Fourier series expansion of the converter waveform then is performed in a piecewise fashion because the converter waveforms all consist of piecewise waveforms. The final actual result will need to be denormalized by multiplying the normalization factor of the base current.

Consider the resonant inductor current (equal to the switch current) of the half-wave zero-current switching quasi-resonant converter in Fig. 1-3. The piecewise resonant inductor current is normalized with respect to the input voltage V_g and the characteristic impedance of the resonant tank R_0, where R_0 is equal to $\sqrt{L_r/C_r}$; i.e., $j_{Lr} = i_{Lr} / (V_g/R_0)$. There are three expressions for the three piecewise conduction intervals during a switching period:

$$\begin{aligned} j_{Lr}(t) &= \omega_0 t && 0 \le t \le t_1 \\ j_{Lr}(t) &= \frac{1}{2} + \sin \omega_0 (t-t_1) && t_1 \le t \le t_2 \\ j_{Lr}(t) &= 0 && t_2 \le t \le T_s \end{aligned} \qquad (2\text{-}6)$$

The time intervals t_1 and t_2 can be found from the interval boundary conditions, and ω_0 is the radian frequency of the tank [1-3]. The Fourier series expansion of $j_{Lr}(t)$ is :

$$j_{Lr}(t) = \sum_{n=-\infty}^{\infty} F_n e^{jn\omega_s t} \qquad (2\text{-}7)$$

where ω_s is the radian switching frequency. The complex Fourier coefficient for each harmonic is :

$$F_n = \frac{1}{T_s}\int_0^{T_s} j_{Lr}(t)e^{-n\omega_s t}dt \tag{2-8}$$

, which can be integrated in a piecewise fashion,

$$F_n = \frac{1}{T_s}\left[\int_0^{t_1} (\omega_0 t)e^{-n\omega_s t}dt + \int_{t_1}^{t_2} \left(\frac{1}{2} + \sin(\omega_0(t-t_1)\right)e^{-n\omega_s t}dt\right] \tag{2-9}$$

This integral can be solved by means of integration by parts, and the result is :

$$F_n = \frac{1}{T_s}\left\{ j\frac{t_1\omega_0 e^{-jn\omega_s t_1}}{n\omega_s} + \frac{\omega_0(e^{-jn\omega_s t_1}-1)}{(n\omega_s)^2} + j\frac{e^{-jn\omega_s t_2}-e^{-jn\omega_s t_1}}{2n\omega_s} + \frac{(n\omega_s)^2}{(n\omega_s)^2 - \omega_0^2}\left[e^{-jn\omega_s t_2}\left(\frac{\omega_0\cos\omega_0(t_2-t_1)}{(n\omega_s)^2} + j\frac{\sin\omega_0(t_2-t_1)}{n\omega_s}\right) - \frac{\omega_0}{(n\omega_s)^2}e^{-jn\omega_s t_1}\right]\right\} \tag{2-10}$$

The magnitude of the spectral content can be computed:

$$|F_n| = \sqrt{R_e^2(F_n) + I_m^2(F_n)} = |j_{Lr}(n\omega_s t)| \tag{2-11}$$

The actual current magnitude i_{Lr} can be obtained by multiplication of (6) by the base current V_g / R_o. This procedure can be applied to all of the converter waveforms. When the magnitude of each frequency harmonic is known, the Fourier spectrum can be plotted. Figure 2-1 shows the spectrum of the inductor current of half-wave zero-current switching quasi-resonant converter. The same procedure can be applied to find the inductor current (equal to input current) spectra of ZCS-1, ZVS-1/2, and ZVS-1 quasi-resonant converters and the switch current spectrum of PWM converter (Appendix A). These spectra are shown from Fig. 2-2 to Fig. 2-5. The catch diode current spectra of quasi-resonant converters (ZCS-1/2, ZCS-1, ZVS-1/2, ZVS-1) are shown in Appendix B.

Note that the inductor current is equal to the switch current for both the half and full wave zero-current switching quasi-resonant converters, but not for the half and full wave

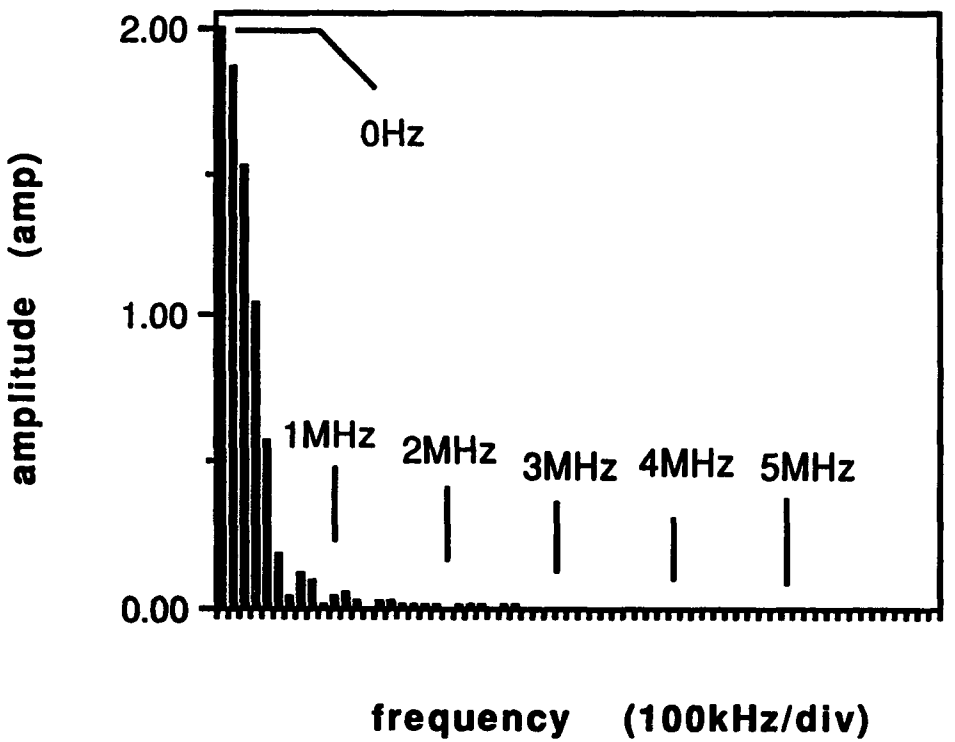

Fig. 2-1 ZCS-1/2 QRC input current Fourier spectrum (output resistance 3.25 Ω).

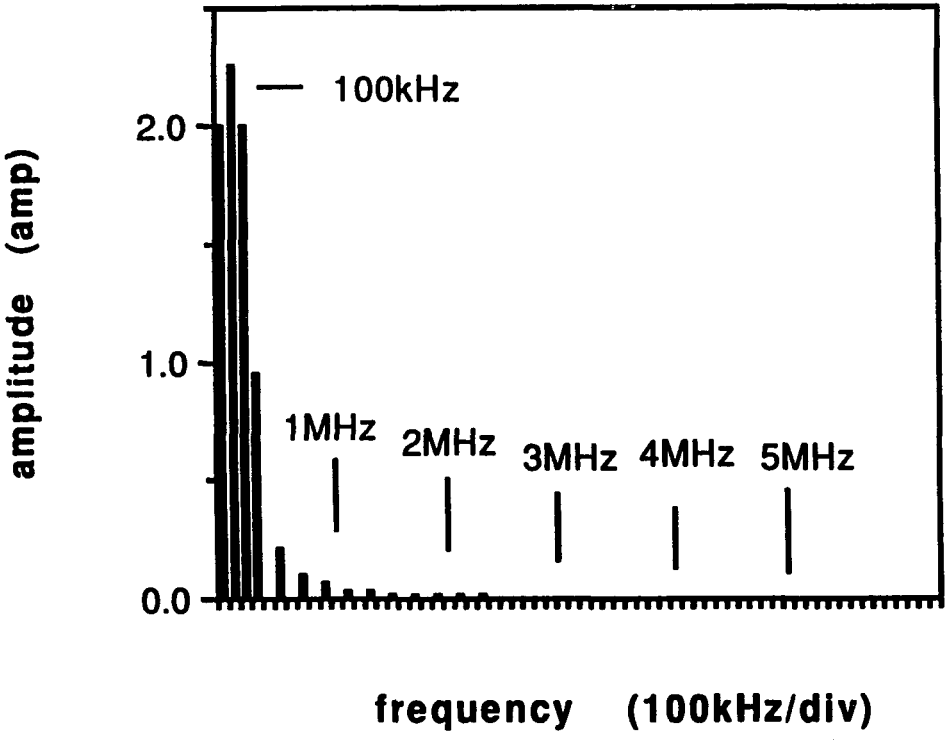

Fig. 2-2 ZCS-1 QRC input current Fourier spectrum (output resistance 3.25 Ω).

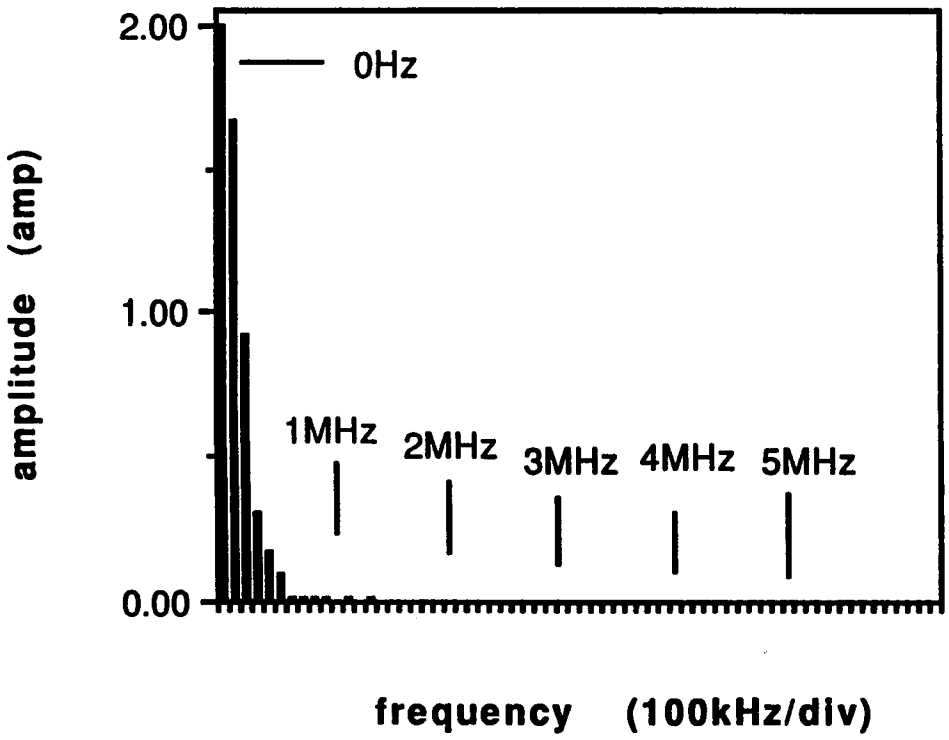

Fig. 2-3 ZVS-1/2 QRC input current Fourier spectrum (output resistance 3.25 Ω).

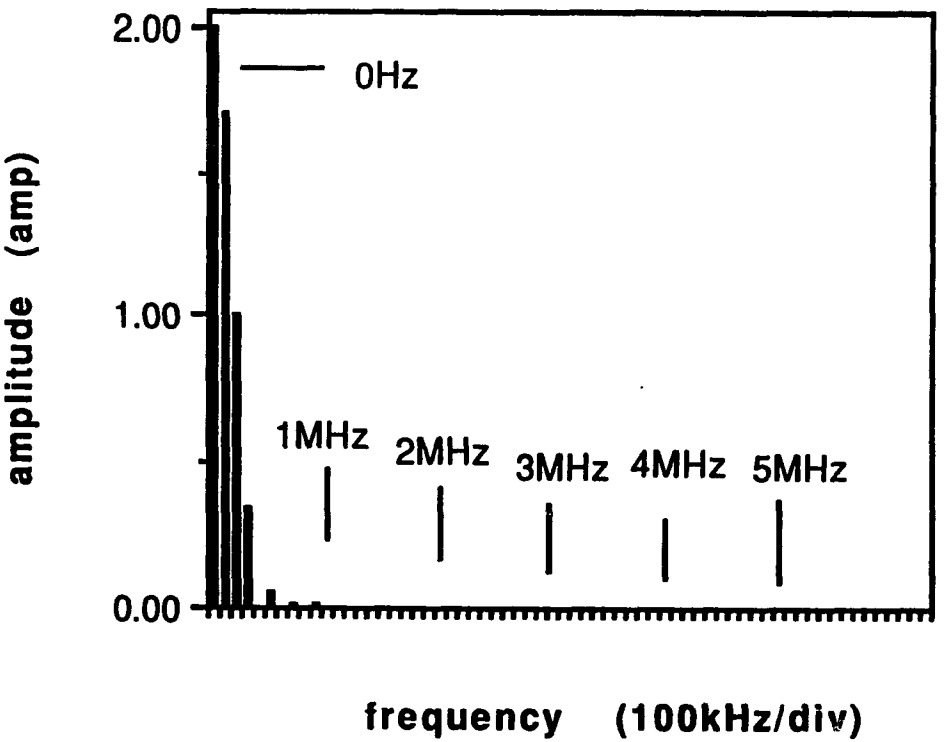

Fig. 2-4 ZVS-1 QRC input current Fourier spectrum (output resistance 3.25 Ω).

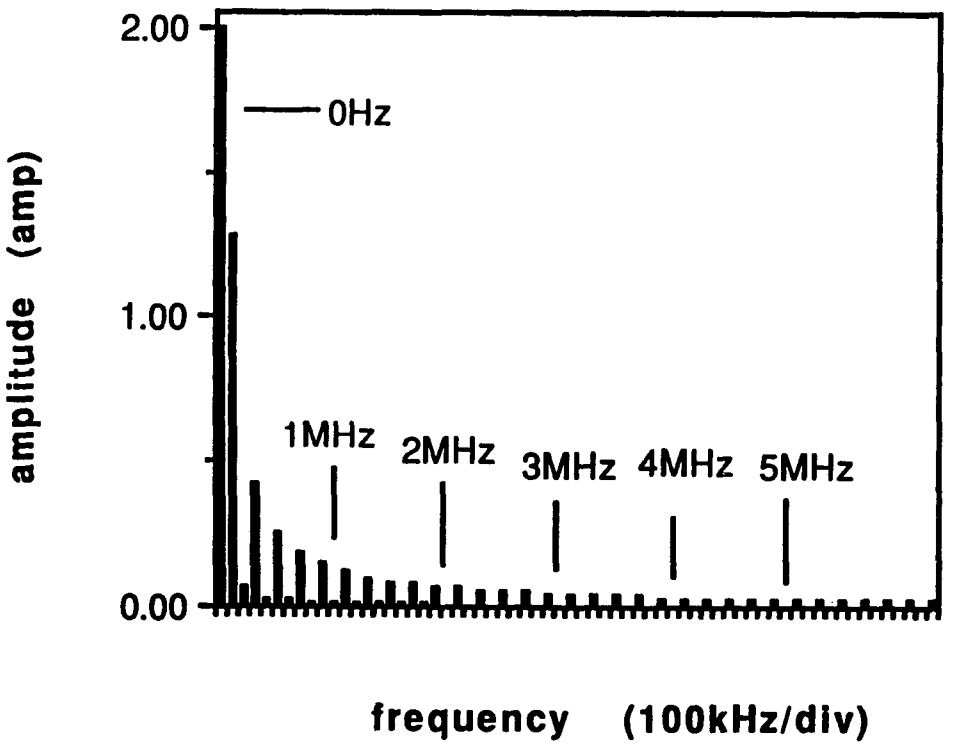

Fig. 2-5 PWM converter input current Fourier spectrum (output resistance 3.25 Ω).

zero-voltage switching quasi-resonant converters. The transistor current and mode diode current waveforms (Figs. 2-6, 2-7) of ZVS-QRC have sharp edges and are different from the quasi-sinusoidal inductor current. Although the transistor current and mode diode current will not affect conducted interference, they may contribute to radiated interference. The ZVS-1/2 transistor and mode diode current Fourier spectra and the ZVS-1 transistor current spectrum are shown in Appendix B. The spectrua of quasi-resonant converter resonant inductor waveforms contain odd and even harmonics. For ideal square PWM converter waveform, the spectrum should contain odd harmonics only. The reason the spectrum in Fig. 2-5 has any even harmonics at all is that the square waveform has been more practically superimposed a 10% current ripple.

2.2 Comparison of Fourier Spectra

Since the Fourier spectra of these five switching converter input current waveforms are known, the EMI generation of the quasi-resonant and PWM converters can be compared on the basis of spectral harmonic frequency content. The Fourier spectrum of the PWM switch current (input current) is shown in Fig. 2-5. Compared to the input current spectra of quasi-resonant converters (ZCS-1/2, ZCS-1, ZVS-1/2, ZVS-1) from Fig. 2-1 to Fig. 2-4, the PWM converter is seen to have a wider bandwidth for its input current. The spectra result from the same Fourier analysis procedure for the catch diode current of these five switching converters is shown in Appendix B. The PWM converter has wider catch diode current waveform spectral bandwidth frequency than the quasi-resonant converters also.

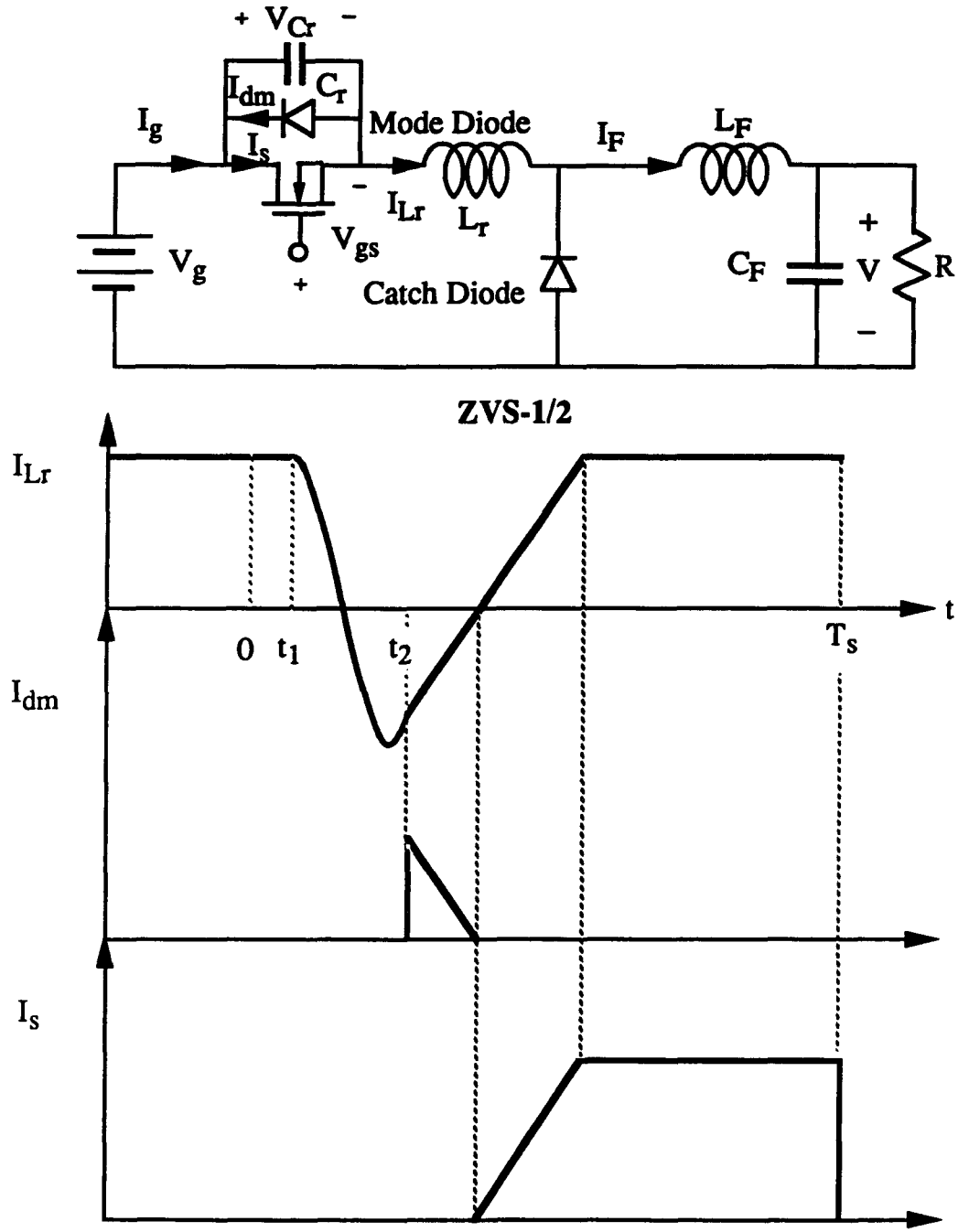

Fig. 2-6 ZVS-1/2 QRC circuit and the waveforms of I_{Lr}, I_{dm}, and I_s.

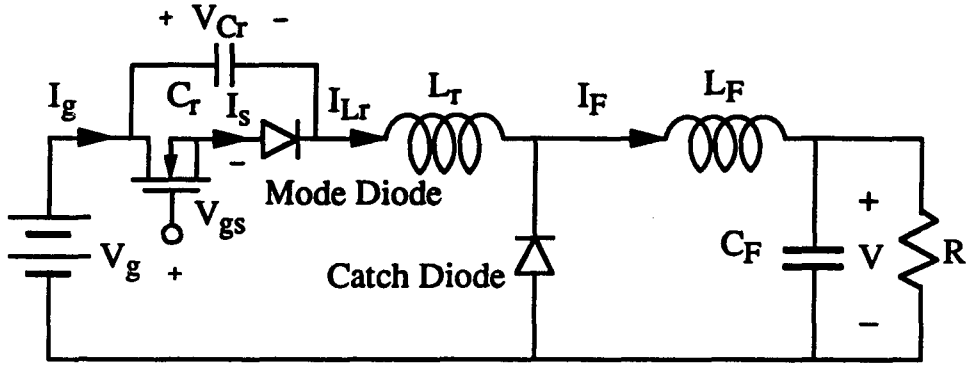

ZVS- 1

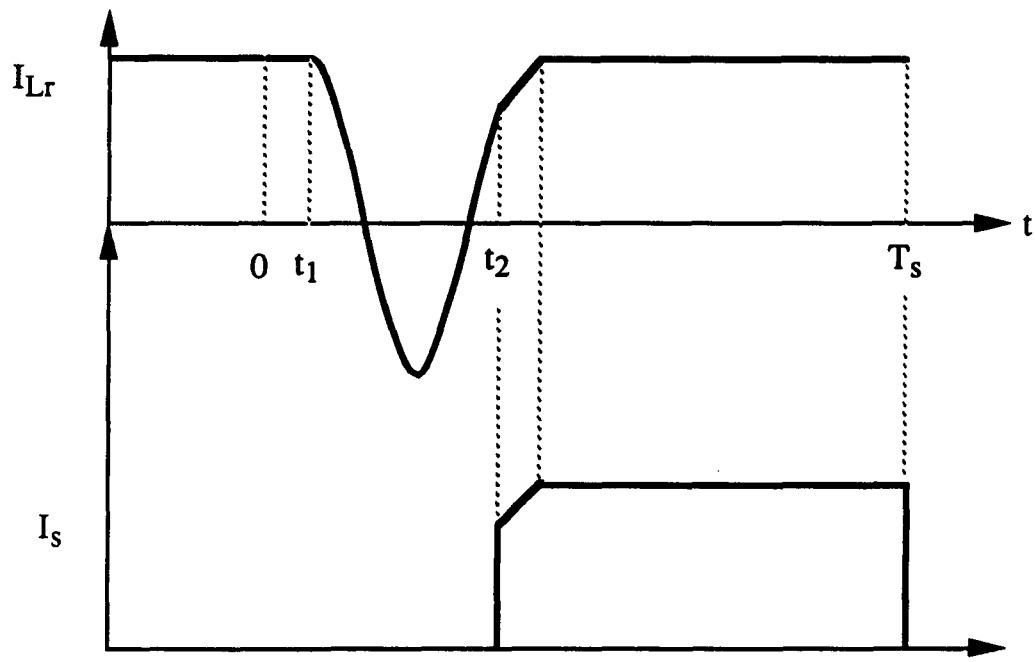

Fig. 2-7 ZVS-1 QRC circuit and the waveforms of I_{Lr}, and I_s.

However, when considering how output load current change affects the spectra, quasi-resonant converters seem more likely to have bigger spectral changes than the PWM converters because of their variable switching frequency control. For the PWM converters, the switching frequency is not changed, because the output voltage is controlled by the duty cycle and the output load current is almost independent of the switching frequency. It is therefore interesting to know how the spectra of the quasi-resonant converters is affected by load current change.

Two other operating points are evaluated to obtain the answer. The load current is changed from 4 A up to 5.4 A and down to 2.6 A. For the PWM converter, the ZCS-1 and the ZVS-1 converters, the switching frequency stays approximately the same, because the switching frequency of full wave quasi-resonant converters is nearly load-insensitive. The new switching frequencies for ZCS-1/2 and ZVS-1/2 are found to be 142 kHz and 85.8 kHz respectively for the case I_o = 5.4 A , and 79.5 kHz and 117 kHz respectively for the case I_o = 2.6 A [1-3].

Since the switching frequencies are not equal in the presence of load current variation, the comparison cannot be based on the relative switching frequency harmonic spectral content. To obtain a general quantitative comparison, two figures of merit are introduced and defined to evaluate various spectra no matter what the converter switching frequency is. The " 3dB bandwidth " (BW_3) is defined by

$$|I_n(BW_3)| \leq \frac{I_0}{\sqrt{2}} \tag{2-12}$$

and the " total bandwidth " (BW_T) is defined by

$$|I_n(BW_T)| \leq \frac{I_0}{100} \tag{2-13}$$

By adoption of the measure defined above, the 3dB and total bandwidth of these five switching schemes evaluated are shown in Table-I for all the three operating points (spectra of these current waveforms at the other different operating points from nominal point are shown in Appendix B).

2.3 Discussion of the Results from the Fourier Analysis

In the following, the observations about input current I_{in} of these converters from Table I is discussed first. Then the results for catch diode current of these converters from I_d column of Table I are discussed. Beyond the result can be observed in Table I, the comparison of conducted and radiated interference behavior of these converters is addressed. An intuitive insight of why the spectral bandwidth of the ZVS quasi-resonant converters increases when the load changes is explained. Concluding this discussion, ZVS-1 is found to be the best choice for generating less interference.

From input current column of Table I, the switching frequency change from the load current change is seen to increase the total bandwidth of quasi-resonant converter input current. Nevertheless, each of the input currents I_{in} (equal to the inductor current) of quasi-resonant converters still has lower total bandwidth than that of the PWM converter. Hence, quasi-resonant converters should have less conducted harmonic interference at the input than does the equivalent PWM converter. However, the 3dB-bandwidth of the quasi-resonant converters is higher than that of the PWM converter. In other words, the spectra of the quasi-resonant converters are more "square-like" in the frequency domain, i.e., contain more power in the lower harmonics, than the PWM converter. Hence, quasi-resonant converters will be easier to filter at high frequencies, i.e., ideal filter performance

Table I The 3dB and total bandwidth of five switching schemes at three different operating points (unit: MHz).

		I_{in}		I_d	
	f_s	BW_3	BW_T	BW_3	BW_T
	I_o = 5.4 A				
PWM	0.1	0.1	6.4	0.1	6.4
ZCS-1/2	0.14	0.14	3.08	0.14	5.18
ZCS-1	0.1	0.2	3.4	0.1	4.0
ZVS-1/2	0.086	0.086	3.44	0.086	3.44
ZVS-1	0.1	0.1	0.6	0.1	0.6
	I_o = 4 A				
PWM	0.1	0.1	6.4	0.1	6.4
ZCS-1/2	0.1	0.2	1.6	0.1	6.1
ZCS-1	0.1	0.2	1.6	0.1	5.7
ZVS-1/2	0.1	0.1	0.6	0.1	0.6
ZVS-1	0.1	0.1	0.6	0.1	0.6
	I_o = 2.6 A				
PWM	0.1	0.1	6.4	0.1	6.4
ZCS-1/2	0.08	0.24	1.76	0.08	4.88
ZCS-1	0.1	0.3	1.9	0.1	5.3
ZVS-1/2	0.12	0.12	0.96	0.12	0.96
ZVS-1	0.1	0.1	0.8	0.1	0.8

at high frequencies is not required, but a lower filter cutoff frequency is needed to achieve the same ripple magnitude as a PWM converter for lower order harmonics.

From the catch diode current I_d column of Table I, the zero-current switching quasi-resonant converter has a square catch diode current waveform, which is known from Table I to have a wide spectrum, but the zero-voltage switching quasi-resonant converter has a quasi-sinusoidal catch diode current waveform with a narrow spectrum. Since the ZVS converter is the topological dual of the ZCS converter, if the radiated interference coupling mechanism is magnetic, the ZVS converter is better because of the quasi-sinusoidal catch diode current, and if the mechanism is electric, the ZCS converter is better because of the quasi-sinusoidal catch diode voltage. The multi-resonant converter (MRC) has a ZVS-like switch waveform and a ZCS-like catch diode waveform, hence the EMI generation behavior of the MRC can be predicted by combining the ZVS switch waveform and the ZCS catch diode waveform.

As discussed earlier in this section, from the standpoint of conducted interference, the quasi-resonant converters are better than the PWM converter (Table I), especially the input current. But from the standpoint of radiated interference, both the quasi-resonant and the PWM converters have wide bandwidth spectra (ZCS has square diode current and ZVS has quasi-square switch current as in Figs. 2-6, 2-7). Hence, the intuition that quasi-resonant converter is better than the PWM converter in generating less EMI caused by switching frequency harmonic interference is not necessarily correct from the standpoint of radiated interference (the comparison of the interference from parasitic oscillations of these converters are addressed in section IV).

Some of the reasons why the spectral bandwidth of the ZVS quasi-resonant converters increases when the load changes can be explained quite intuitively. The examination of the resonant inductor current total bandwidth after the load change indicates that variable switching frequency control changes the total bandwidth of the ZVS quasi-resonant converters. The half wave quasi-resonant converters are dependent on load current. For the ZVS-1/2, increasing the output load current will increase the resonant amplitude while decreasing the resonant interval. This changes the resonant inductor current waveform from quasi-sinusoidal to a more triangular waveform which will have a higher total bandwidth than that of the quasi-sinusoidal waveform. For the ZVS-1 converter, increasing the output load current will increase both the resonant amplitude and the resonant interval. There is only a little change in the resonant inductor current waveform and therefore the total bandwidth does not change significantly. It is not easy to find the intuitive reason for the ZCS quasi-resonant converters, however. For the ZCS-1/2 and ZCS-1, increasing or decreasing the output load current from the nominal value of 4 A will increase the total bandwidth of resonant inductor current but will decrease the total bandwidth of the catch diode current.

Concluding all the observation discussed before, from Table I, the ZVS–1 quasi-resonant converter is found to be the best of the five converters analyzed because: 1) both the input current and catch diode current total bandwidth of ZVS-1 are lower than that of the others, 2) the variant switching frequency almost does not change either the input current or the catch diode current total bandwidth at all, 3) there is no switching frequency change from the load current change, which makes the control easy because of the fixed filter bandwidth instead of some filter bandwidth range otherwise. Notice that, like ZVS-1, the switching frequency of ZCS-1 stays the same when the output load current changes,

however, the total bandwidth of the input current and catch diode current changes significantly, which is worse than that of ZVS-1.

CHAPTER 3
DESIGN AND CONSTRUCTION OF THE EXPERIMENTAL PROTOTYPE

In the previous chapter, the theoretical Fourier analysis on ideal converter waveforms has been done which reveals the effect of switching frequency harmonics. However, as been pointed out in 1.1.3, some higher parasitic frequency noise are also found in switching converters. To find the actual noise mechanism, an experimental approach is best. In addition, efficient methods to reduce the interference effect are investigated experimentally in this study. Therefore, a good prototype circuit is built for experiment. In the following, the prototype circuit construction and design consideration is pointed out in section 3.1. The design constraints for these converters being examined are given in section 3.2.

3.1 Prototype Circuit Construction and Design Consideration

The prototype circuit construction and layout is considered to allow six different switching converter configurations on the same circuit board, and to isolate the relationship between noise generation and the converter topology. Hence, the fewest components possible are changed from one topology to the other (as seen in Fig. 3-1, only the switch part of the converters is changed), and the components of the same converter function (e.g., resonant inductors) in the circuit are kept in the same physical position in the circuit layout (Fig. 3-2(a) shows the layout of these converters). In addition, the resonant frequency of the quasi-resonant converters is kept as constant as possible to make the comparison more meaningful.

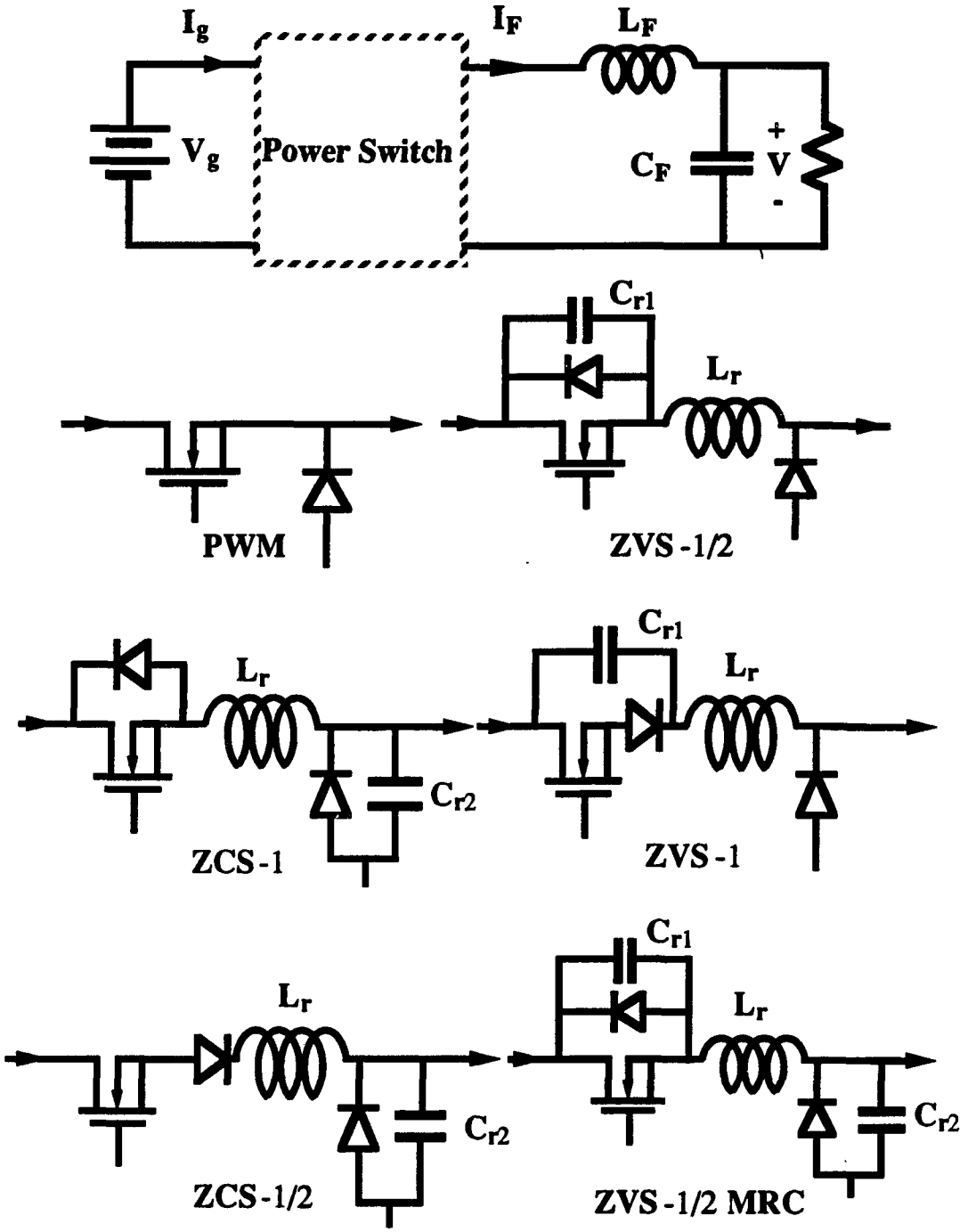

Fig. 3-1 Buck converter with six different power switch schemes.

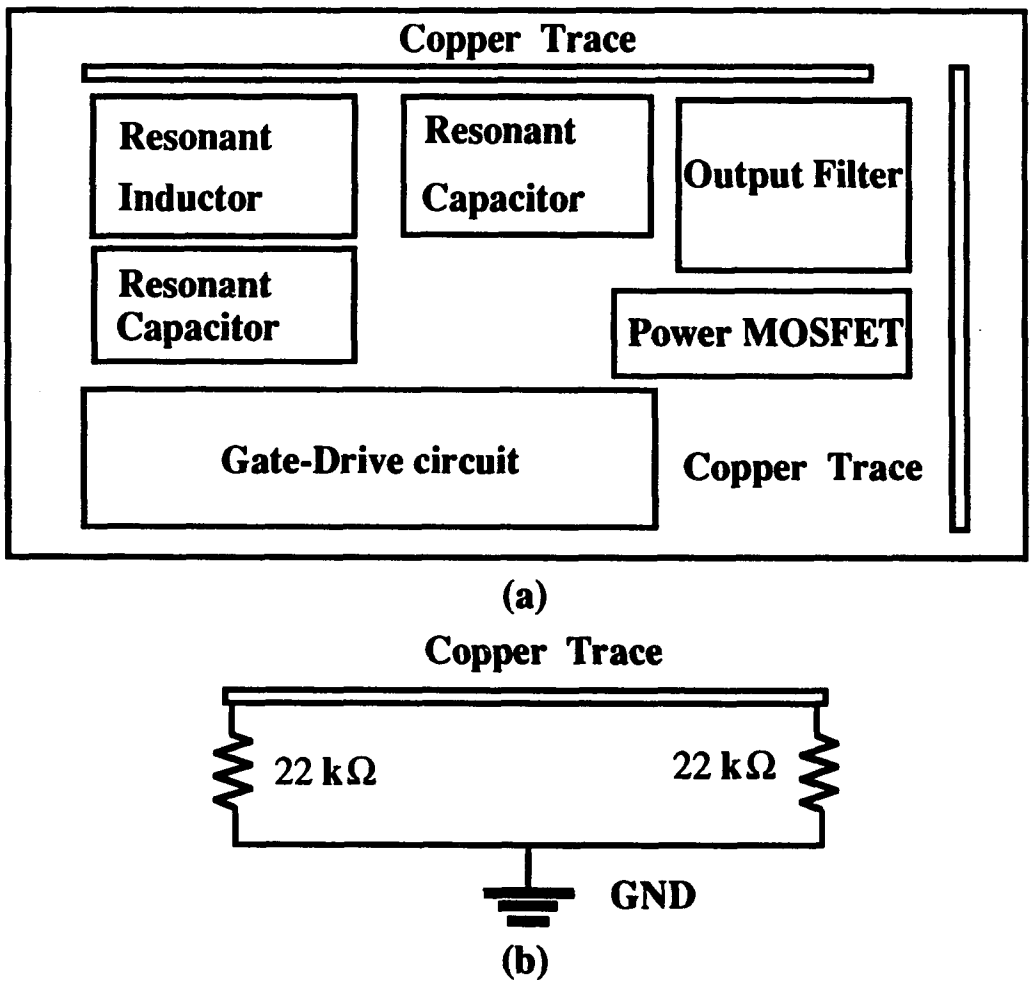

Fig. 3-2 (a) Prototype circuit layout.
(b) Radiated signal pick-up setting.

3.2 Prototype Circuit Design Constraints

There are two design constraints for these converters in the construction of the prototype circuit. First, as in the Fourier analysis in chapter 2, six switching converters (shown in Fig. 3-1) are operated nominally at the same input voltage V_g (26 V), output voltage V_o (13 V), output current I_o (4 A) and switching frequency f_s (100 kHz). This is the most important design constraint so that the comparison are based on the same output power delivery from each converter and the same switching harmonic frequencies. Second, the design consideration mentioned in 3.1, that the resonant frequency of the quasi-resonant converters is kept the same as much as possible, constrains the values of the resonant components. Therefore, from the first design constraint, the conversion ratio $M = V_o/V_g = 1/2$ is chosen for all the quasi-resonant converters. From the second design constraint, the switching frequency is 100 kHz for all converters in this particular nominal operating point.

For quasi-resonant converters, the output voltage (hence conversion ratio) is a function of both the switching frequency and the output current. In the following, the formula of the conversion ratio for these quasi-resonant converetrs are given to demonstrate the procedure to obtain the values of the resonant components [1-3]. First, define the normalized average resonant capacitor voltage as:

$$\langle m_{Cr} \rangle = \langle V_{Cr} \rangle / V_g \tag{3-1}$$

the normalized resonant inductor current as:

$$\langle j_{Lr} \rangle = \frac{\langle I_{Lr} \rangle}{V_g / R_o} \tag{3-2}$$

the normalized frequency:

$$\gamma = \pi f_o / f_s \tag{3-3}$$

and the normalized output load current:

$$J = \frac{I}{V_g / R_o} \tag{3-3}$$

where I is the output load current. For convenience, denote J_C for ZCS-QRC and J_V for ZVS-QRC. For ZCS-1/2,

$$M = \langle m_{Cr} \rangle = \frac{1}{2\gamma} K_{1/2}(J_C) \tag{3-4}$$

$$K_{1/2}(J_C) = \frac{1}{2} J_C + \pi + \sin^{-1}(J_C) + \frac{1}{J_C}(1 + \sqrt{1 - J_C^2}) \tag{3-5}$$

For ZCS-1,

$$M = \langle m_{Cr} \rangle = \frac{1}{2\gamma} K_1(J_C) \tag{3-6}$$

$$K_1(J_C) = \frac{1}{2} J_C + 2\pi - \sin^{-1}(J_C) + \frac{1}{J_C}(1 - \sqrt{1 - J_C^2}) \tag{3-7}$$

For ZVS-1/2,

$$M = 1 - \langle m_{Cr} \rangle = 1 - \frac{1}{2\gamma} K_{1/2}\left(\frac{1}{J_V}\right) \tag{3-8}$$

$$K_{1/2}\left(\frac{1}{J_V}\right) = \frac{1}{2J_V} + \pi + \sin^{-1}\left(\frac{1}{J_V}\right) + J_V + \sqrt{J_V^2 - 1} \tag{3-9}$$

For ZVS-1,

$$M = 1 - \langle m_{Cr} \rangle = 1 - \frac{1}{2\gamma} K_1\left(\frac{1}{J_V}\right) \tag{3-10}$$

$$K_1\left(\frac{1}{J_V}\right) = \frac{1}{2J_V} + 2\pi - \sin^{-1}\left(\frac{1}{J_V}\right) + J_V - \sqrt{J_V^2 - 1} \tag{3-11}$$

If the input voltage, output voltage, output current, switching frequency, and resonant frequency are kept the same for these converters, there are too many boundary conditions (five) to satisfy four set of equations of each quasi-resonant converters at the same time.

Therefore, the reasonable choice is let the resonant frequency be a free variable. It is desired that half wave converters are operated at one resonant frequency and full wave converters at another, which is the third design constraint. Notice that the conversion ratio is equal to 1/2 (M = 1/2) for all quasi-resonant converters, which sets Eq. (3-4) equal to Eq. (3-8) and Eq. (3-6) equal to Eq. (3-10). The third constraint then gives that Eq. (3-5) equals Eq. (3-9) and Eq. (3-7) equals Eq. (3-11). These computations show that J_C equals 1/2 and J_V equals 2. At nominal operating point (f_s = 100 kHz), half wave converter resonant frequency is found to be 243 kHz, and full wave converter resonant frequency is 200 kHz. The values of resonant components according to these constrains now can be calculated from J (J_C or J_V) and f_0 of each quasi-resonant converter [1-3].

The values for the multi-resonant converter (MRC) are evaluated by the method presented in [7-8]. The minimum capacitor ratio C_N chosen is equal to two. The normalized resistance R_N is chosen to be 0.5. With the conversion ratio M known as 0.5, and C_N and R_N specified, the normalized frequency f_N equals to 0.8 can be read from the output plane provided by [7-8]. The MRC in this particular study is designed for the operation with the catch diode voltage going to zero first. Since f_N and R_N are found, the resonant component values can be calculated. The values obtained are shown in Table II.

The output filter is the same for all converters. To determine the values of filter inductance and capacitance, two constraints are chosen: 1) the output current ripple is limited to 10 % of the output current, 2) the quality factor Q of the filter is chosen to be 1.5 to limit the peaking in the frequency response. All the values of the filter and the resonant inductance and capacitance are listed in Table II.

Table II Summary of filter and resonant inductance and capacitance.

Type	L(filter)	C(filter)	L(resonant)	C_1(resonant)	C_2(resonant)
PWM	81.25 uH	17.31 uF			
ZCS-QRC 1/2	81.25 uH	17.31 uF	2.125 uH		.2012 uF
ZCS-QRC 1	81.25 uH	17.31 uF	2.589 uH		.2451 uF
ZVS-QRC 1/2	81.25 uH	17.31 uF	8.5 uH	.0503 uF	
ZVS-QRC 1	81.25 uH	17.31 uF	10.35 uH	.0613 uF	
ZVS-MRC 1/2	81.25 uH	17.31 uF	8.379 uH	.1983 uF	.3972 uF

CHAPTER 4
EXPERIMENTAL RESULTS

4.0 Introduction

Besides the inevitable harmonic frequency interference generated by switching, two other high frequency interference caused by excitation of parasitic elements have been found, which significantly influence both the conducted and radiated emissions. One oscillation happens when the catch diode turns on (ZCS), or off (ZVS), the other effect arises from the exponential gate charge current waveform when the MOSFET turns on or off. The effects of these sources on the radiated-field-induced waveforms, on the output voltage, and on the input current are discussed in the following sections. Approaches for reducing the effect of these parasitic frequencies on the output and input waveforms are given. It is found that the effect of gate charge current is greater than that from the catch diode turn-on or turn-off.

4.1 Radiated Interference

In this section, experimental results show the parasitic interference effect on several converter waveforms. The experimental setting for picking up the radiated interference signal is demonstrated. By examining the picked-up signal, the parasitic interference sources are identified.

Spurious oscillations have been found in converter waveforms. For zero-current switching converters, the interference on the experimental waveforms is generated by the

parasitic oscillation of the catch diode junction capacitor and the catch diode leads when the catch diode turns on. The length of the diode leads affects the value of the parasitic inductance and changes the oscillation frequency (Figs. 4-1, 4-2). For zero-voltage switching converters, the interference on the experimental waveforms is also generated from the parasitic oscillation of the catch diode junction capacitor and the catch diode leads. However, it occurs when the catch diode turns off and the catch diode lead length does not appear to significantly affect the oscillation frequency (Figs. 4-3, 4-4).

In order to find the interference sources in these switching converter circuits and then to find efficient methods suppressing these sources, the following experimental setting is employed. To determine the actual radiated noise waveforms picked up by electrical coupling to the circuits surrounding the converter, two copper traces of 8.3 cm long and 0.17 cm wide terminated by a 22 kΩ resistor to ground on both sides are added to the circuit in different physical orientations (Fig. 3-2(b)) [9].

The comparison between the picked-up radiated noise waveforms and the quasi-resonant converter waveforms allows identification of the respective noise sources contributing to the actual noise waveforms. For example, a typical picked-up radiated signal (experimental waveforms will be shown later) from the copper trace in ZCS-1/2 and ZVS-1/2 (Figs. 4-5, 4-6) is divided into three portions for indicating different interference sources causing the respective picked-up noise. These interference sources are the gate charge current spikes, the catch diode parasitic oscillation, and the electrostatic effect of the switching frequency harmonics. The experimental proof for ZCS-1/2 and ZVS-1/2 waveforms are shown in Figs. 4-7, 4-8. In zero-current switching converters, the parasitic oscillation from catch diode occurs when the catch diode turns on (Fig. 4-7). In zero-

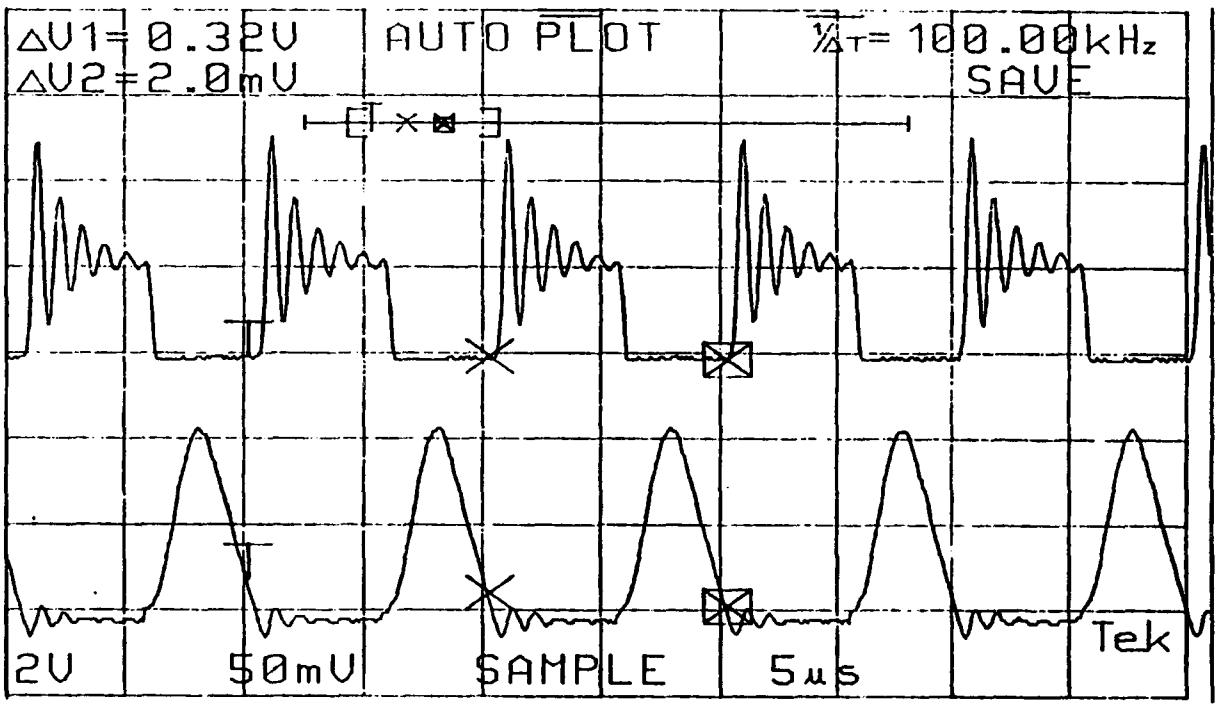

Fig. 4-1 ZCS-1/2 diode current (top, 2.5 A/ div) and diode voltage (bottom, 20 V/ div) waveforms observed on oscilloscope with a short diode lead.

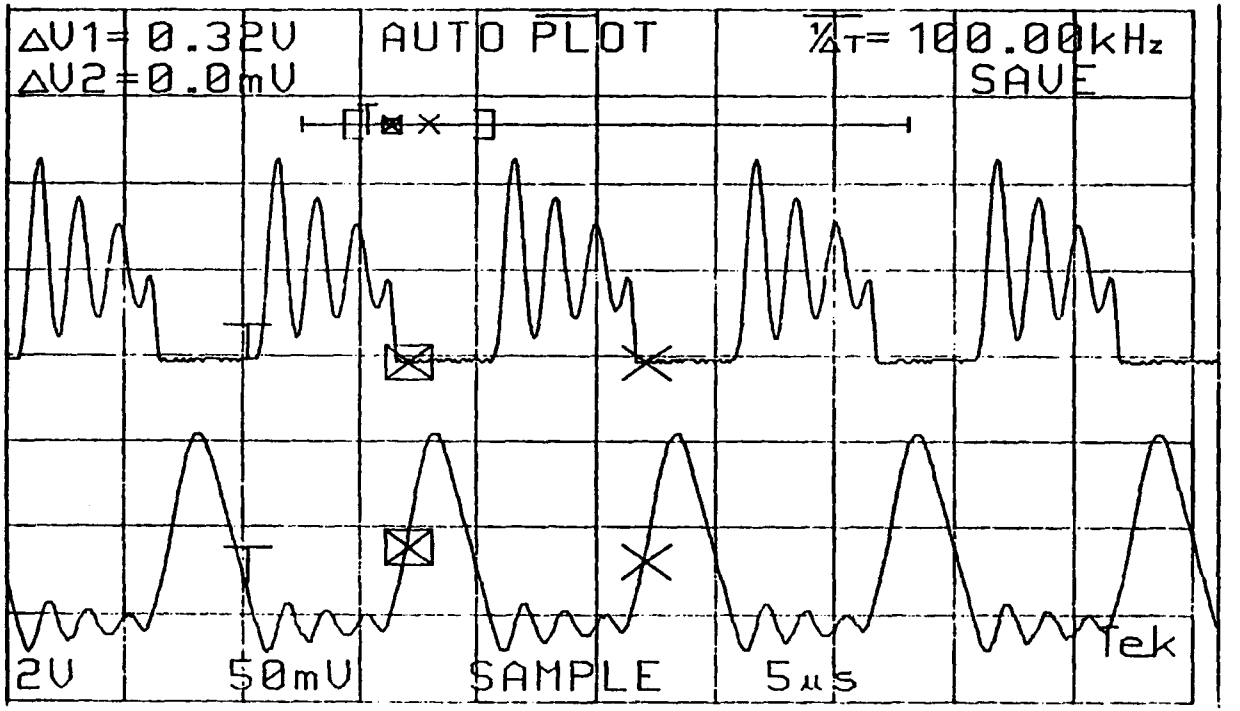

Fig. 4-2 ZCS-1/2 diode current (top, 2.5 A/ div) and diode voltage (bottom, 20 V/ div) waveforms observed on oscilloscope with a long diode lead.

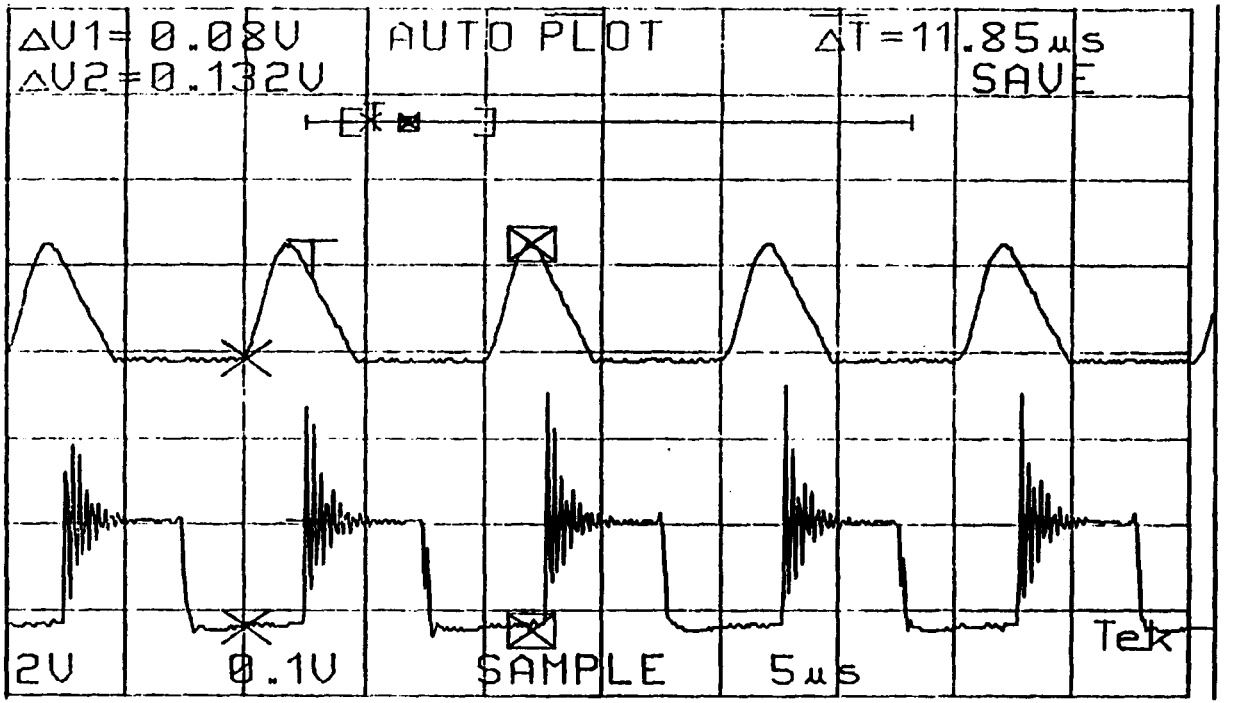

Fig. 4-3 ZVS-1/2 diode current (top, 5 A/ div) and diode voltage (bottom, 20 V/ div) waveforms observed on oscilloscope with a short diode lead.

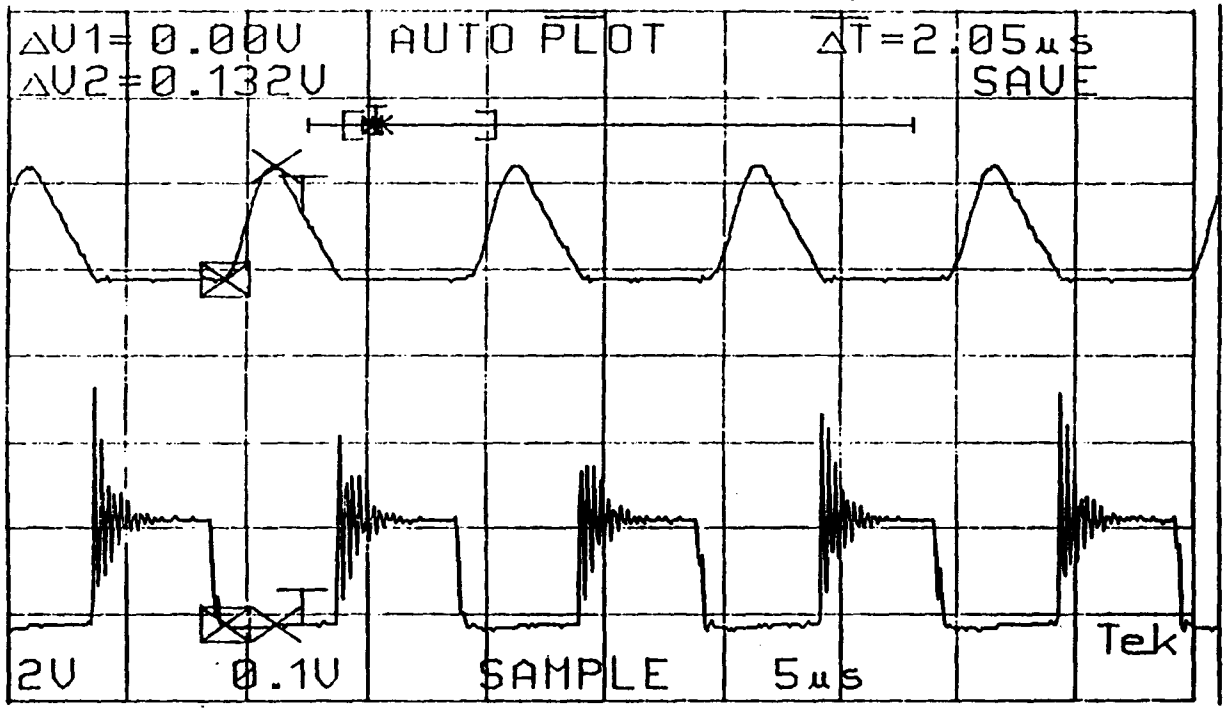

Fig. 4-4 ZVS-1/2 diode current (top, 5 A/ div) and diode voltage (bottom, 20 V/ div) waveforms observed on oscilloscope with a short diode lead.

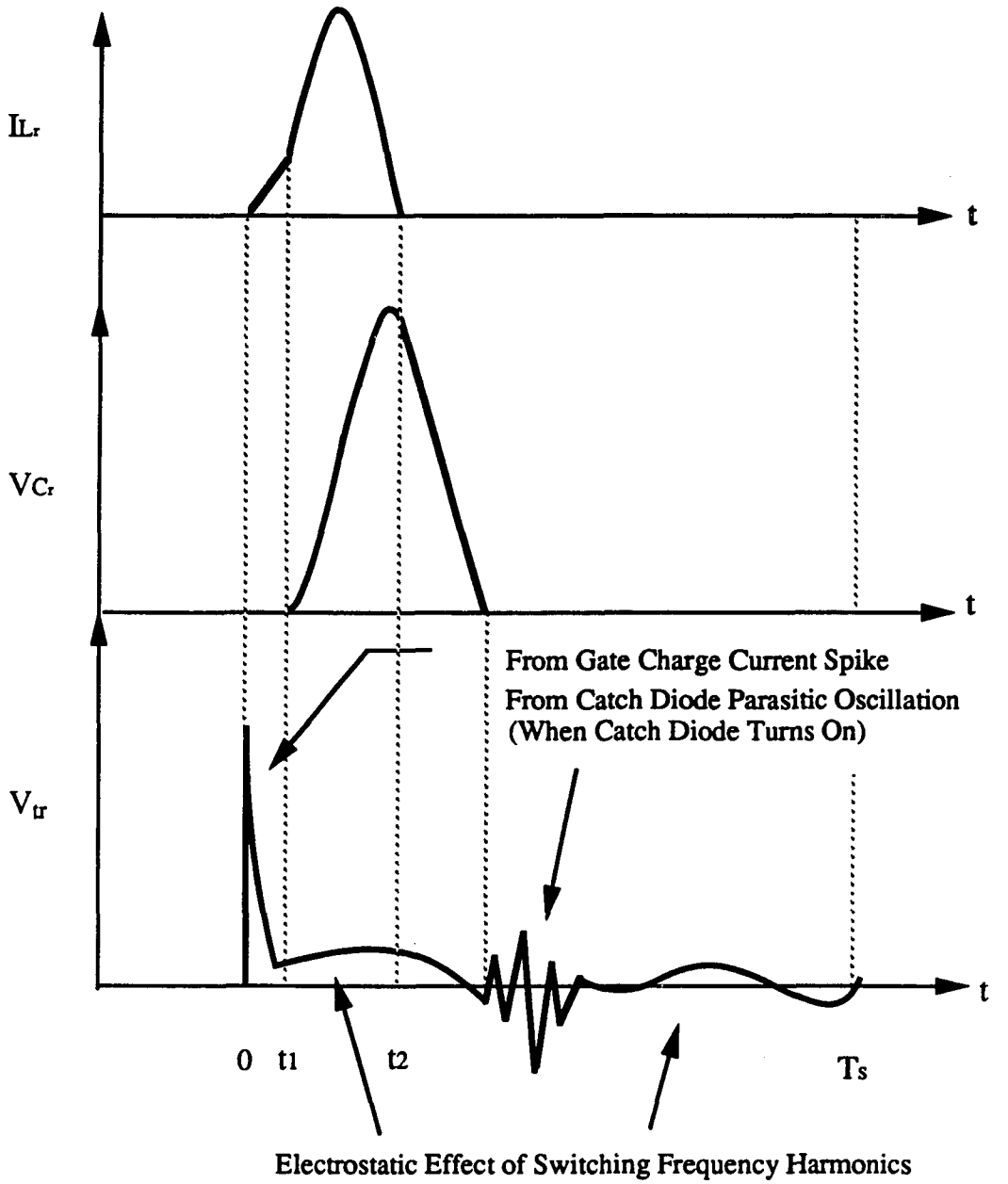

Fig. 4-5 Typical waveform of picked-up signal in ZCS-1/2.

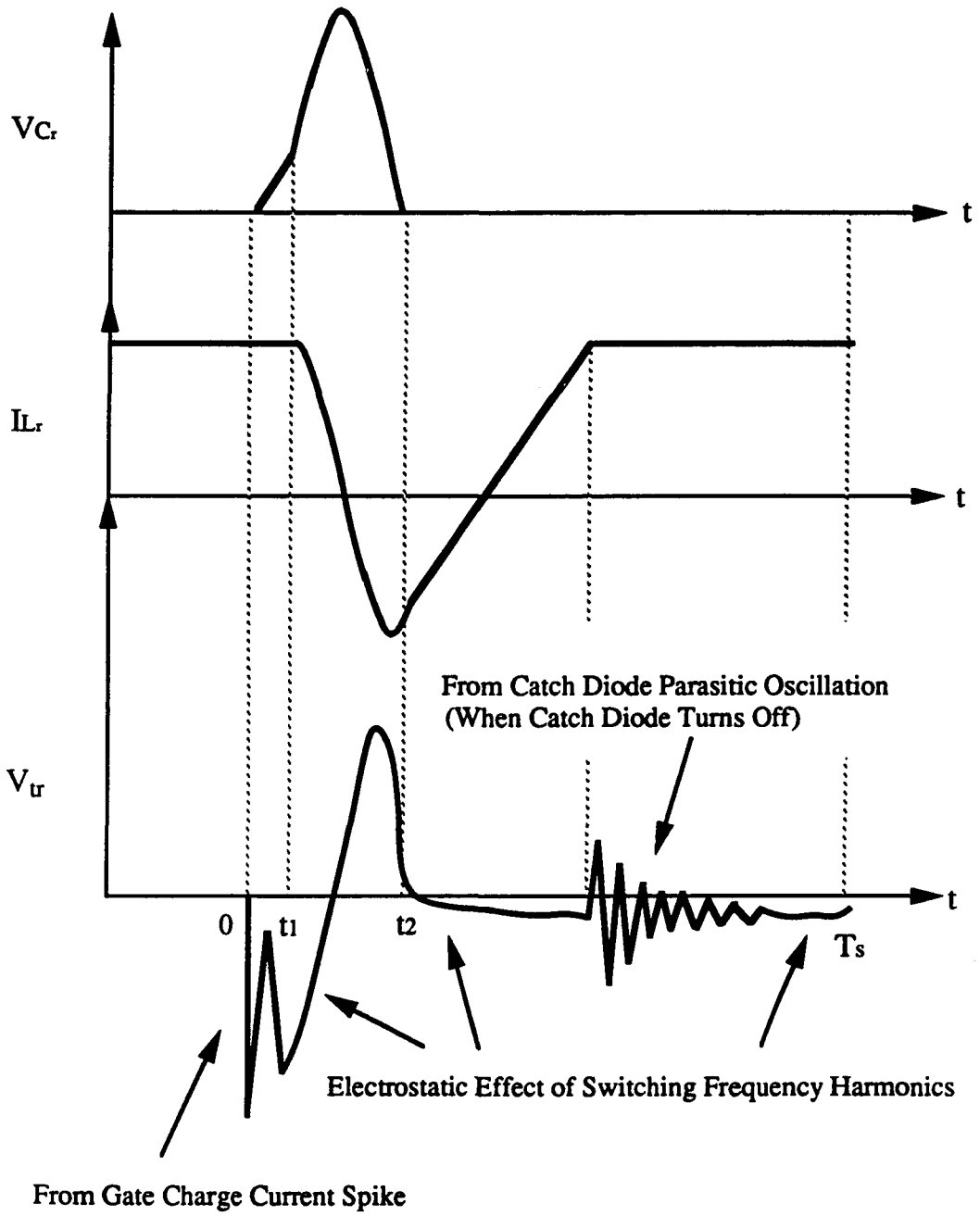

Fig. 4-6 Typical waveform of picked-up signal in ZVS-1/2.

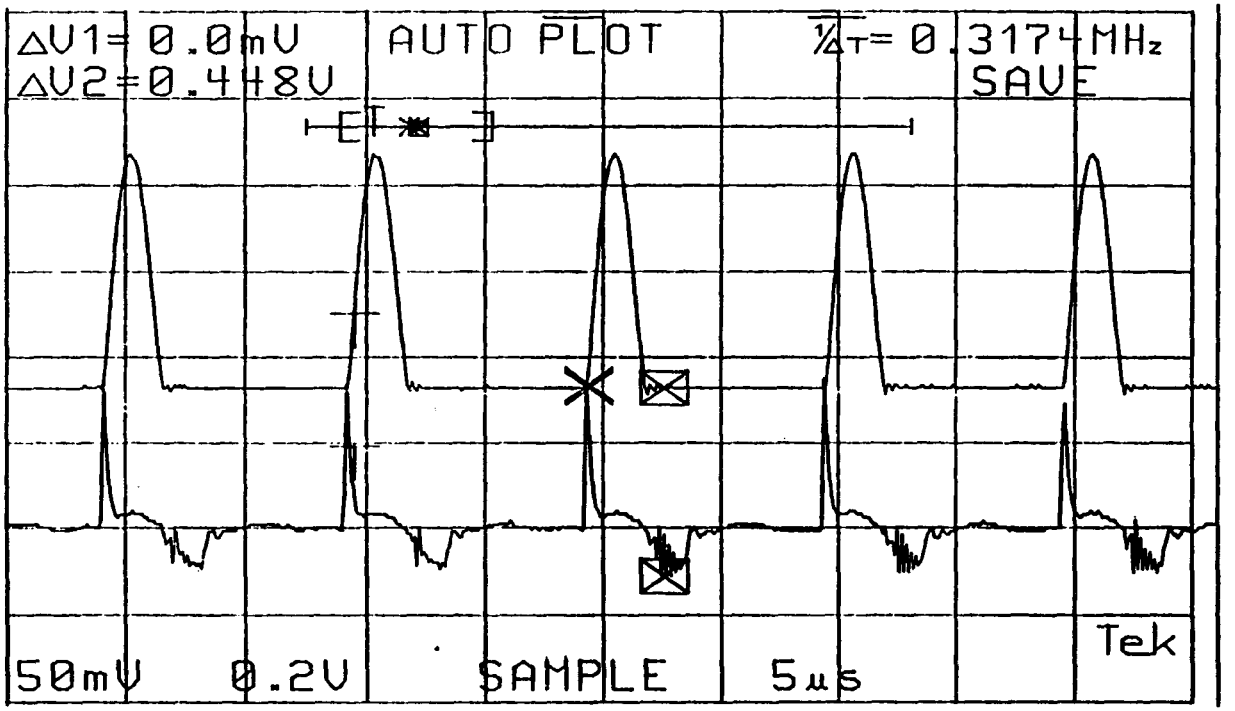

Fig. 4-7 ZCS-1/2 noise waveform (bottom, 0.2 V/ div) picked up from copper trace. The resonant inductor current waveform (top, 2.5 A/ div) is given as a time reference.

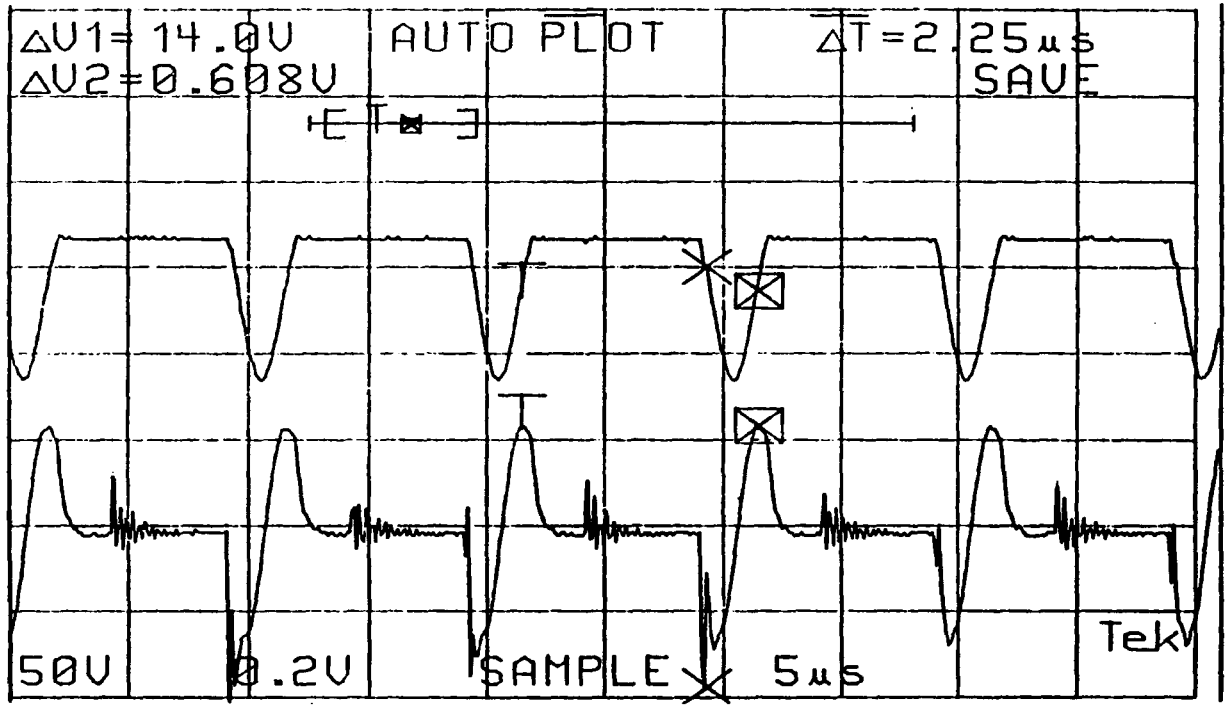

Fig. 4-8 ZVS-1/2 noise waveform (bottom, 0.2 V/ div) picked up from copper trace. The inverted resonant capacitor voltage waveform (top, 50 V/ div) is given as a time reference.

voltage switching converters, the parasitic oscillation from catch diode occurs when the catch diode turns off (Fig. 4-8). Furthermore, some high-frequency spikes from gate charge current appear in the pick-up waveforms (Figs. 4-7, 4-8) when the MOSFET switch turns on and off in the PWM and all the quasi-resonant converter circuits. It is further proved that these radiated noise spikes are due to the gate charge current turn-on and turn-off pulses, and are present on the traces even if the drain is disconnected and carries no current, as shown in Fig. 4-9, in which only the gate drive circuit is operating. It is important to observe that the influence of the turn-on and turn-off spikes from the MOSFET switch gate charge current appears to be much greater in magnitude than that of the parasitic oscillation of the catch diode (Figs. 4-7 and 4-8). This phenomenon will be discussed in more detail below. The other portion of the experimental results are simply the electrostatic effect of the switching frequency harmonics generated from the natural switching function. This electrostatic effect however could be important when the converter is in close proximity to signal processing circuitry board mounted.

4.2 Conducted Interference

The conducted interference of ZVS-1/2 quasi-resonant converter is investigated by examining the interference effect on the output voltage and input current. The interference on the output voltage is studied in 4.2.1. The interference on the input current is studied in 4.2.2. The methods to remove interference are demonstrated in both sections.

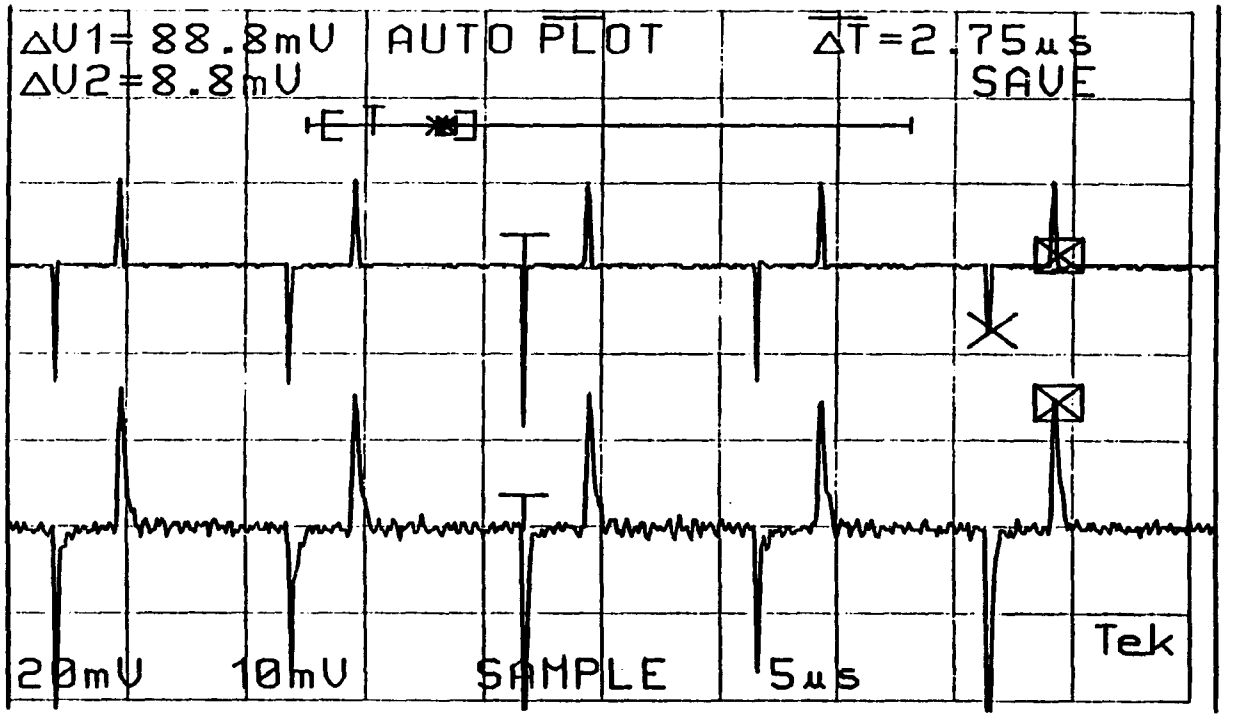

Fig. 4-9 MOSFET gate charge current waveform (top, 0.1 A/ div) and the noise waveform picked up from the copper trace (bottom, 20 mA/ div). Only the gate-drive circuit is operating, with the converter disconnected.

4.2.1 Interference on the Output Voltage

When examining the ZVS-1/2 quasi-resonant converter, high-frequency radiated noise (from gate charge current), high-frequency conducted noise (from the parasitic oscillation of the catch diode), and low-frequency conducted harmonics (from the normal switching operation) are found on the output load voltage waveform. In the following discussion, the mechanisms contributing to the radiated and conducted noise on the output voltage are identified, and methods of reducing these noise from interference sources are demonstrated.

The influence of the load inductance on the conducted noise at the output is very important. Before the output load resistor can be used to examine the converter circuit, the parasitic inductance of the output resistor must be reduced to a reasonable amount. Many spurious high frequency components were present in the first load, which was composed of several connecting wires and resistors in parallel and series. A much cleaner output voltage waveform was obtained by using only one resistor, mounted on a large aluminum heat sink with the shortest possible lead lengths.

The output load voltage as measured by a differential voltage probe is shown in Fig. 4-10 for a ZVS-1/2 converter. The components of the ripple arise from switching frequency harmonics, catch diode turn-off oscillation, and gate current spikes. To reduce the interference from the catch diode oscillation, the addition of ferrite beads on the catch diode leads is found to be effective as shown in Fig. 4-11 where one cylindrical ferrite bead is added on each catch diode lead.

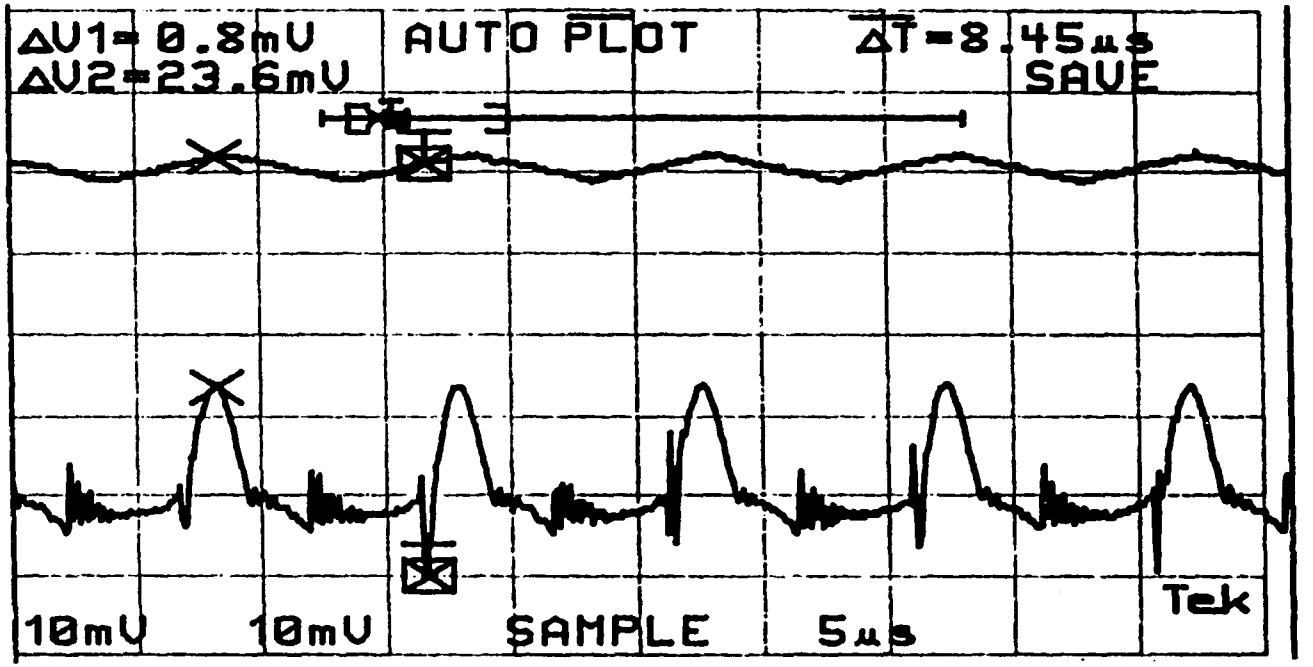

Fig. 4-10 ZVS-1/2 output voltage (bottom, 10 mV/ div). The experiment used new load and with no ferrite beads on catch diode leads and without using slow switching in the gate drive circuit.

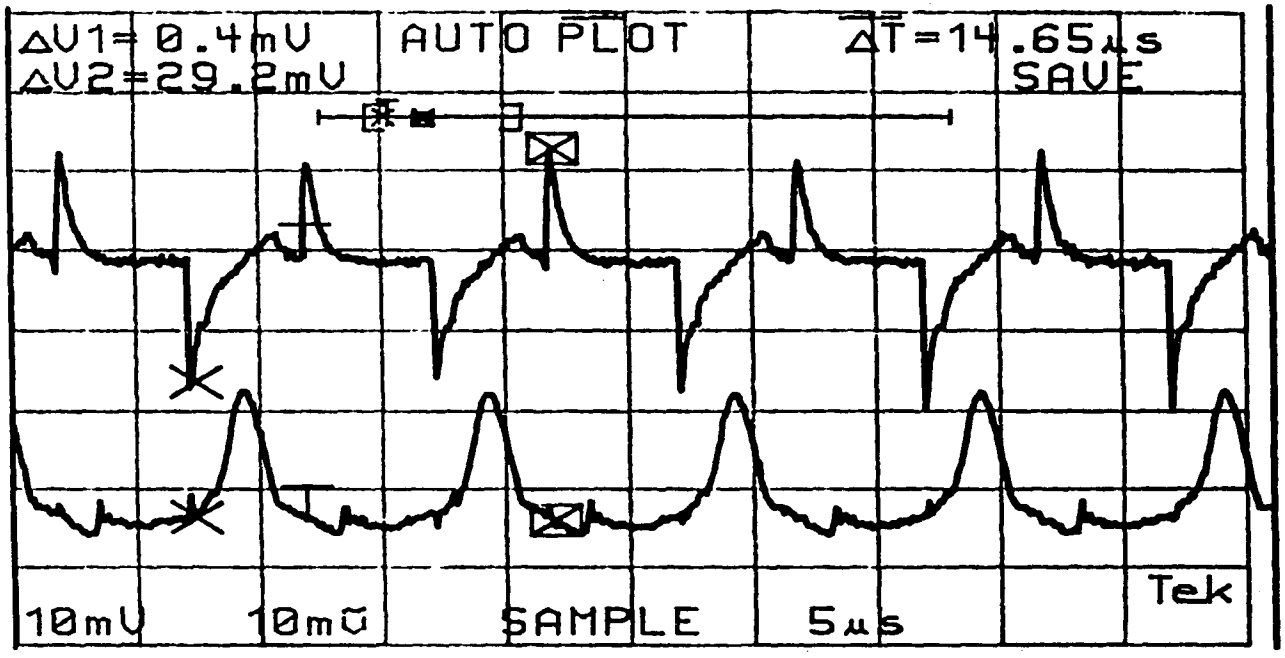

Fig. 4-11 ZVS-1/2 gate charge current (top, 20 mA/ div) and output voltage (bottom, 10 mV/ div). The experiment used new load and 320 Ω resistor in the gate drive circuit with one ferrite bead on each catch diode lead.

To reduce the interference from the gate charge current, the gate can be switched with longer rise time or fall time. Both zero-voltage switching and zero-current switching converters can use slow switching without a significant loss of efficiency (it approximately only increases the power dissipation of the resistor putting into the gate drive circuit for slow switching). Slow-switching does not increase the power dissipation in the converter circuit because in the increased switch conduction interval the switch current (ZCS-1/2 and ZVS-1) or switch voltage (ZCS-1 and ZVS-1/2) is nearly zero as shown from Fig. 4-12 to Fig. 4-15. The ZVS converters can have longer rise time; the ZCS converters can have longer fall time. If longer fall time is used by ZVS converters or longer rise time is used by ZCS converters, there is only a little switching loss, because the resonant components help keeping the switch voltage or current at zero. However, for the PWM converter, the slow switching significantly reduces efficiency because of significant switch current and voltage levels present during switching. The slow switching is implemented in the experimental prototype by adding a resistor of proper value in the gate-drive circuit (Fig. 4-16). For half wave zero-voltage switching, the maximum rise time is approximately given by the length of the t_{on} interval in which the mode diode is conducting the negative inductor current as shown in Fig. 4-14 (t_{on} = 1.13 μs, for the nominal operating point of I_o = 4 A). In practice, a resistance of R = 320 Ω is found to increase the rise time and reduce the amplitude of the gate current pulses, and hence causes the noise shown on the output load voltage earlier (Fig. 4-10) to disappear (note the change in the gate charge current scale from Fig. 4-9 to Fig. 4-11). For ZCS-1/2, ZCS-1, and ZVS-1, the maximum slow-switching intervals are indicated in Figs. 4-12, 4-13, and 4-15.

To suppress the switching-frequency sinusoidal ripple on the output voltage waveform, another capacitor is added across the output load. The ripple is not appreciably

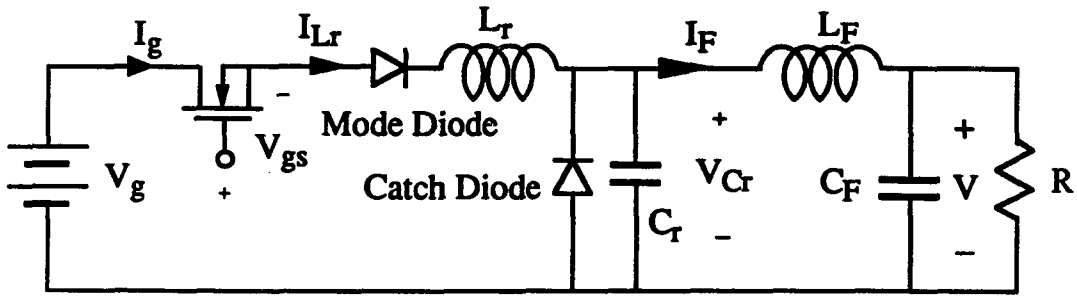

ZCS-1/2

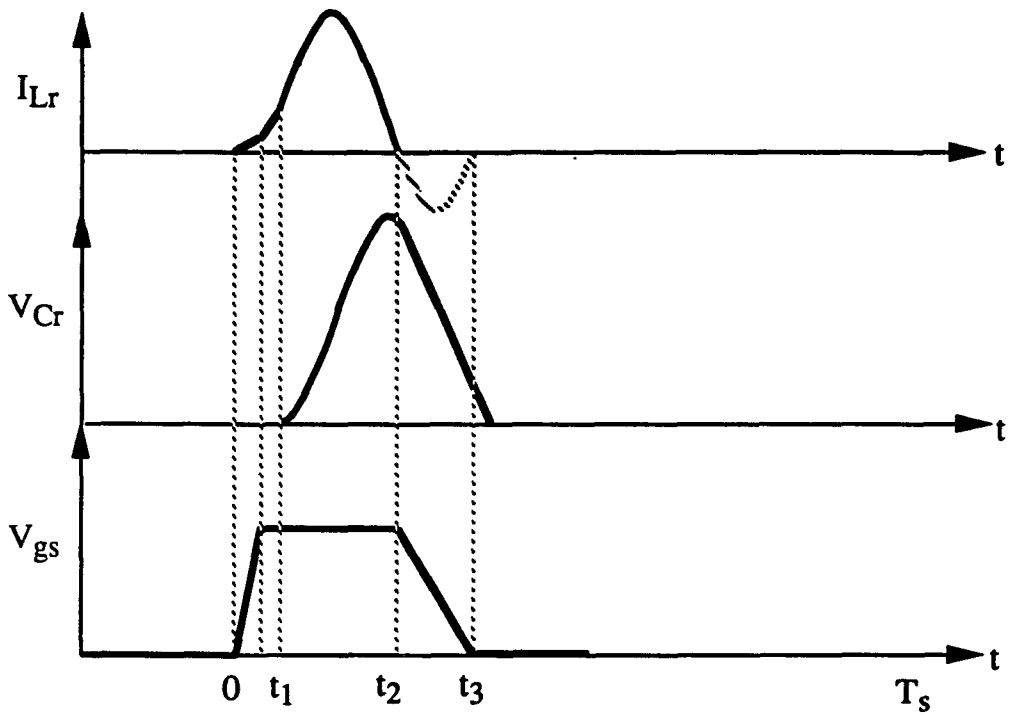

Fig. 4-12 The slow-switching interval of ZCS-1/2 QRC. Interval t_2 to t_3 can be used for slow switching, because the switch current is zero. (The mode diode is blocking the negative resonant inductor current.)

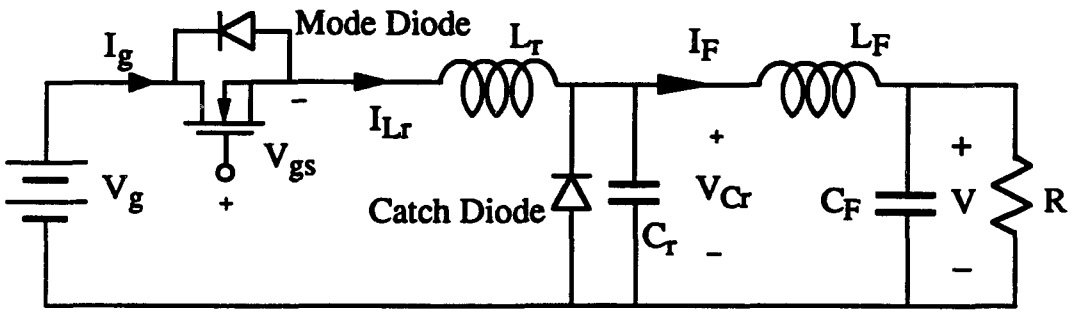

ZCS-1

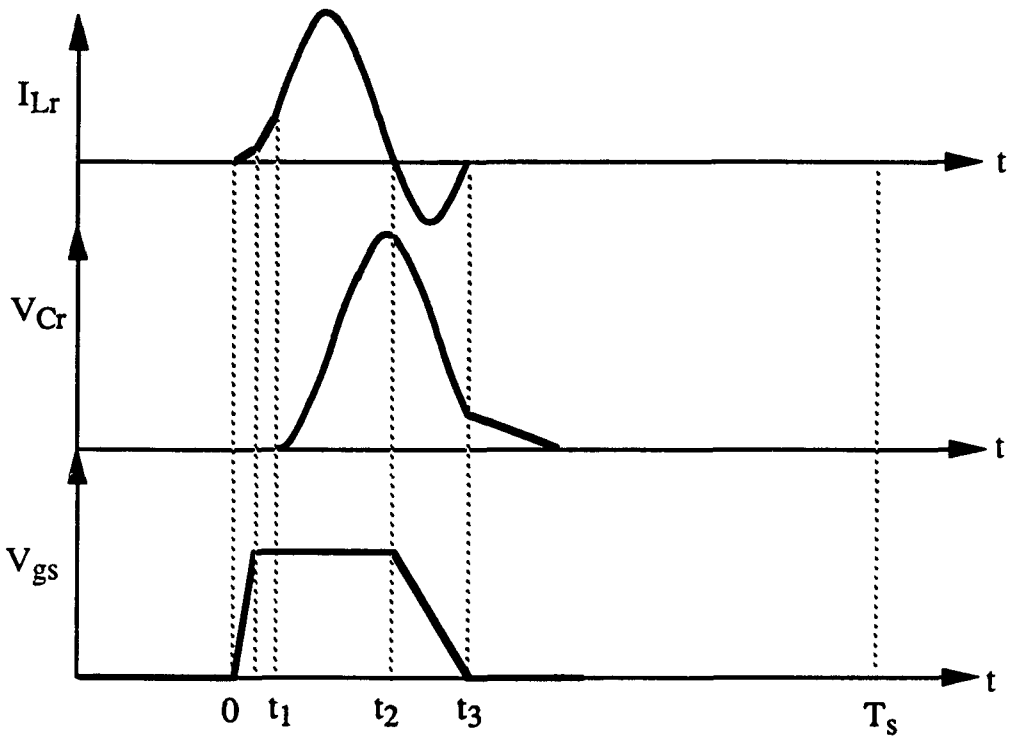

Fig. 4-13 The slow-switching interval of ZCS-1 QRC. Interval t_2 to t_3 can be used for slow switching, because the voltage across the switch is zero. (The mode diode is conducting the negative resonant inductor current.)

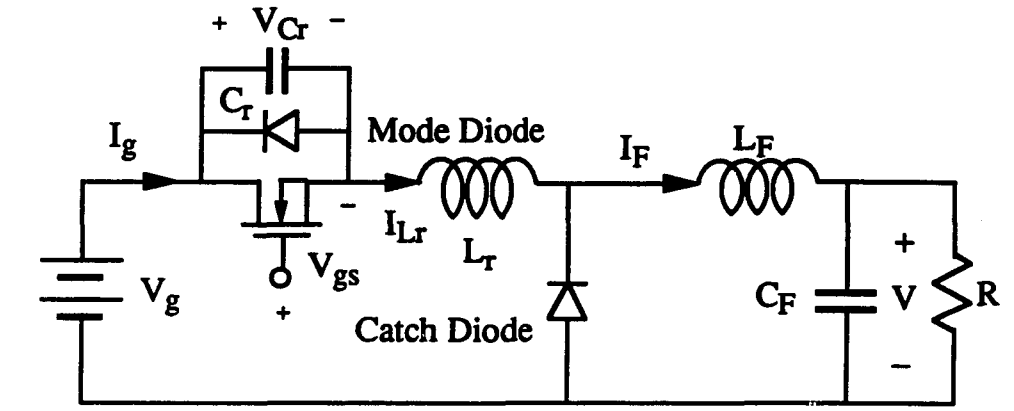

ZVS-1/2

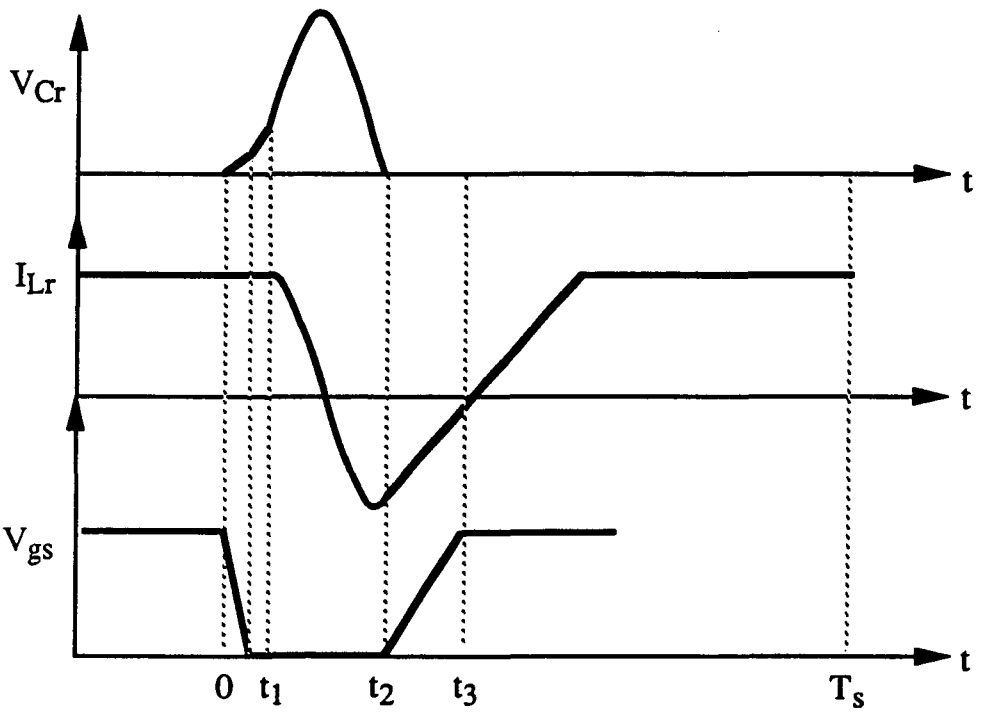

Fig. 4-14 The slow-switching interval of ZVS-1/2 QRC. Interval t_2 to t_3 can be used for slow switching, because the voltage across the switch is zero. (The mode diode is conducting the negative resonant inductor current.)

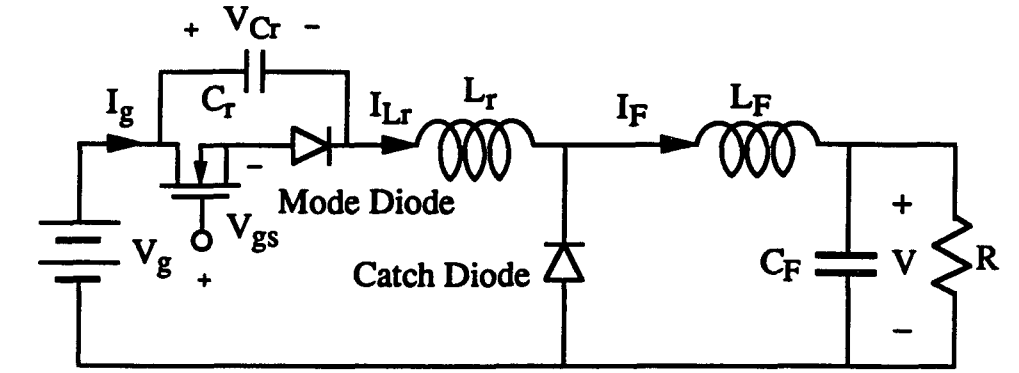

ZVS- 1

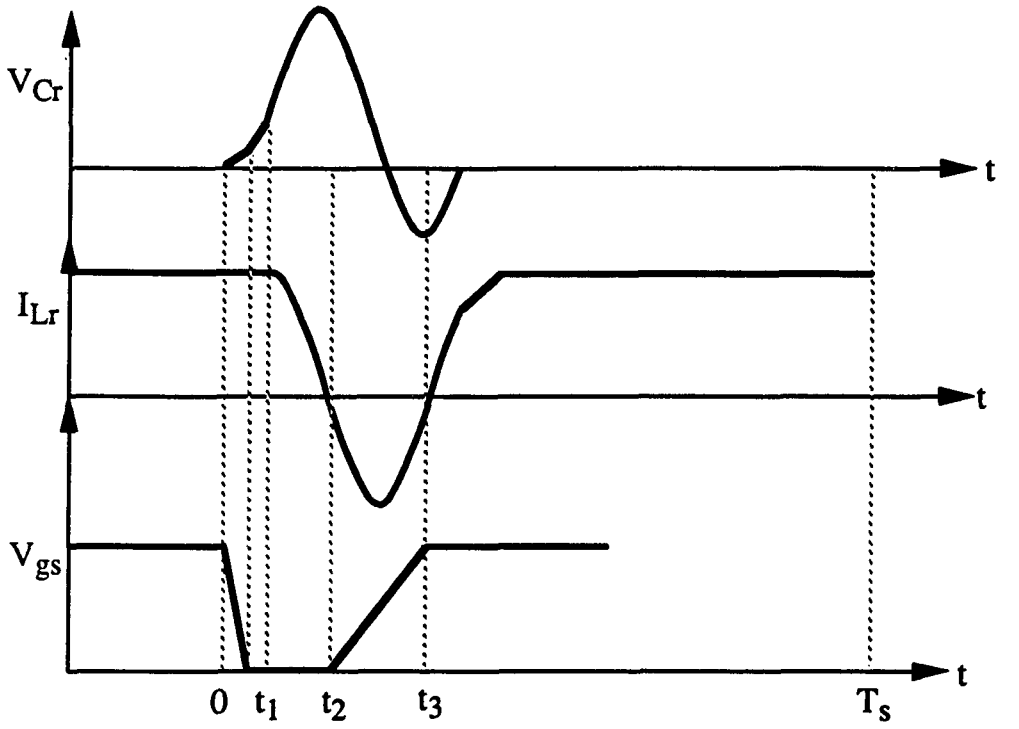

Fig. 4-15 The slow-switching interval of ZVS-1 QRC.
Interval t_2 to t_3 can be used for slow switching, because the switch current is zero.
(The mode diode is blocking the negative resonant inductor current.)

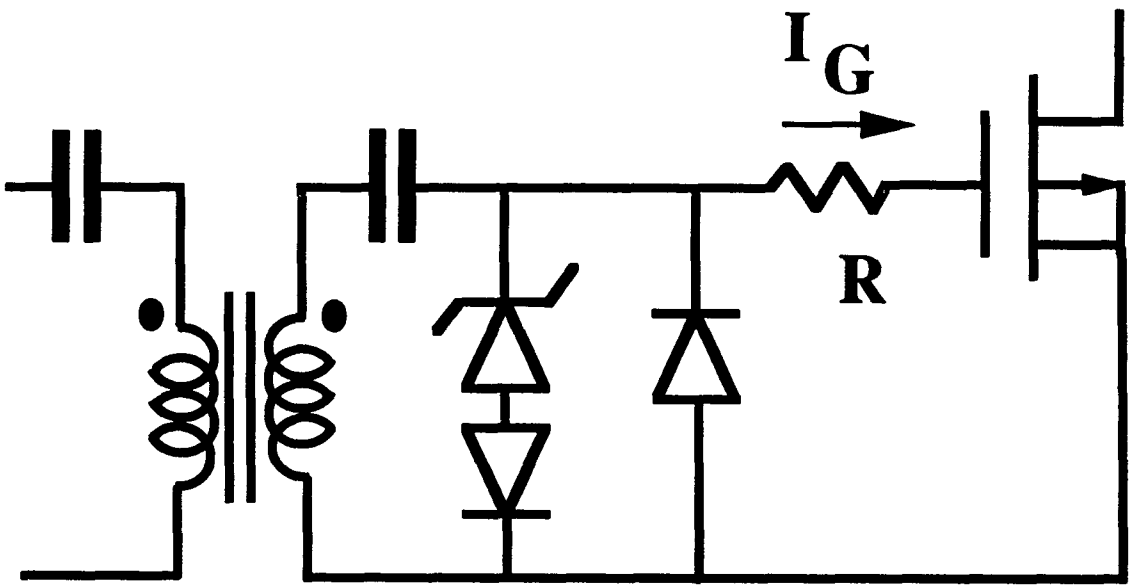

Fig. 4-16 Circuit scheme of slow switching by adding a resistor (320Ω for ZVS-1/2) in the gate drive circuit.

reduced using electrolytic capacitors even up to 2200 μF, therefore, higher quality capacitors are needed, because the low frequency sinusoidal ripple is attributed to the ESR (equivalent series resistance) of the filter capacitor. Another stage of output filter composed of a 50 μH inductor and a 23.5 μF ceramic capacitor is added to the existing filter. The low frequency ripple is successfully suppressed, as shown in Fig. 4-17.

4.2.2 Interference on the Input Current

When examining the ZVS-1/2 converter, high-frequency radiated noise (from gate charge current) and low-frequency conducted harmonics (from the normal switching operation) are found on the input current waveform. The input current waveform measured by a current probe is shown in Fig. 4-18, with the input filter consisting of a capacitor only. The low frequency harmonics are related to the natural switching operation. A two pole input filter obtained by adding a 50 μH inductor to the original filter reduces the low frequency harmonics (Fig. 4-19). The other observable spikes on the input current waveform (Figs. 4-18 and 4-19) are induced from the gate charge current spikes. Using the slow switching, these spikes can be reduced effectively (Fig. 4-20). Note that the two pole input filter could effectively reduce the low-frequency harmonics but could not effectively reduce the high-frequency noise. The high-frequency noise can only be suppressed by the slow switching technique as shown in Figs. 4-19 and 4-20.

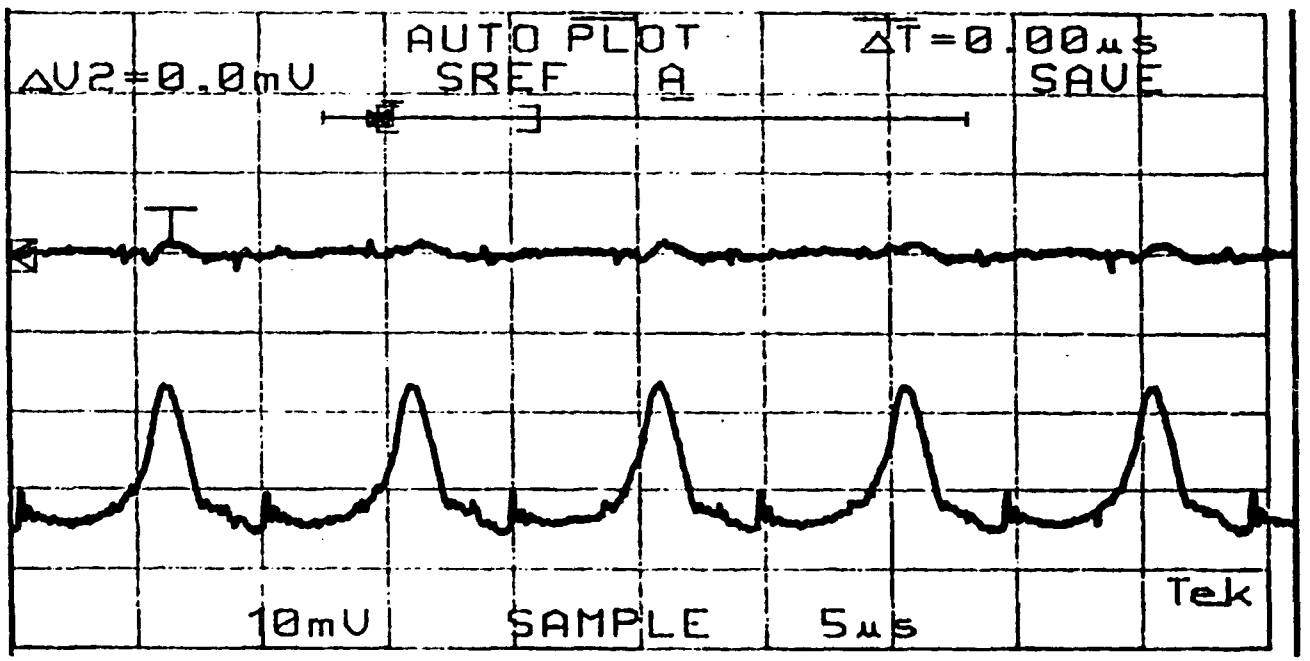

Fig. 4-17 ZVS-1/2 output voltage before adding another output filter (bottom, 10 mV/ div) and output voltage after adding another output filter (top, 10 mV/ div). The experiment used new load and 320 Ω resistor in the gate drive circuit with one ferrite bead on each catch diode lead.

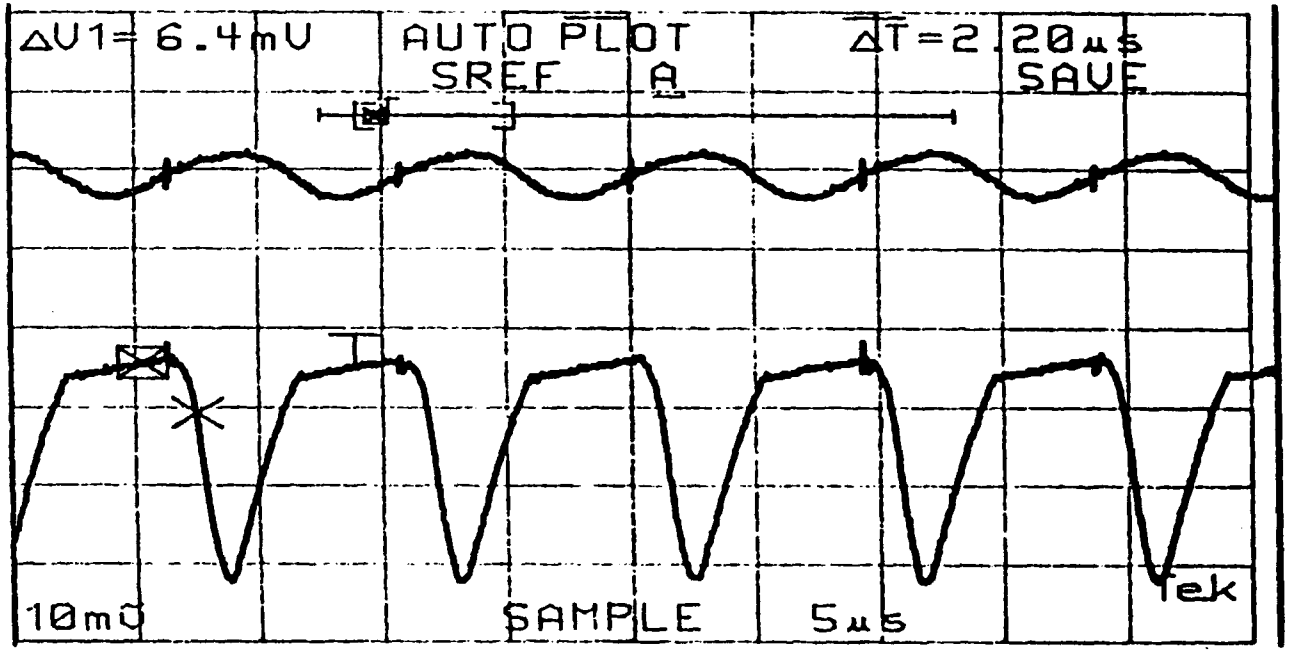

Fig. 4-18 ZVS-1/2 input current before input capacitor (top, 2 A/ div) and input current after input capacitor (bottom, 2 A/ div). The experiment used new load without an input inductor and without a 320 Ω resistor in the gate drive circuit. Note the high frequency spike noise on the waveforms.

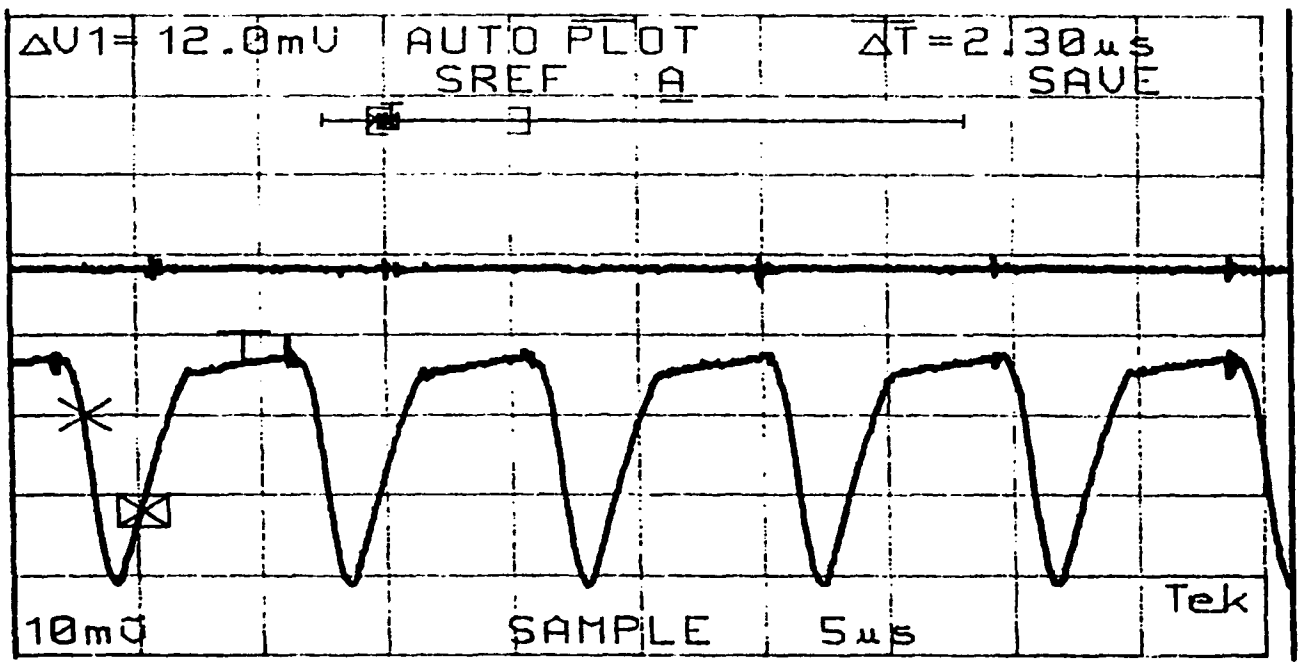

Fig. 4-19 ZVS-1/2 input current before input inductor and capacitor (top, 2 A/ div) and input current after input inductor and capacitor (bottom, 2 A/ div). The experiment used new load without a 320 Ω resistor in the gate drive circuit. Note the high frequency spike noise on the waveforms.

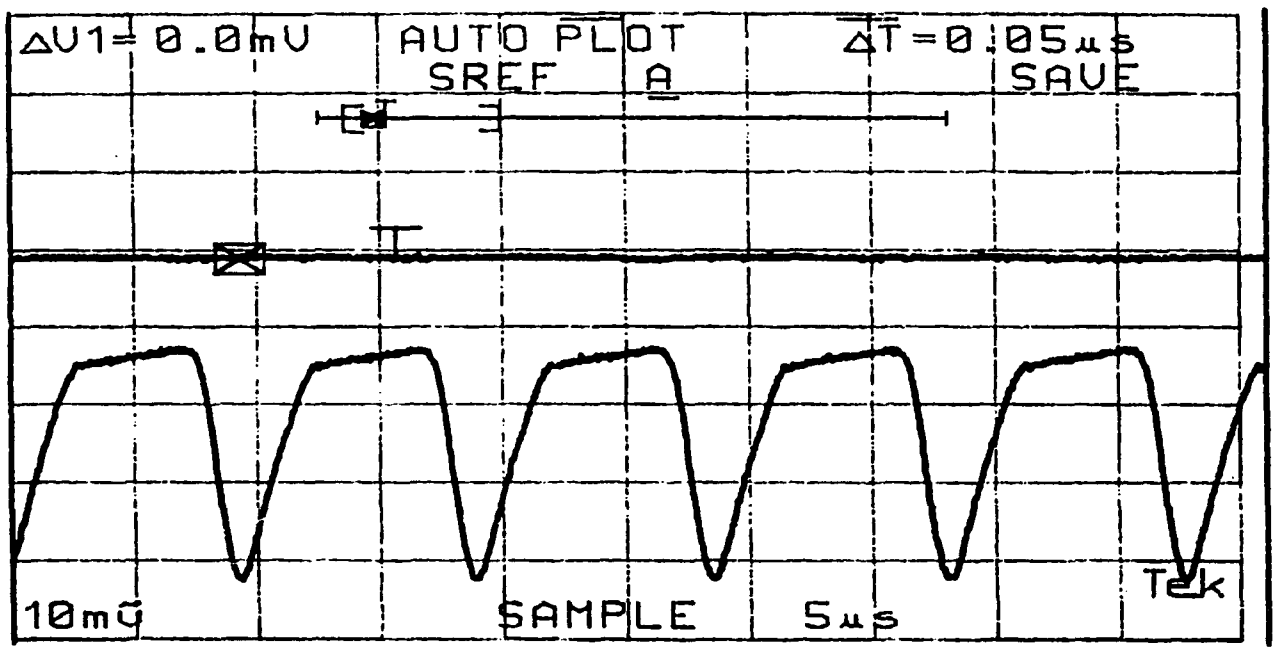

Fig. 4-20 ZVS-1/2 input current before input inductor and capacitor (top, 2 A/ div) and input current after input inductor and capacitor (bottom, 2 A/ div). The experiment used new load with a 320 Ω resistor in the gate drive circuit. Note the high frequency spike noise have been removed.

CHAPTER 5
CONCLUSION

Any switching converter will generate two kinds of electromagnetic interference (EMI): 1) the EMI produced by the natural action of the switch, which occurs at multiples of the switching frequency, and 2) the EMI produced by excitation of parasitic elements when the semiconductor devices are turned on or off. The former is a natural consequence of the switching action, and the latter is a consequence of the non-ideal realization of the switch. To reduce the total EMI, both effects must be considered.

The EMI produced by the switching action can be characterized by Fourier series expansions of the waveform functions. From Table I, for a given load, the total bandwidth of the input current of quasi-resonant converters is only one-half to one-eighth of that of the PWM converter at the same average power level. However, almost all quasi-resonant converters have higher 3dB bandwidth of the input current than does the PWM converter. Hence, for a given low frequency ripple specification, a lower cutoff frequency is needed on the quasi-resonant converter filter than for the PWM converter filter. Although the filter elements may be larger for a quasi-resonant converter than a PWM converter, these filter elements do not have to be ideal over as large a frequency range, whereas a PWM converter requires ideal filter performance over a large switching frequency harmonic range. This consideration is especially important at higher switching frequencies, where ideal filter behavior is difficult to obtain in practice.

The catch diode current is as important to EMI concerns as the transistor current. Fourier analysis on the catch diode current waveform of the quasi-resonant converters

shows that zero-current switching quasi-resonant converters (ZCS-QRCs) have very high total bandwidth comparable to that of the PWM converter, because of their square catch diode current waveform. Although zero-voltage switching quasi-resonant converters (ZCS-QRCs) have low total bandwidth in the quasi-sinusoidal catch diode current waveform, they have quasi-square switch and mode diode current waveforms which have high total bandwidth. Hence, from the standpoint of radiated interference caused by switching harmonics, some quasi-resonant converters will cause severe radiated EMI harmonics like the PWM converter. Moreover, the ZCS-QRC is the topological dual of the ZVS-QRC. Since the ZCS-QRC has a square diode current waveform which will have a wide spectrum, and since the ZVS-QRC has a quasi-sinusoidal diode current waveform with a narrow spectrum, therefore, if the radiated interference coupling mechanism is magnetic, the ZVS-QRC is better, and if the mechanism is electric, the ZCS-QRC is better.

The effects of load current variation, and hence switching frequency variation, are examined in chapter 2 for all converter topologies and given in Table I. Switching frequency control does indeed increase the total bandwidth of the input current waveforms in all schemes except for ZVS-1 quasi-resonant converter. However, the quasi-resonant converters still maintain a lower total bandwidth than the PWM converter at all operating points examined.

The EMI induced by excitation of parasitic elements is investigated by the experimental measurement of the radiated noise-induced waveforms in nearby traces, the converter output voltage, and the converter input current. The parasitic oscillation source from the catch diode and a EMI source from the gate charge current spike are found to be the most significant. The parasitic oscillation of the catch diode is conducted to output load

voltage (Fig. 23) and radiated to the surroundings (Fig. 20, 21). This EMI can be effectively reduced by adding a cylindrical ferrite bead to each catch diode lead (Fig. 25). The EMI from the MOSFET switch gate charge current is radiated to the input current (Fig. 27) and output load voltage (Fig. 23). However, the quasi-resonant converters have a distinct advantage over the PWM converters in that slow gate switching (i.e., using longer gate voltage rise and fall times) has been shown to significantly reduce the effect of the most severe EMI source in the circuit (Fig. 25, 29) without reducing the overall converter efficiency (section 4.2).

Appendix A: Derivation of Fourier Spectral Content Magnitude

In the following discussion, the approach to obtain the Fourier spectral content magnitudes of the quasi-resonant converter (ZCS-1/2, ZCS-1, ZVS-1/2, and ZVS-1) resonant inductor current and the PWM converter filter inductor current at the nominal operating point of $I_o = 4$ A is demonstrated. The normalized spectral content magnitude formula expression of the quasi-resonant converters obtained can be utilized to compute the spectral content magnitude at different operating points by substitution for appropriate parameter values. The actual spectral content magnitude then is obtained by multiplying by the respective base current factor.

When deriving the formula for the PWM converter, the normalized process is not applied because there is no resonant circuit in the PWM converter. Moreover, a more practical PWM converter filter inductor current with a 10 % current ripple is derived instead of the ideal square waveform.

(1) ZCS-1/2

Referring to Fig. 1-3, the normalized resonant inductor current can be expressed by

$$j_{Lr}(t) = \omega_0 t \qquad 0 \le t \le t_1$$

$$j_{Lr}(t) = 1/2 + \sin \omega_0(t-t_1) \qquad t_1 \le t \le t_2$$

$$j_{Lr}(t) = 0 \qquad t_2 \le t \le T_s$$

where ω_o is the radian resonant frequency, T_s is the switching period, and t_1 and t_2 are to be solved from the boundary conditions of the expression above [1-3]. It is found that

$$\omega_o = 2\pi f_{1/2} = 2\pi \times 243 \times 10^3 = 1.53 \times 10^6$$

$$t_1 = 0.33 \times 10^{-6} \text{ second}$$

$$t_2 = 2.72 \times 10^{-6} \text{ second}$$

$$T_s = 1/f_s = 10^{-5} \text{ second} \quad (f_s = 100 \text{ kHz})$$

Following the derivation described in chapter 2.2, the complex Fourier coefficient for each harmonic is:

$$F_n = \frac{1}{T_s}\left[\int_0^{t_1} (\omega_0 t)e^{-jn\omega_s t}\,dt + \int_{t_1}^{t_2} \left(\frac{1}{2} + \sin(\omega_0(t-t_1))\right)e^{-jn\omega_s t}\,dt\right]$$

where ω_s is the radian switching frequency ($\omega_s = 2\pi \times f_s = 2\pi \times 10^5$).

$$F_n = \frac{1}{T_s}\left\{ j\frac{t_1\omega_o e^{-jn\omega_s t_1}}{n\omega_s} + \frac{\omega_o(e^{-jn\omega_s t_1}-1)}{(n\omega_s)^2} + j\frac{e^{-jn\omega_s t_2}-e^{-jn\omega_s t_1}}{2n\omega_s} \right.$$
$$\left. + \frac{(n\omega_s)^2}{(n\omega_s)^2 - \omega_0^2}\left[e^{-jn\omega_s t_2}\left(\frac{\omega_o \cos\omega_o(t_2-t_1)}{(n\omega_s)^2} + j\frac{\sin\omega_o(t_2-t_1)}{n\omega_s} \right) - \frac{\omega_o}{(n\omega_s)^2} e^{-jn\omega_s t_1} \right] \right\}$$

The normalized magnitude of the spectral content can be computed:

$$|F_n| = \sqrt{R_e^2(F_n) + I_m^2(F_n)} = |j_{Lr}(n\omega_s t)|$$

The actual (denormalized) magnitude of the spectral content is obtained by multiplying by the base current V_g / R_o.

(2) ZCS-1

Referring to Fig. 1-4, the normalized resonant inductor current can be expressed by

$$j_{Lr}(t) = \omega_0 t \qquad 0 \le t \le t_1$$

$$j_{Lr}(t) = 1/2 + \sin \omega_0(t-t_1) \qquad t_1 \le t \le t_2$$

$$j_{Lr}(t) = 0 \qquad t_2 \le t \le T_s$$

where ω_o is the radian resonant frequency, T_s is the switching period, and t_1 and t_2 are to be solved from the boundary conditions of the expression above [1-3]. It is found that

$$\omega_o = 2\pi f_1 = 2\pi \times 200 \times 10^3 = 1.26 \times 10^6$$

$$t_1 = 0.4 \times 10^{-6} \text{ second}$$

$$t_2 = 5 \times 10^{-6} \text{ second}$$

$$T_s = 1/f_s = 10^{-5} \text{ second} \quad (f_s = 100 \text{ kHz})$$

Following the derivation described in chapter 2.2, the complex Fourier coefficient for each harmonic is:

$$F_n = \frac{1}{T_s}\left[\int_0^{t_1} (\omega_0 t) e^{-jn\omega_s t}\, dt + \int_{t_1}^{t_2} \left(\frac{1}{2} + \sin(\omega_0(t-t_1)) e^{-jn\omega_s t}\, dt\right]\right.$$

where ω_s is the radian switching frequency ($\omega_s = 2\pi \times f_s = 2\pi \times 10^5$).

$$F_n = \frac{1}{T_s}\left\{ j\frac{t_1 \omega_o e^{-jn\omega_s t_1}}{n\omega_s} + \frac{\omega_o(e^{-jn\omega_s t_1} - 1)}{(n\omega_s)^2} + j\frac{e^{-jn\omega_s t_2} - e^{-jn\omega_s t_1}}{2n\omega_s} \right.$$
$$\left. + \frac{(n\omega_s)^2}{(n\omega_s)^2 - \omega_0^2}\left[e^{-jn\omega_s t_2}\left(\frac{\omega_o \cos \omega_o(t_2-t_1)}{(n\omega_s)^2} + j\frac{\sin \omega_o(t_2-t_1)}{n\omega_s} \right) - \frac{\omega_o}{(n\omega_s)^2} e^{-jn\omega_s t_1} \right] \right\}$$

The normalized magnitude of the spectral content can be computed:

$$|F_n| = \sqrt{R_e^2(F_n) + I_m^2(F_n)} = |j_{Lr}(n\omega_s t)|$$

The actual (denormalized) magnitude of the spectral content is obtained by multiplying by the base current V_g / R_o.

(3) ZVS-1/2

Referring to Fig. 1-5, the normalized resonant inductor current can be expressed by

$$j_{Lr}(t) = 2\cos\omega_o \qquad 0 \le t \le t_1$$

$$j_{Lr}(t) = -\sqrt{3} + \omega_0(t-t_1) \qquad t_1 \le t \le t_2$$

$$j_{Lr}(t) = 2 \qquad t_2 \le t \le T_s$$

where ω_o is the radian resonant frequency, T_s is the switching period, and t_1 and t_2 are to be solved from the boundary conditions of the expression above [1-3]. It is found that

$$\omega_o = 2\pi f_{1/2} = 2\pi \times 243 \times 10^3 = 1.53 \times 10^6$$

$$t_1 = 2.4 \times 10^{-6} \text{ second}$$

$$t_2 = 4.8 \times 10^{-6} \text{ second}$$

$$T_s = 1/f_s = 10^{-5} \text{ second} \quad (f_s = 100 \text{ kHz})$$

Following the derivation described in chapter 2.2, the complex Fourier coefficient for each harmonic is:

$$F_n = \frac{1}{T_s}\left[\int_0^{t1} (2\cos\omega_0 t)e^{-jn\omega_s t}dt + \int_{t1}^{t2} (-\sqrt{3} + (\omega_0(t-t_1))e^{-jn\omega_s t}dt + \int_{t2}^{T_s} 2e^{-jn\omega_s t}dt\right]$$

where ω_s is the radian switching frequency ($\omega_s = 2\pi \times f_s = 2\pi \times 10^5$).

$$F_n = \frac{1}{T_s}\left\{ j\frac{-\sqrt{3}(e^{-jn\omega_s t_2} - e^{-jn\omega_s t_1}) + 2 + (\omega_0(t_2-t_1)-1)e^{-jn\omega_s t_2}}{n\omega_s} + \frac{\omega_o e^{-jn\omega_s t_2} - e^{-jn\omega_s t_1}}{(n\omega_s)^2} + \frac{(n\omega_s)^2}{(n\omega_s)^2 - \omega_0^2}\left[\frac{-2\omega_o \sin\omega_0 t_1 e^{-jn\omega_s t_1}}{(n\omega_s)^2} + j\frac{2\cos\omega_0 t_1 e^{-jn\omega_s t_1} - 2}{n\omega_s}\right]\right\}$$

The normalized magnitude of the spectral content can be computed:

$$|F_n| = \sqrt{R_e^2(F_n) + I_m^2(F_n)} = |j_{Lr}(n\omega_s t)|$$

The actual (denormalized) magnitude of the spectral content is obtained by multiplying by the base current V_g / R_o.

(4) ZVS-1

Referring to Fig. 1-6, the normalized resonant inductor current can be expressed by

$$j_{Lr}(t) = 2\cos\omega_o \qquad 0 \le t \le t_1$$

$$j_{Lr}(t) = \sqrt{3} + \omega_0(t-t_1) \qquad t_1 \le t \le t_2$$

$$j_{Lr}(t) = 2 \qquad t_2 \le t \le T_s$$

where ω_o is the radian resonant frequency, T_s is the switching period, and t_1 and t_2 are to be solved from the boundary conditions of the expression above [1-3]. It is found that

$$\omega_o = 2\pi f_1 = 2\pi \times 200 \times 10^3 \approx 1.26 \times 10^6$$

$$t_1 = 4.6 \times 10^{-6} \text{ second}$$

$$t_2 = 4.8 \times 10^{-6} \text{ second}$$

$$T_s = 1/f_s = 10^{-5} \text{ second} \quad (f_s = 100 \text{ kHz})$$

Following the derivation described in chapter 2.2, the complex Fourier coefficient for each harmonic is:

$$F_n = \frac{1}{T_s}\left[\int_0^{t1} (2\cos\omega_0 t)e^{-jn\omega_s t}\,dt + \int_{t1}^{t2} (\sqrt{3} + (\omega_0(t-t_1))e^{-jn\omega_s t}\,dt + \int_{t2}^{T_s} 2e^{-jn\omega_s t}\,dt\right]$$

where ω_s is the radian switching frequency ($\omega_s = 2\pi \times f_s = 2\pi \times 10^5$).

$$F_n = \frac{1}{T_s}\left\{ j\frac{\sqrt{3}(e^{-jn\omega_s t2} - e^{-jn\omega_s t1}) + 2 + (\omega_o(t_2-t_1)-1)e^{-jn\omega_s t2}}{n\omega_s} + \frac{\omega_o e^{-jn\omega_s t2} - e^{-jn\omega_s t1}}{(n\omega_s)^2} + \frac{(n\omega_s)^2}{(n\omega_s)^2 - \omega_0^2}\left[\frac{-2\omega_o \sin\omega_o t_1 e^{-jn\omega_s t1}}{(n\omega_s)^2} + j\frac{2\cos\omega_o t_1 e^{-jn\omega_s t1} - 2}{n\omega_s}\right]\right\}$$

The normalized magnitude of the spectral content can be computed:

$$|F_n| = \sqrt{R_e^2(F_n) + I_m^2(F_n)} = |j_{Lr}(n\omega_s t)|$$

The actual (denormalized) magnitude of the spectral content is obtained by multiplying by the base current V_g / R_o.

(5) PWM

The filter inductor current of PWM converter actually has ripple. To make a more practical comparison, Fourier analysis on PWM converter will include 10% current ripple.

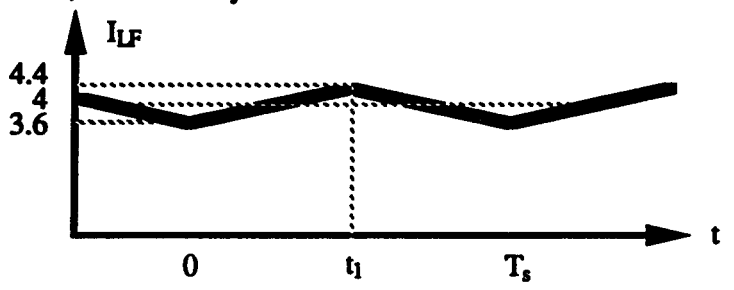

From the figure above, the filter inductor current can be expressed by

$$i_g(t) = 3.6 + \frac{V_g}{2L_F} t \qquad 0 \le t \le t_1$$

$$i_g(t) = 4.4 - \frac{V_g}{2L_F} (t - t_1) \qquad 0 \le t \le T_s$$

where $t_1 = T_s/2 = 5 \times 10^{-6}$ second

$T_s = 1/f_s = 10^{-5}$ second ($f_s = 100$ kHz)

Following the derivation described in chapter 2.2, the complex Fourier coefficient for each harmonic is:

$$F_n = \frac{1}{T_s} \left[\int_0^{t_1} \left(3.6 + \frac{V_g}{2L_F} t \right) e^{-jn\omega_s t} dt + \int_{t_1}^{T_s} \left(4.4 - \frac{V_g}{2L_F} (t - t_1) \right) e^{-jn\omega_s t} dt \right]$$

where ω_s is the radian switching frequency ($\omega_s = 2\pi \times f_s = 2\pi \times 10^5$).

$$F_n = \frac{1}{T_s} \left\{ j \frac{(3.6 - 4.4) + \frac{V_g}{2L_F}}{n\omega_s} e^{-jn\omega_s t_1} + j \frac{4.4 - 3.6 - \frac{V_g}{2L_F} (T_s - t_1)}{n\omega_s} + \frac{\frac{V_g}{L_F} (e^{-jn\omega_s t_1} - 1)}{(n\omega_s)^2} \right\}$$

The normalized magnitude of the spectral content can be computed:

$$|F_n| = \sqrt{R_e^2(F_n) + I_m^2(F_n)} = |I_{LF}(n\omega_s t)|$$

Appendix B: The Fourier Spectra at Three Operating Points

From the spectral content magnitude formulas in appendix A, the spectral content magnitudes at switching frequency multiples can be calculated and used to depict the Fourier spectra. In the following, several Fourier spectra of the quasi-resonant converter resonant inductor current and catch diode current are shown.

1) At the nominal operating point ($I_o = 4$ A):

(a) The spectra of the quasi-resonant converter resonant inductor current are shown earlier from Fig. 2-1 to Fig. 2-4, chapter 2.

(b) The spectra of the quasi-resonant converter catch diode current are shown from Fig. B-1 to Fig. B-4.

(c) The spectrum of the ZVS-1/2 quasi-resonant converter switch current is shown in Fig. B-5.

(d) The spectrum of the ZVS-1/2 quasi-resonant converter mode diode current is shown in Fig. B-6.

(e) The spectrum of the ZVS-1 quasi-resonant converter switch current is shown in Fig. B-7.

2) At the operating point $I_o = 5.4$ A:

(a) The spectra of the quasi-resonant converter resonant inductor current are shown from Fig. B-8 to Fig. B-11.

(b) The spectra of the quasi-resonant converter catch diode current are shown from Fig. B-12 to Fig. B-15.

3) At the operating point $I_o = 2.6$ A:

(a) The spectra of the quasi-resonant converter resonant inductor current are shown from Fig. B-16 to Fig. B-19.

(b) The spectra of the quasi-resonant converter catch diode current are shown from Fig. B-20 to Fig. B-23.

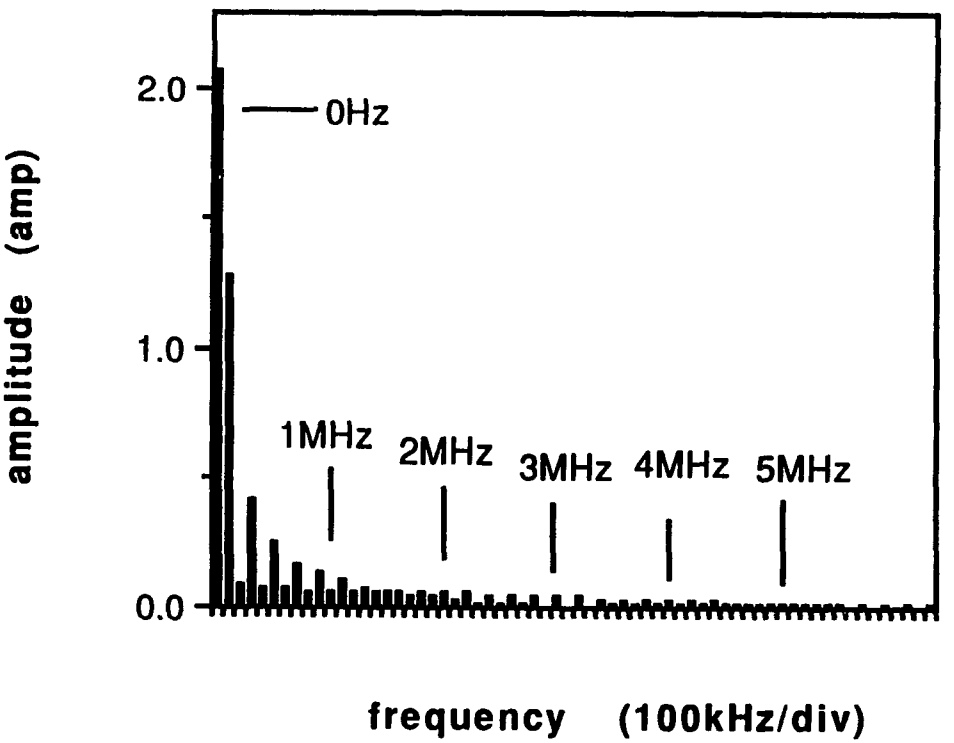

Fig. B-1 ZCS-1/2 QRC catch diode current Fourier spectrum (output resistance 3.25 Ω).

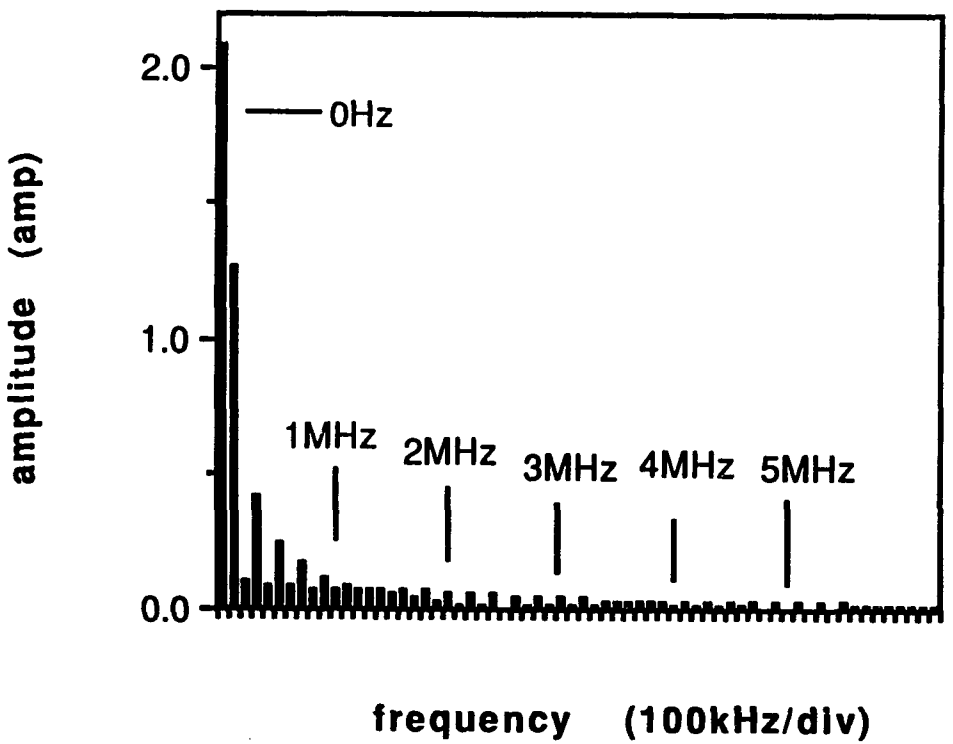

Fig. B-2 ZCS-1 QRC catch diode current Fourier spectrum (output resistance 3.25 Ω).

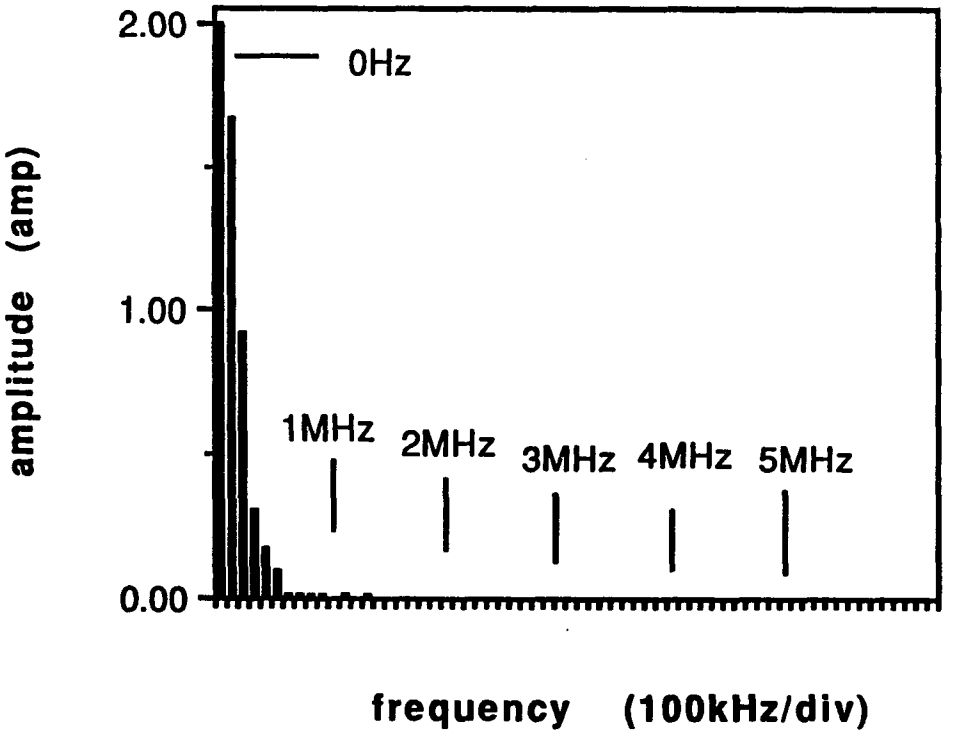

Fig. B-3 ZVS-1/2 QRC catch diode current Fourier spectrum (output resistance 3.25 Ω).

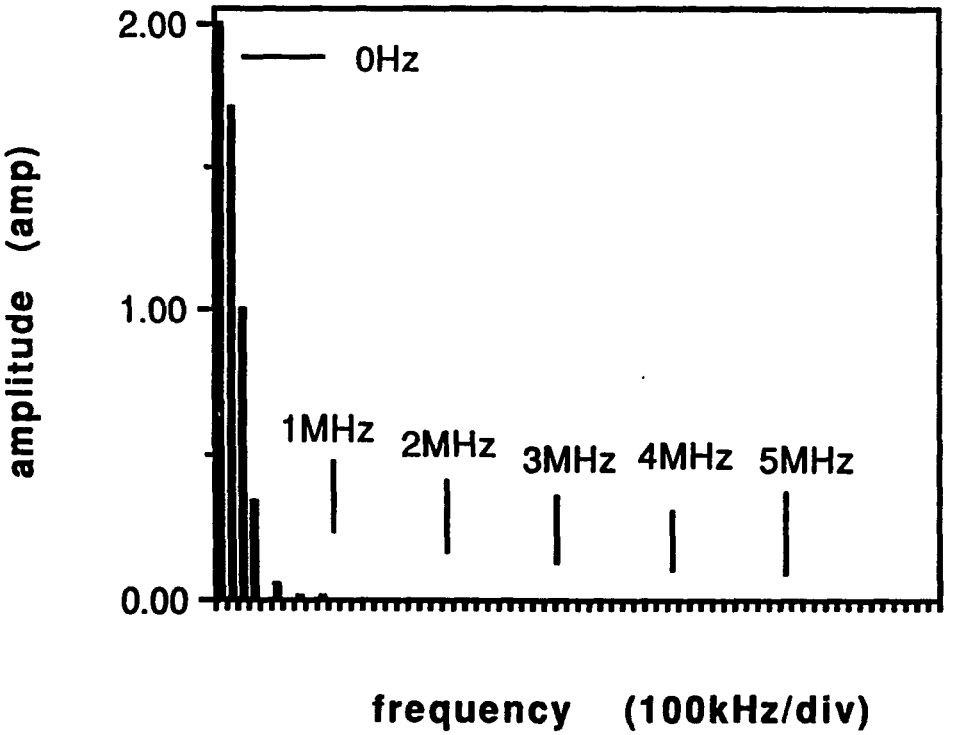

Fig. B-4 ZVS-1 QRC catch diode current Fourier spectrum (output resistance 3.25 Ω).

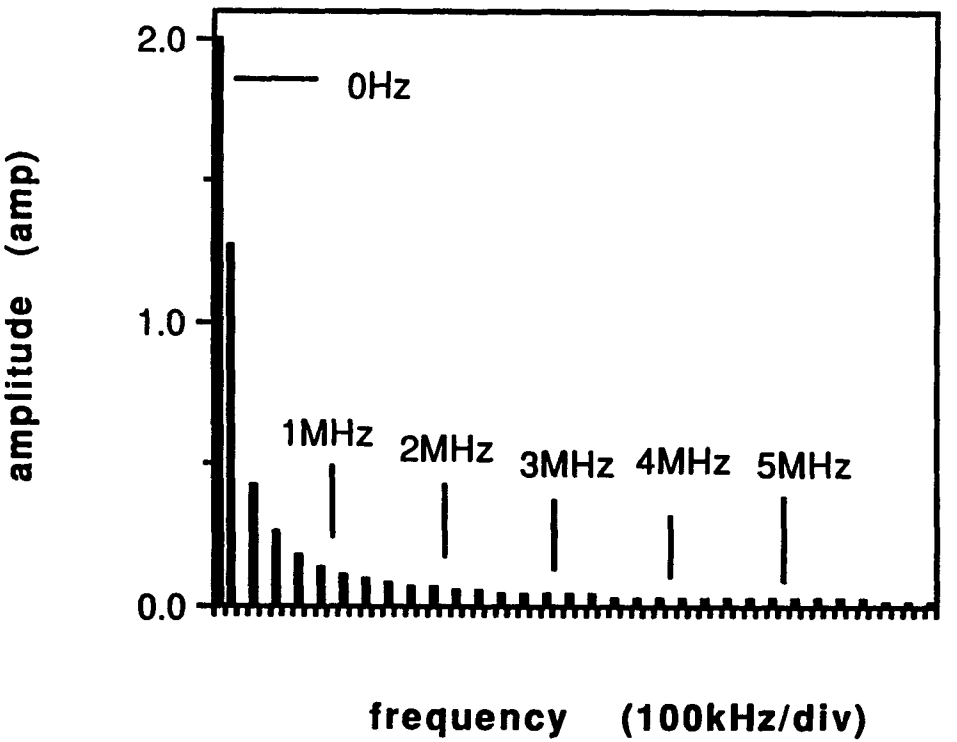

Fig. B-5 ZVS-1/2 QRC switch current Fourier spectrum (output resistance 3.25 Ω).

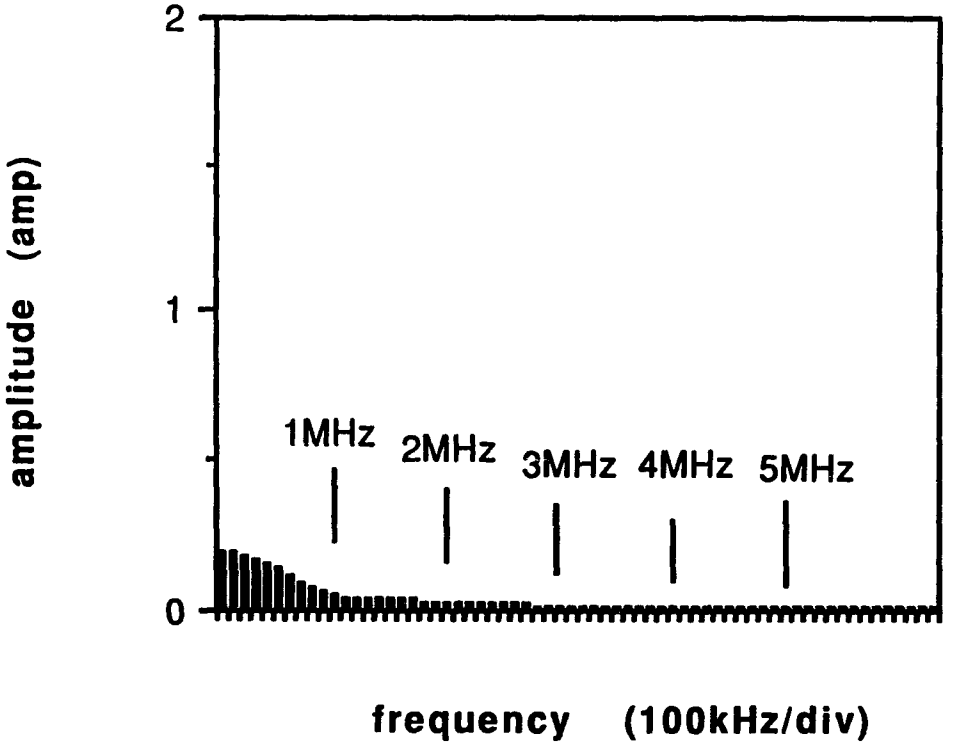

Fig. B-6 ZVS-1/2 QRC mode diode current Fourier spectrum (output resistance 3.25 Ω).

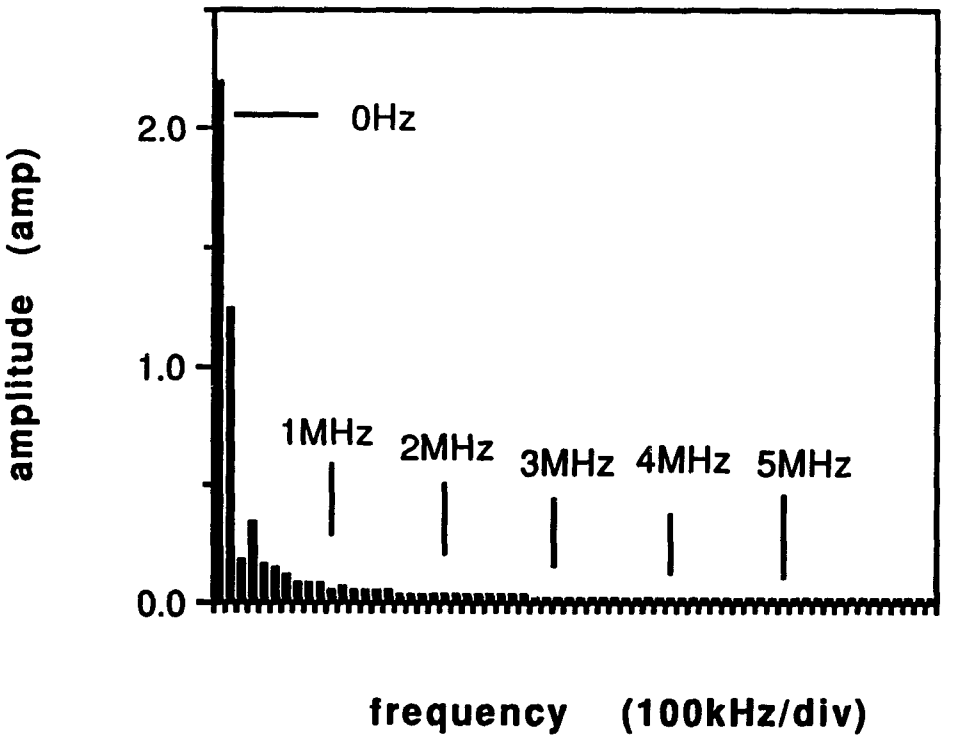

Fig. B-7 ZVS-1 QRC switch current Fourier spectrum (output resistance 3.25 Ω).

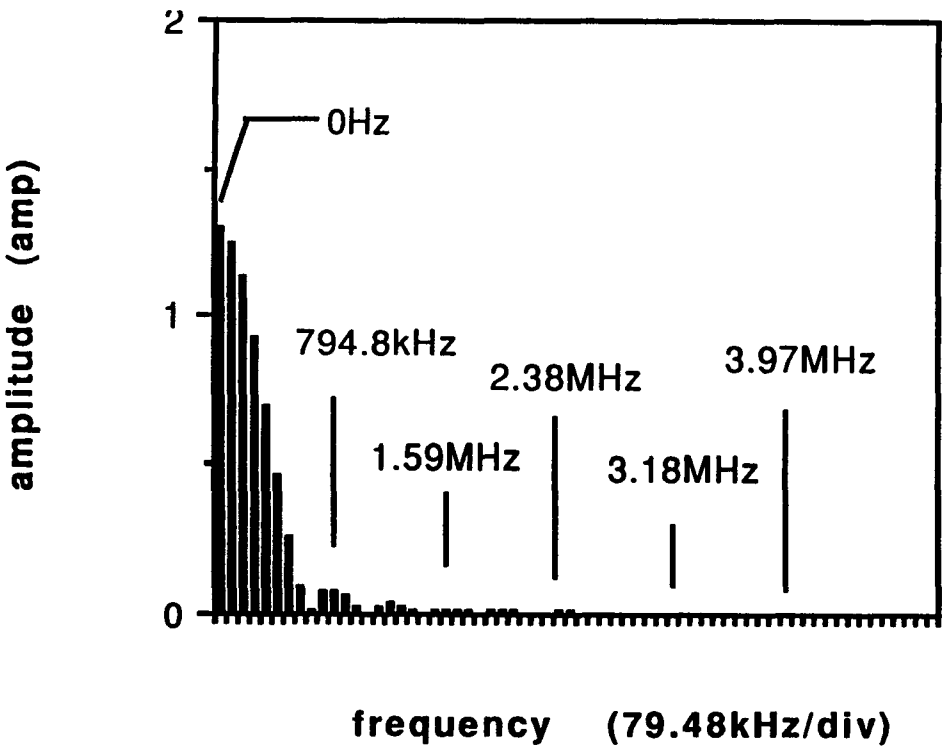

Fig. B-8 ZCS-1/2 QRC input current Fourier spectrum (output resistance 5 Ω).

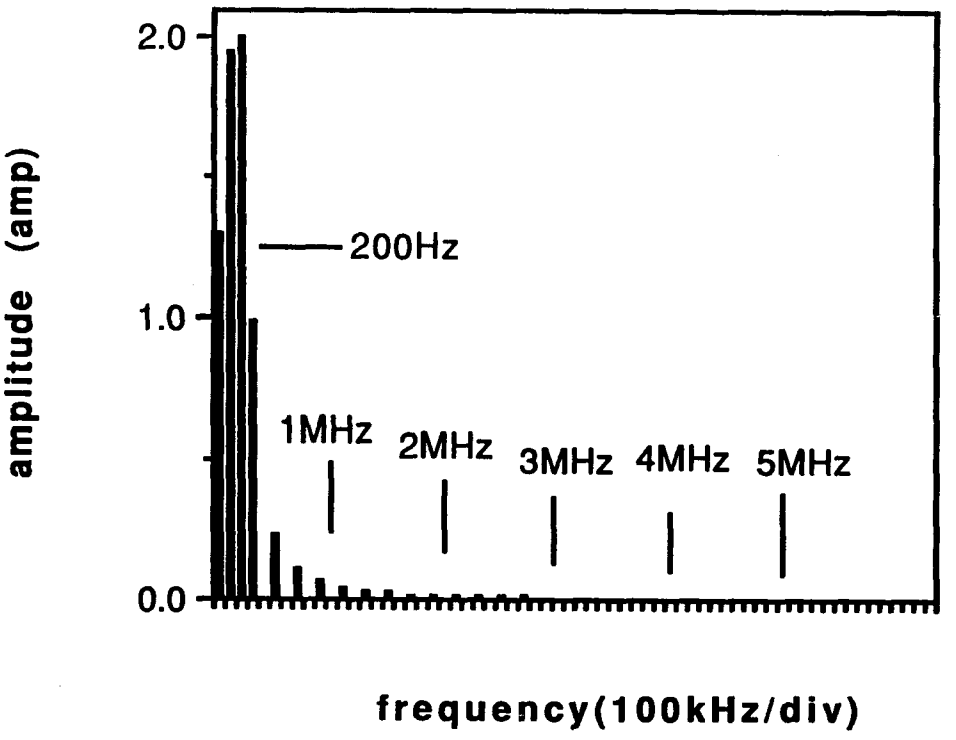

Fig. B-9 ZCS-1 QRC input current Fourier spectrum (output resistance 5 Ω).

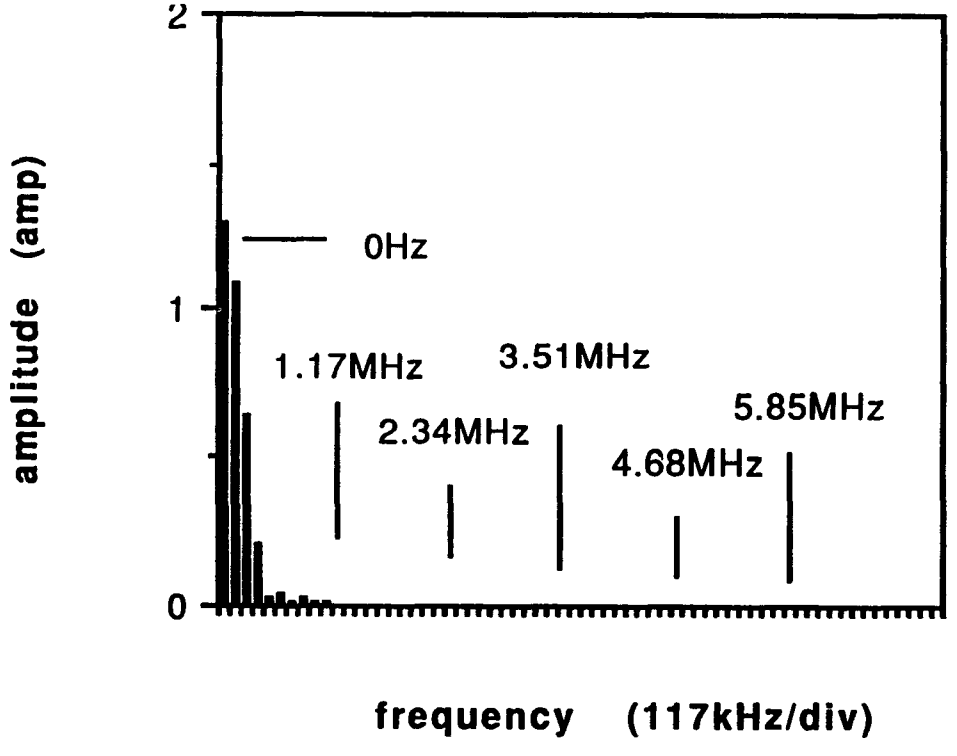

Fig. B-10 ZVS-1/2 QRC input current Fourier spectrum (output resistance 5 Ω).

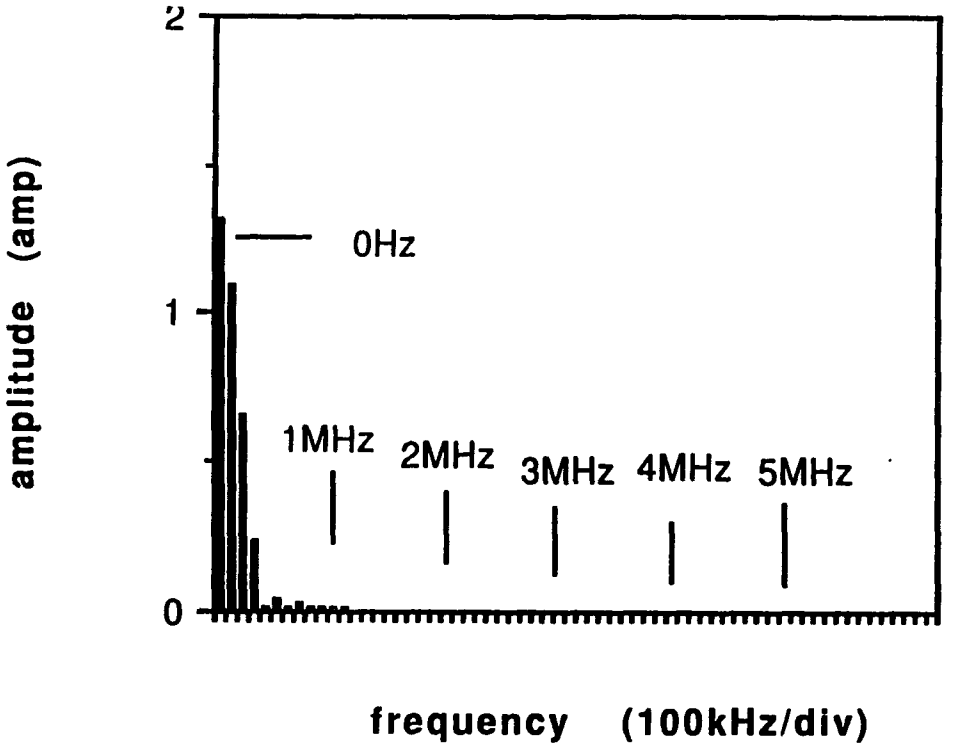

Fig. B-11 ZVS-1 QRC input current Fourier spectrum (output resistance 5 Ω).

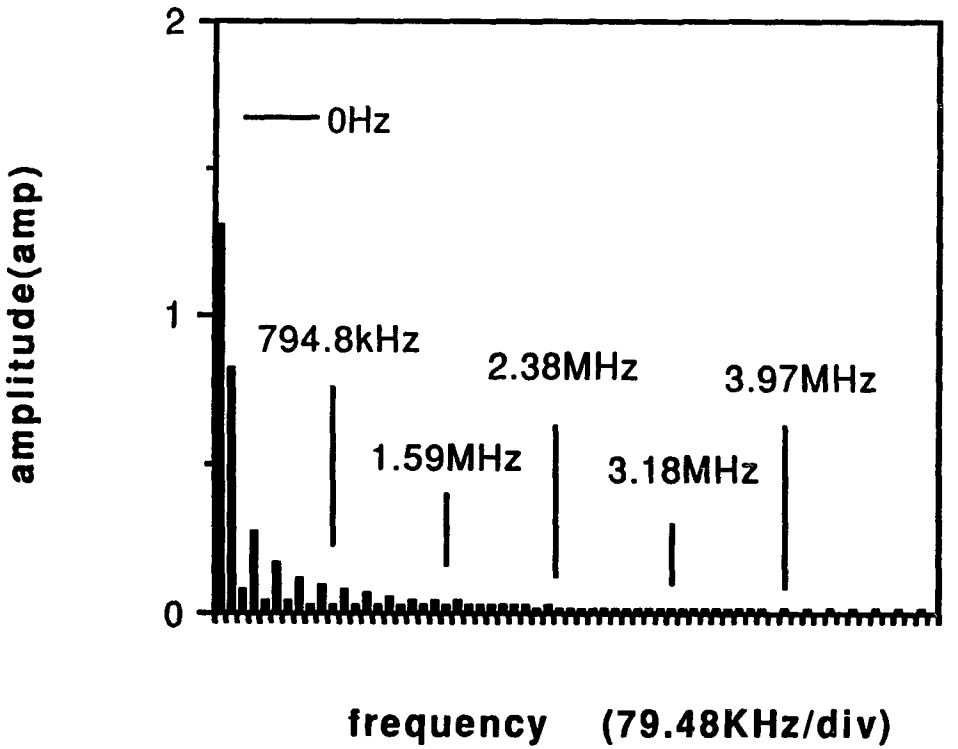

Fig. B-12 ZCS-1/2 QRC catch diode current Fourier spectrum (output resistance 5 Ω).

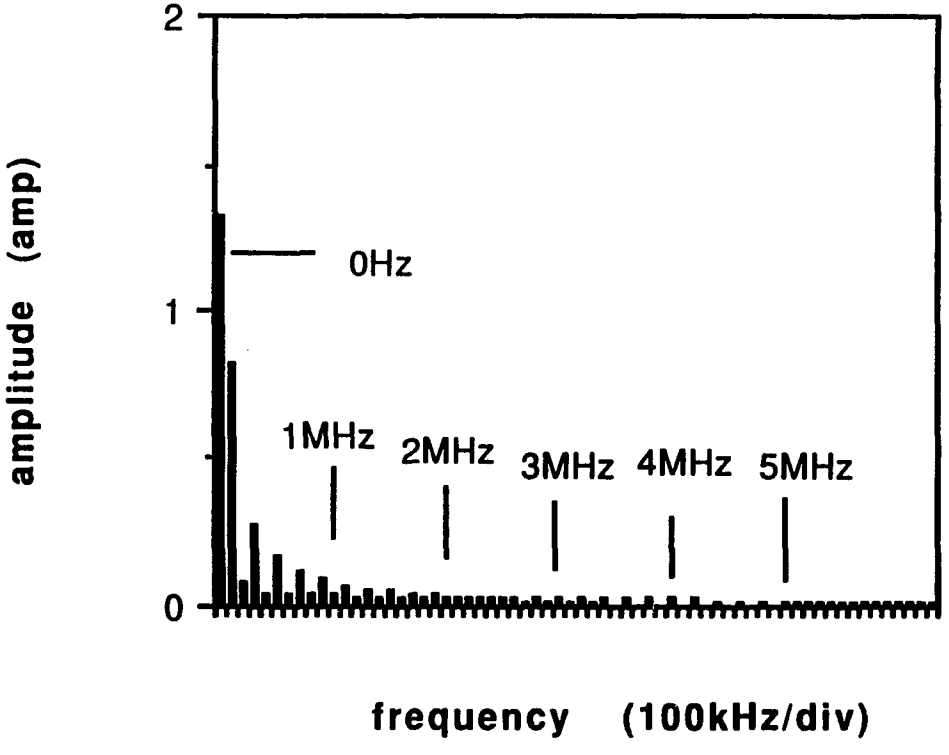

Fig. B-13 ZCS-1 QRC catch diode current Fourier spectrum (output resistance 5 Ω).

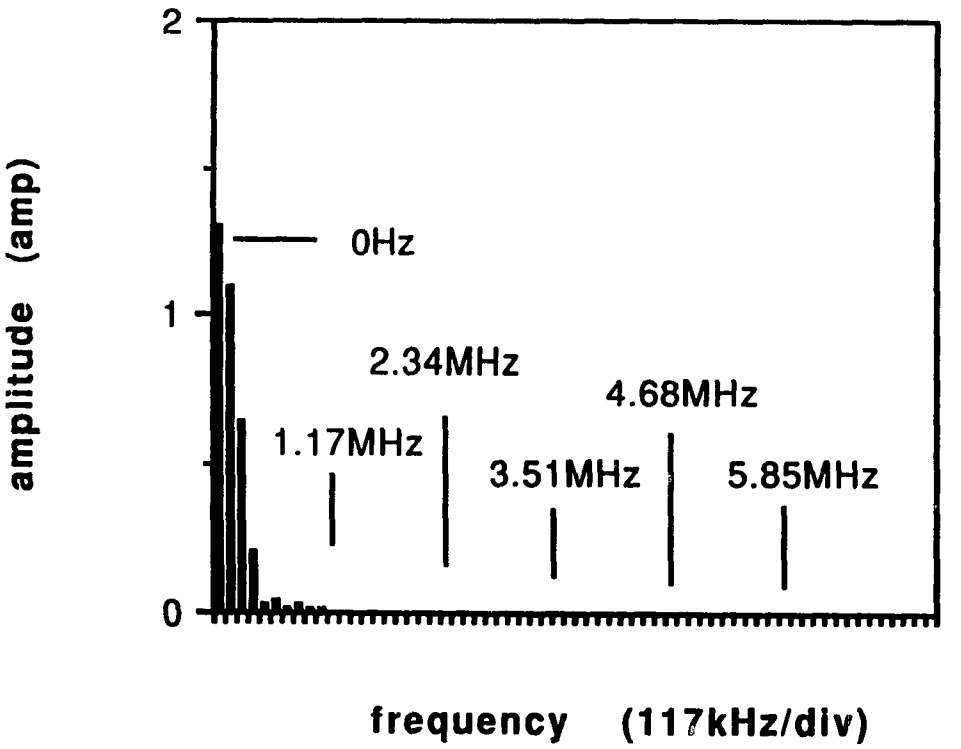

Fig. B-14 ZVS-1/2 QRC catch diode current Fourier spectrum (output resistance 5 Ω).

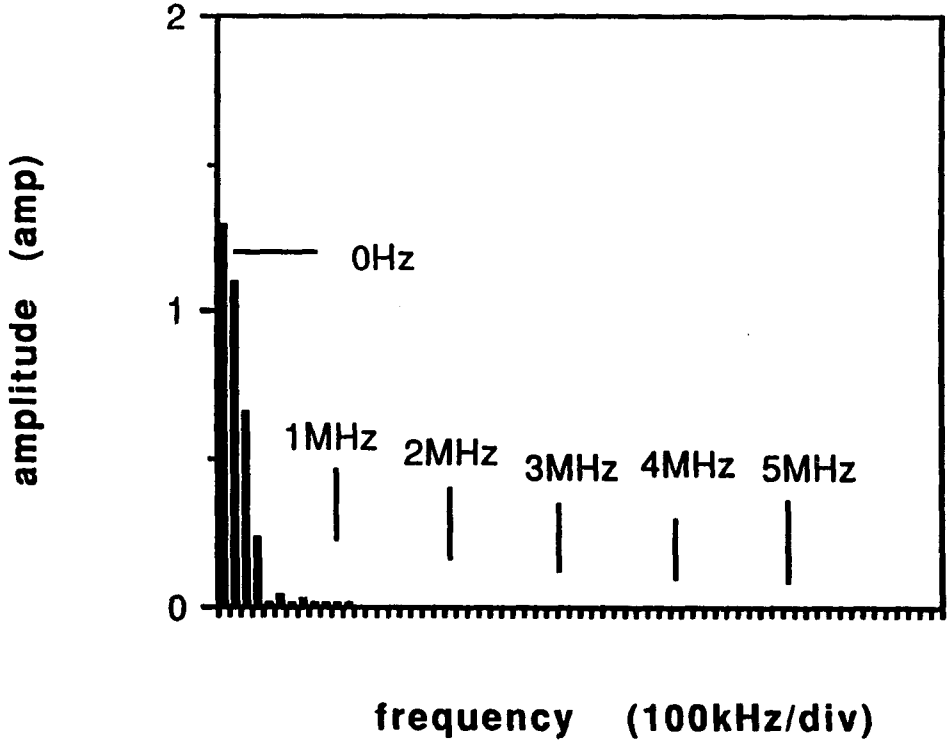

Fig. B-15 ZVS-1 QRC catch diode current Fourier spectrum (output resistance 5 Ω).

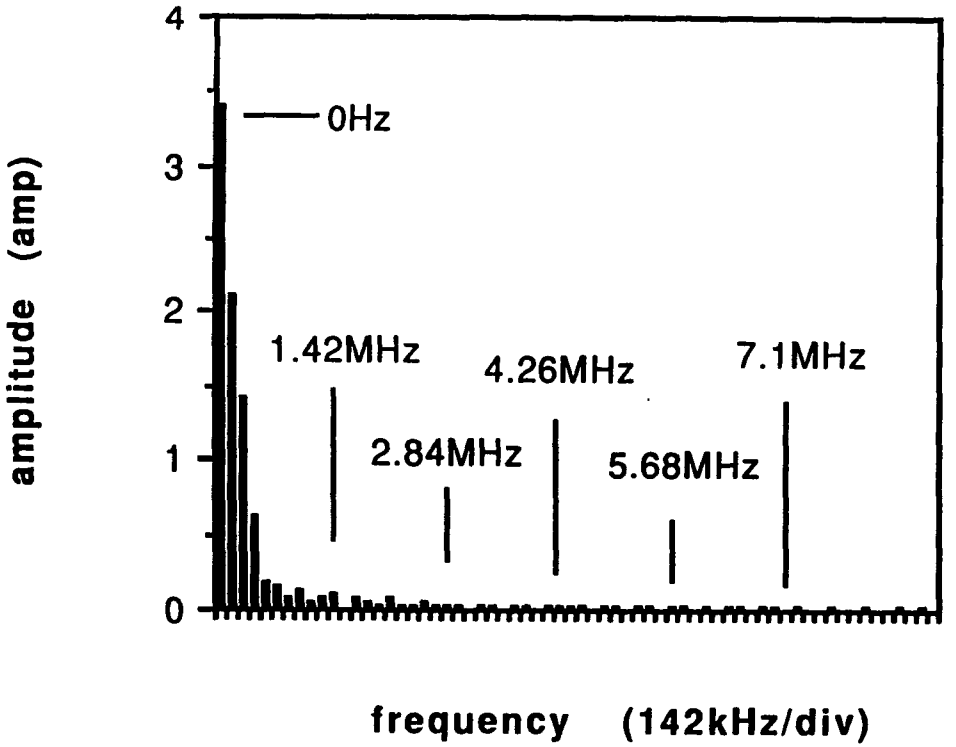

Fig. B-16 ZCS-1/2 QRC input current Fourier spectrum (output resistance 2.4 Ω).

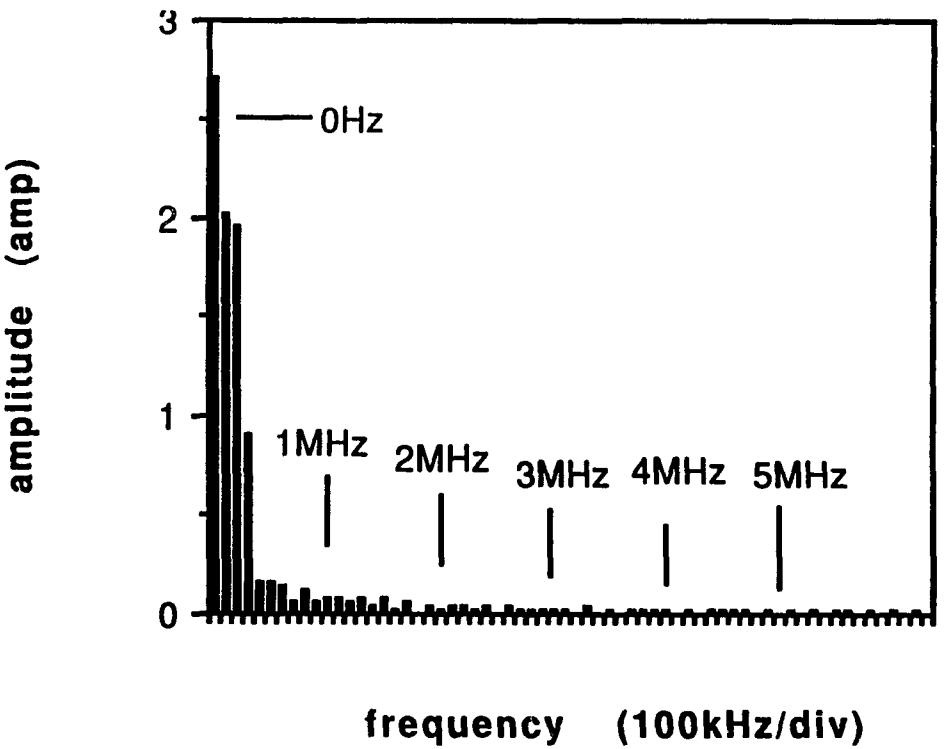

Fig. B-17 ZCS-1 QRC input current Fourier spectrum (output resistance 2.4 Ω).

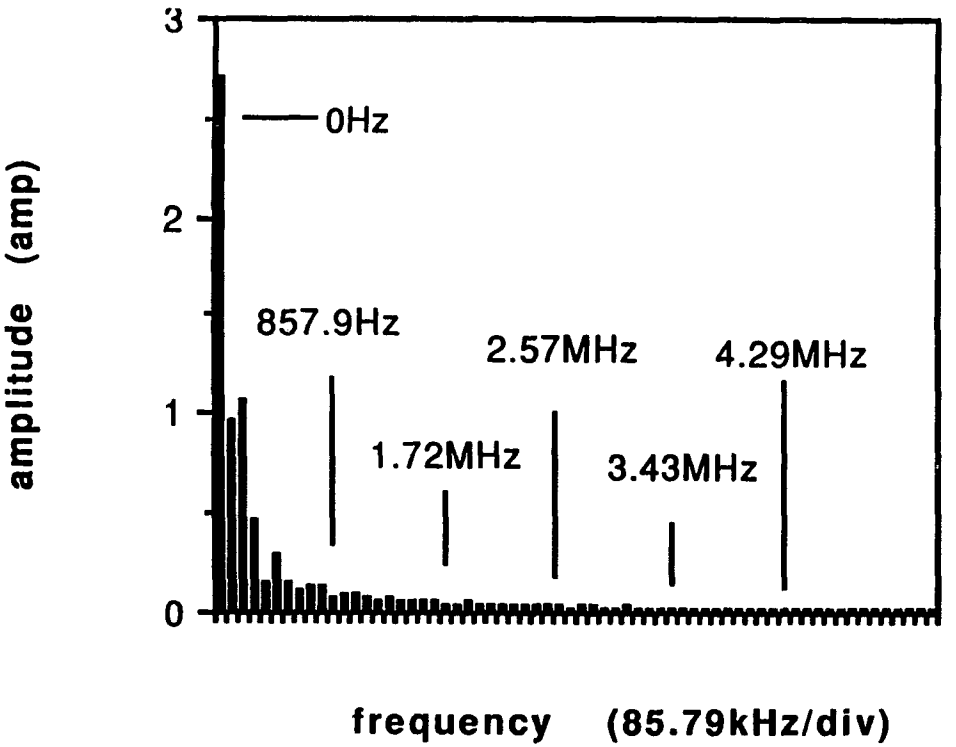

Fig. B-18 ZVS-1/2 QRC input current Fourier spectrum (output resistance 2.4 Ω).

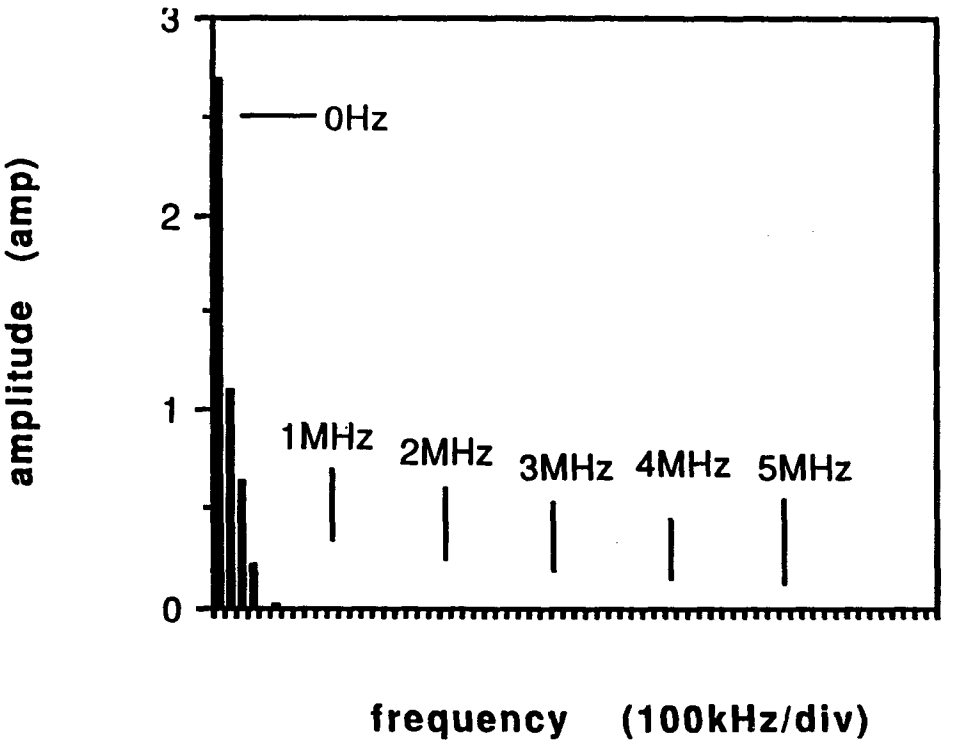

Fig. B-19 ZVS-1 QRC input current Fourier spectrum (output resistance 2.4 Ω).

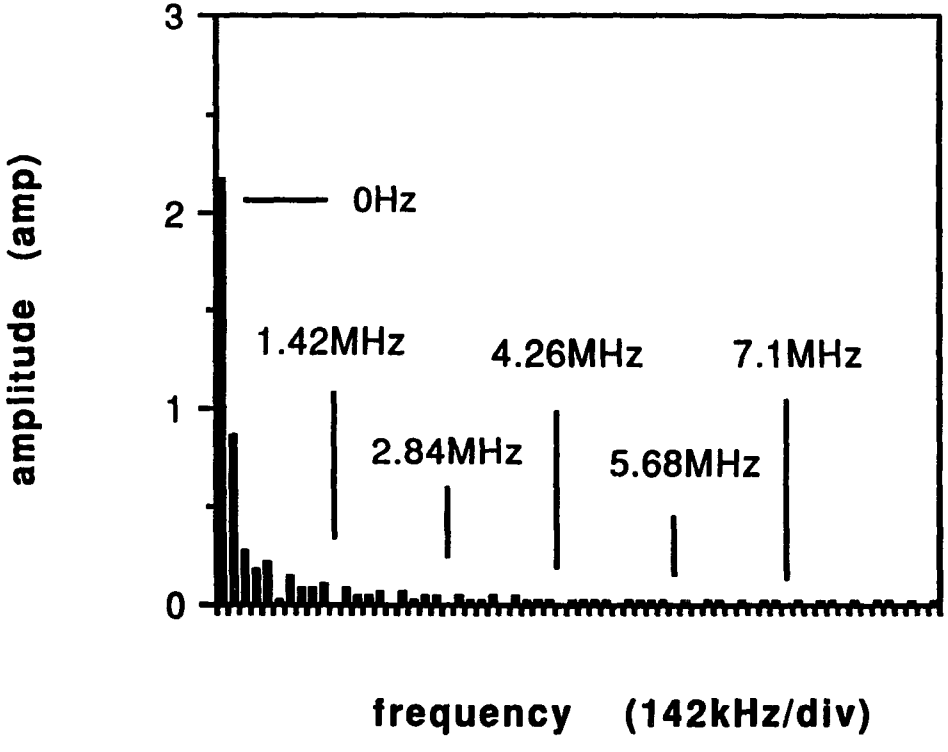

Fig. B-20 ZCS-1/2 QRC catch diode current Fourier spectrum (output resistance 2.4 Ω).

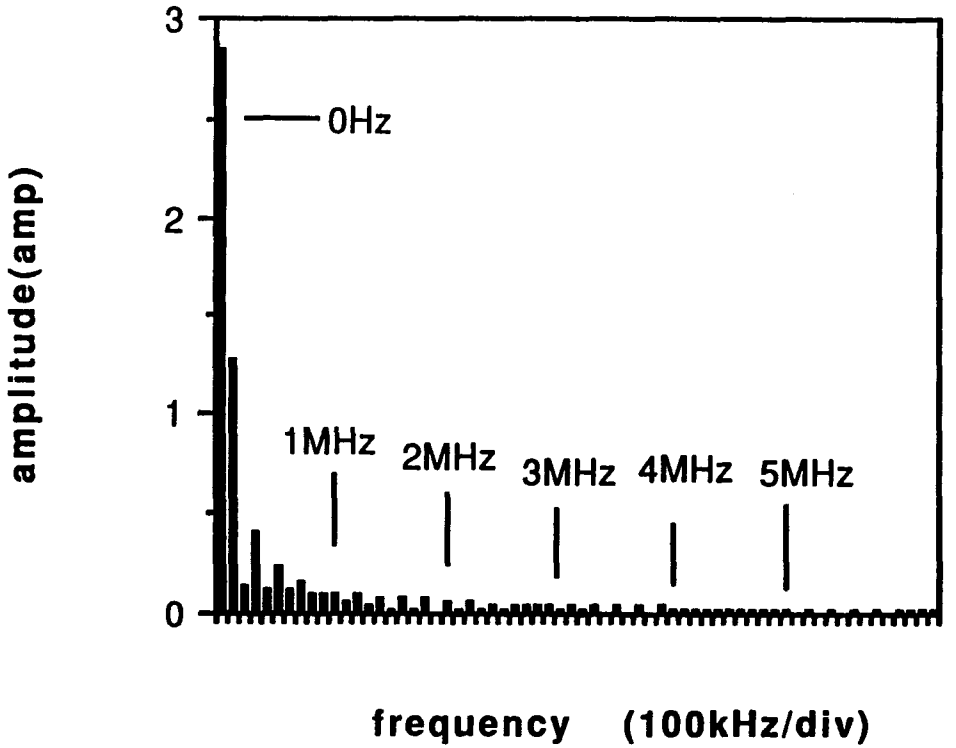

Fig. B-21 ZCS-1 QRC catch diode current Fourier spectrum (output resistance 2.4 Ω).

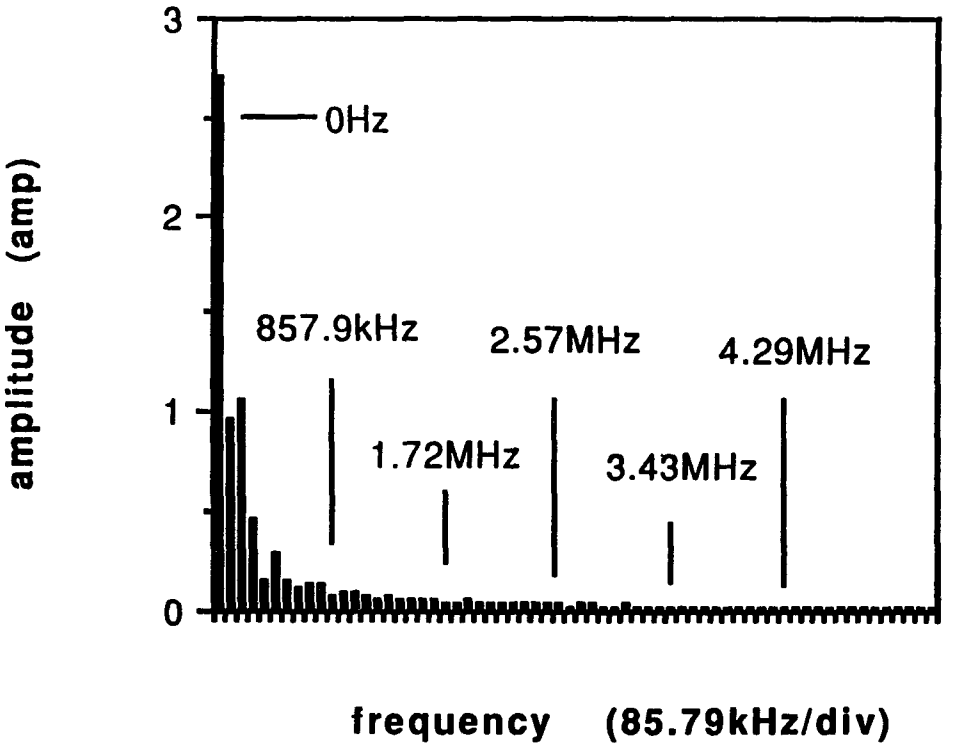

Fig. B-22 ZVS-1/2 QRC catch diode current Fourier spectrum (output resistance 2.4 Ω).

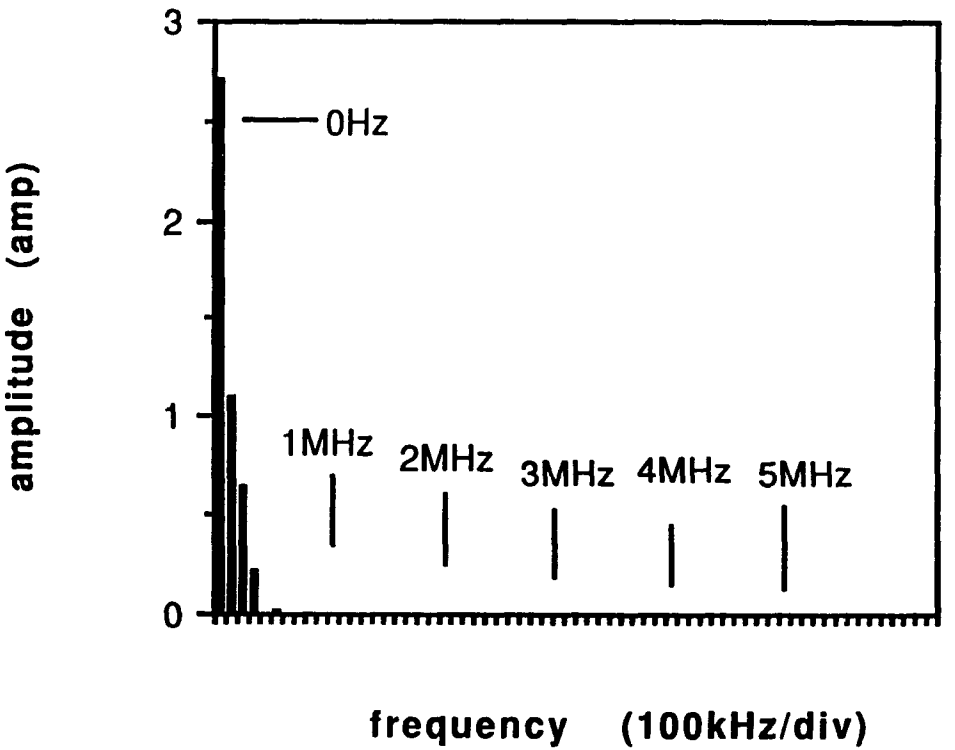

Fig. B-23 ZVS-1 QRC catch diode current Fourier spectrum (output resistance 2.4 Ω).

References

[1] K. H. Liu, R. Oruganti, and F. C. Lee, "Resonant Switches - Topologies and Characteristics", IEEE Power Electronics Specialists Conference, 1985 Record, pp. 106-116.

[2] K. D. T. Ngo, "Generalization of Resonant Switches and Quasi-Resonant DC-DC Converters", IEEE Power Electronics Specialists Conference, 1987 Record, pp. 395-403.

[3] M. M. Jovanovic, K. H. Liu, R. Oruganti, and F. C. Lee, "State Plane Analysis of Quasi-Resonant Converters", IEEE Transaction on Power Electronics, Vol.PE-2, pp. 36-44, Jan 1987.

[4] R. D. Middlebrook, "Design Consideration and Noise Reduction in Switching Converters", Advances in Switched-Mode Power Conversion, Teslaco, Vol III, 1983, pp. 313-324.

[5] M. Nakahara, T. Ninomiya, and K. Harada, "Noise generation in a forward dc-to-dc converter", Proceedings of INTELEC 83' (October 1983), PP. 276-283 .

[6] M. Nakahara, T. Ninomiya, and K.Harada, "Analysis of Surge and Noise Generation in a Forward DC-TO-DC Converter", 1984 IEEE, PP. 339-349.

[7] M. Nakahara, T. Ninomiya, and K.Harada, "Surge and Noise Generation in a Forward DC-to-DC Converter", IEEE Transactions on Aerospace and Electronic Systems Vol. AES-21, No. 5, September 1985, pp. 619-629.

[8] Wojciech A. Tabisz and Fred C. Lee, "DC Analysis and Design of Zero-Voltage-Switched Multi-Resonant Converters", IEEE Power Electronics Specialists Conference, 1989 Record, pp. 243-251.

[9] Wojciech A. Tabisz and Fred C. Lee, "Zero-Voltage-Switching Multi-Resonant Technique-A Novel Approach to Improve Performance of High-Frequency Quasi-Resonant Converters", IEEE Power Electronics Specialists Conference, 1988 Record, pp. 9-17.

[10] Mark Jutras and Mike Ingemi, "Determining and Reducing EMI Sources in On-board Switching Regulators", 1987 IEEE Applied Power Electronics Conference, pp. 199-206.